



HAL
open science

Transboundary particulate matter in Europe – Status report 2013

Wenche Aas, Karl Espen Yttri, Andreas Stohl, Cathrine Lund Myhre, Matthias Karl, Svetlana Tsyro, Katarína Marečková, Robert Wankmüller, Zbigniew Klimont, Chris Heyes, et al.

► To cite this version:

Wenche Aas, Karl Espen Yttri, Andreas Stohl, Cathrine Lund Myhre, Matthias Karl, et al.. Transboundary particulate matter in Europe – Status report 2013. EMEP Co-operative Programme for Monitoring and Evaluation of the Long-Range Transmission of Air Pollutants in Europe. 2013. hal-04244937

HAL Id: hal-04244937

<https://hal.science/hal-04244937v1>

Submitted on 16 Oct 2023

HAL is a multi-disciplinary open access archive for the deposit and dissemination of scientific research documents, whether they are published or not. The documents may come from teaching and research institutions in France or abroad, or from public or private research centers.

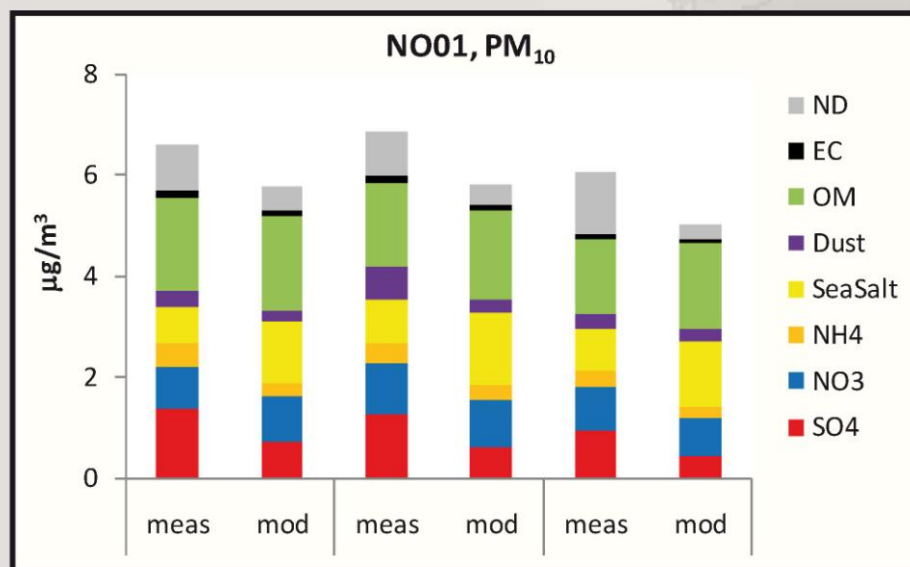
L'archive ouverte pluridisciplinaire **HAL**, est destinée au dépôt et à la diffusion de documents scientifiques de niveau recherche, publiés ou non, émanant des établissements d'enseignement et de recherche français ou étrangers, des laboratoires publics ou privés.



Distributed under a Creative Commons Attribution - NonCommercial 4.0 International License

Transboundary particulate matter in Europe

Status Report 4/2013



NILU: EMEP Report 4/2013
REFERENCE: O-7726
DATE: AUGUST 2013
ISSN: 1504-6109 (print)
1504-6192 (online)

**EMEP Co-operative Programme for Monitoring and Evaluation of the
Long-Range Transmission of Air Pollutants
in Europe**

Transboundary particulate matter in Europe Status report 2013

**Joint
CCC, MSC-W, CEIP and CIAM
Report 2013**



Norwegian Institute for Air Research
P.O. Box 100, NO-2027 Kjeller, Norway



Norwegian Meteorological Institute
P.O. Box 43 Blindern, NO-0313 Oslo, Norway



Umweltbundesamt GmbH
Spittelauer Lände 5, AT-1090 Vienna, Austria



**IIASA – International Institute for Applied
Systems Analysis**
Schlossplatz 1, AT-2361 Laxenburg, Austria

List of Contributors

Wenche Aas¹, Karl Espen Yttri¹, Andreas Stohl¹, Cathrine Lund Myhre¹,
 Matthias Karl¹, Svetlana Tsyro², Katarína Marečková³, Robert Wankmüller³,
 Zbigniew Klimont⁴, Chris Heyes⁴, Andres Alastuey⁵, Xavier Querol⁵,
 Noemí Pérez⁵, Teresa Moreno⁵, Franco Lucarelli⁶, Hans Areskoug⁷,
 Violeta Balan⁸, Fabrizia Cavalli⁹, Jean-Phillippe Putaud⁹, John N. Cape¹⁰,
 Maria Catrambone¹¹, Darius Ceburnis¹², Sebastien Conil¹³, Lusine Gevorgyan¹⁴,
 Jean Luc Jaffrezo¹⁵, Christoph Hueglin¹⁶, Nikos Mihalopoulos¹⁷,
 Marta Mitosinkova¹⁸, Véronique Riffault¹⁹, Karine Sellegri²⁰, Gerald Spindler²¹,
 Tanja Schuck²², Ulrich Pfeffer²², Ludger Breuer²², Dorothee Adolfs²²,
 Lyudmila Chuntanova²³, Marine Arabidze²⁴, Emil Abdulazizov²⁵

¹ Norwegian Institute for Air Research, Kjeller, Norway

² Norwegian Meteorological Institute, Oslo, Norway

³ Umweltbundesamt, Vienna, Austria

⁴ International Institute for Applied Systems Analysis, Laxenburg, Austria

⁵ Institute of Environmental Assessment and Water Research (IDAEA-CSIC), Barcelona, Spain

⁶ Dipartimento di Fisica e Astronomia and INFN, Firenze, Italy

⁷ Stockholm University, ITM, Stockholm, Sweden

⁸ Hydrometeorologic State Service, Ministry Ecology and Natural Resources, Chisinau, Moldova

⁹ European Commission – DG Joint Research Centre, Ispra, Italy

¹⁰ Centre for Ecology and Hydrology (CEH), Bush Estate, UK

¹¹ CNR, The Institute for Atmospheric Pollution, Rome, Italy

¹² School of Physics, National University of Ireland Galway, Galway, Ireland

¹³ ANDRA - DRD - Observation Surveillance, Observatoire Pérenne de l'Environnement, France

¹⁴ Environmental Impact Monitoring Center, Yerevan, Armenia

¹⁵ Laboratoire de Glaciologie et Géophysique de l'Environnement, France

¹⁶ Air Pollution, Environmental Technology, EMPA, Dübendorf, Switzerland

¹⁷ Environmental Chemical Processes Laboratory Dept of Chemistry, University of Crete, Greece

¹⁸ Slovak Hydrometeorological Institute, Bratislava, Slovak Republic

¹⁹ Département Chimie et Environnement, Ecole des Mines de Douai, France

²⁰ Laboratoire de Météorologie Physique LaMP-CNRS/OPGC, Aubiere, France

²¹ Leibniz Institute for Tropospheric Research (TROPOS), Leipzig, Germany

²² Landesamt für Natur, Umwelt und Verbraucherschutz (LANUV), NRW, Essen, Germany

²³ HydroMeteorological Monitoring Center (Kazhydromet), Astana, Republic of Kazakhstan

²⁴ Environment Pollution Monitoring Center, State Dept. Hydrometeorology, Tbilisi, Georgia

²⁵ Centre of Mon. Env. Pollution, Ministry of Ecology and Natural Resources, Baku, Azerbaijan

¹ EMEP Chemical Coordinating Centre

² EMEP Meteorological Synthesizing Centre – West

³ EMEP Centre on Emission Inventories and Projections

⁴ EMEP Centre on Integrated Assessment Modelling

Contents

	Page
Executive Summary	7
1 Status of emissions.....	11
1.1 Status of reporting emission data for 2011	11
1.2 Uncertainty of PM emissions.....	11
1.3 PM emission per capita and per GDP	13
1.4 Contribution of key categories to total PM emissions	13
1.5 PM emission trends.....	14
1.6 Emission data prepared for modellers	18
2 Global emission data set developed with the GAINS model for the period 2005 to 2050	19
2.1 Emission scenarios.....	20
2.2 Example of findings using the ECLIPSE dataset	22
3 Measurement and model assessment of particulate matter in Europe in 2011	24
3.1 Introduction.....	24
3.2 The measurement network.....	24
3.3 The EMEP model and runs setup for 2011	24
3.4 Annual PM ₁₀ , PM _{2.5} and PM ₁ concentrations in 2011	25
3.4.1 PM ₁₀ and PM _{2.5} in 2011 compared to 2010.....	27
3.4.2 PM size fractions.....	27
3.5 Exceedances of EU limit values and WHO Air Quality Guidelines in the regional background environment in 2011	29
3.6 Evaluation of the model performance for PM in 2011	32
3.6.1 Overall statistical analysis.....	32
3.6.2 Individual stations.....	36
4 A closer look at episodes of high PM₁₀ concentration in Central Europe	37
4.1 EMEP observations and model.....	37
4.2 High PM ₁₀ -episodes in Germany in November 2011	41
5 Time series of PM₁₀ and PM_{2.5} and their chemical composition.....	44
5.1 Time series of PM ₁₀ and PM _{2.5}	44
5.2 Time series in chemical composition.....	47
6 The EMEP intensive measurement period in summer 2012 – Mineral dust and trace metals in PM₁₀	52
6.1 Introduction.....	52
6.2 Methods	53
6.2.1 Sampling sites	53
6.2.2 Sampling and analysis.....	53
6.3 Levels of PM ₁₀	54
6.4 Spatial variation	55
6.5 African dust outbreaks: time evolution and spatial influence.....	59
6.6 Trace metals	61

6.7	Factor analysis	65
6.8	Conclusions.....	66
7	Measurements of particulate matter in the EECCA countries.....	67
7.1	Introduction.....	67
7.2	Mass concentration of PM ₁₀	69
7.3	Concentrations of EC and OC in PM ₁₀	70
7.4	Concentrations of CO ₃ ²⁻ in PM ₁₀	72
7.5	Concentrations of levoglucosan in PM ₁₀	73
7.6	Contribution of carbonaceous aerosol to PM ₁₀	74
7.7	General remarks.....	76
8	EMEP development endeavours towards better characterisation of atmospheric aerosol	77
8.1	Improved and extended measurement platform in EMEP.....	77
8.2	EMEP-MAFOR: size-resolved aerosol model under development.....	78
8.2.1	Short description of model approaches and process description.....	79
8.2.2	Sensitivity studies	83
8.2.3	Preliminary results and comparison with measurements.....	83
9	References	88
	APPENDIX A	97

Executive Summary

The current report presents the status and progress of the emission reporting, observations and modelling activities undertaken under EMEP in relation to particulate matter in the European rural background environment. In addition to the assessment of PM concentration levels for the year 2011, we take a closer look at two high pollution episodes in Central Europe in 2011. Time series of PM₁₀ and PM_{2.5} and their chemical composition for the period 2000-2011 is presented.

The report also includes a chapter dedicated to the EMEP intensive measurements of mineral dust during the summer of 2012. One chapter discusses the results of a one year campaign of measurements of particulate matter in the EECCA region, and finally a chapter describes new development in both the measurement platform and the EMEP model towards better characterisation of the atmospheric aerosol.

The main findings presented in the status report for 2011 are described below.

Emission reporting

The total number of Parties which has provided primary particulate matter emissions data for 2011 was 40; out of 51 Parties to the Convention. It has been a slight improvement in the number of Parties reporting PM emissions since year 2008. For 2011, PM sectoral data has been reported for less than 50% of the extended EMEP domain, however more or less complete emission data is available for Europe, except for some Balkan countries. No PM emissions were reported by a number of EECCA countries and for the “Russian Federation extended EMEP domain”.

The most significant source of PM emission is the combustion of fossil fuels, contributing more than 40% of PM emissions. Not all Parties report emissions from all the emissions sectors, and especially for countries outside EU/EFTA region there is a relatively low contribution of “Small Combustion” to the total PM emissions, indicating that emissions from this sector are underestimated.

According to the data submitted by countries and gap-filled by expert estimates, PM emissions in the EMEP area are gradually decreasing, but in individual Parties emission trends vary quite considerably. For the 38 countries which reported full PM₁₀ and/or PM_{2.5} time series (2000-2011), emissions increased in 18 Parties

A section devoted to the updated global emission data set developed with the GAINS model for the period 2005 to 2050 within the EU FP7 project ECLIPSE, shows the importance of including emissions from gas flaring in oil and gas industry and their explicit spatial allocation on a global scale; it is the first time emissions from this source are integrated in the global emission dataset.

Measurement and model assessment of particulate matter

For 2011, mass concentrations of PM are reported for 65 regional or global background sites (55 for PM₁₀ and 44 for PM_{2.5}); that is four less than in 2010.

Combined maps based on model results and measurements show a pronounced north to south gradient, with the annual mean PM₁₀ concentrations varying from 2-5 $\mu\text{g m}^{-3}$ in Northern Europe to 15-25 $\mu\text{g m}^{-3}$ in southern Europe. The corresponding range for PM_{2.5} is from 1-3 $\mu\text{g/m}^3$ to 5-20 $\mu\text{g/m}^3$. The average observed annual mean PM₁₀ concentration for all sites was 16.1 $\mu\text{g/m}^3$, ranging from 3.0 $\mu\text{g/m}^3$ at the high altitude global site Jungfraujoch in Switzerland to 29.9 $\mu\text{g/m}^3$ at the Montelibretti site in Italy. The average observed annual mean PM_{2.5} concentration for all sites was 10.1 $\mu\text{g/m}^3$, ranging from 1.9 $\mu\text{g/m}^3$ at Breckälén in Sweden to 22.2 $\mu\text{g/m}^3$ in Northern Italy (Ispra).

On average for all sites with measurements of PM₁₀ in both 2011 and 2010, it was an increase in mass concentration of 7%. 75% of the sites showed an increase, however, there are large variations between sites. The observed increase in concentrations is confirmed by the EMEP model, which shows higher concentrations in most parts of Europe, except from the eastern part of EMEP domain. These differences in PM concentrations are most likely due to the differences in precipitation amounts between 2010 and 2011 and less to changes in anthropogenic emissions. It was drier in Western/Central/Southern Europe and wetter in most of the other regions in 2011 when compared to 2010.

The combined model and observation maps show that the annual mean regional background PM₁₀ concentrations were below the EU limit value of 40 $\mu\text{g/m}^3$ over all of Europe in 2011, with the exception of the Central Asian area affected by desert dust. However, the annual mean PM₁₀ concentrations calculated by the model exceed the WHO recommended air quality guidelines (AQG) of 20 $\mu\text{g/m}^3$ in the Benelux countries, in parts of central Europe and in the Po Valley (in addition to the Caucasus and Central Asia). The regional background annual mean PM_{2.5} concentrations were above the EU target value (25 $\mu\text{g/m}^3$) and WHO recommended AQG (10 $\mu\text{g/m}^3$) value in the Po Valley and Central Asia in 2011.

The exceedance days for the Central European sites in 2011 were mainly seen in February and November. At several of these sites, the recorded number of days with PM₁₀ exceedance of 50 $\mu\text{g/m}^3$ was the highest in 5 years. On average 80% of the exceedance days took place during the two pollution episodes caused by unfavourable meteorological situation and probably enhanced emissions from residential heating. The EMEP/MS-CW model manages quite well to reproduce the November pollution period, whereas it is not successful in calculating that for February 2011. This illustrates that accurate meteorological input is a prerequisite for successful prediction of the occurrence of pollution episodes by the model, as are emissions from residential wood burning.

There is a relatively obvious decrease in the observed mass concentration in Europe over the last decade although large inter-annual variability can occur. Trend analysis from sixteen sites shows an average decrease of 18% \pm 13% for the period 2000 to 2011. 56% of the sites show a significant decrease, non with a

significant increase. Similar numbers are observed for PM_{2.5}; an average decrease of $26 \pm 16\%$. The downward tendency of the observed annual mean concentration of PM corresponds to a reduction in the emissions of primary PM and gaseous precursors of secondary PM in Europe in the actual period. The EMEP/MSC-W model manages to reproduce these time trends, though with an underestimation of the measured PM by about 20%. There are only a few sites with long time series of chemical composition of the particulate matter. Nevertheless, it is quite clear that the relative contribution of sulphate has decreased in both PM₁₀ and PM_{2.5} in both modelled and measured estimates. For nitrogen and total carbonate the picture is more scattered.

EMEP intensive measurements on mineral dust in PM₁₀

One of the major aims during the EMEP intensive measurements periods in summer 2012 and winter 2013 was to measure the chemical speciation of PM₁₀, focusing in particular on the mineral dust and trace metal content. Thirteen regional sites across Europe participated in this initiative, which has provided a unique data set, which is comparable beyond any other data set currently available for Europe, and which enables an extensive evaluation of sources, transport, and regional distribution of mineral dust across the European continent.

The concentration of mineral dust and trace metals in PM₁₀ across Europe during the summer period is described in the present report, showing the importance of African dust outbreaks on the PM mineral content and concentrations in Southern Europe, and that of local/regional sources in Eastern Europe. The importance of shipping emissions as a regional source in the Mediterranean region, metallurgic industry in Central and Eastern Europe, and coal combustion in Eastern European countries were predicted from the observed concentrations.

Measurements of particulate matter in the EECCA countries

In order to improve our current understanding of PM pollution in the EECCA region, a one year measurement program was initiated to determine the ambient mass concentration of PM₁₀ at five sites in Armenia, Azerbaijan, Georgia, Kazakhstan and Moldova. The measurements also included elemental (EC) and organic carbon (OC), as well as the biomass burning tracer levoglucosan, in order to learn more about the relative contribution of carbonaceous aerosol sources, and biomass burning sources in particular, to PM₁₀.

A substantial fraction of PM₁₀ is attributed to the carb aerosol in the EECCA countries. I.e. in excess of 40% on an annual basis at the Georgian site Abastumani. Further, approximately 30% of OC and 40% of EC is estimated to originate from biomass burning sources, which in turn is found to be more important in winter than in summer, indicating residential wood burning

Although there is a positive trend with more measurements in the EECCA region, there are still issues related to data quality and long term commitments, which needs to be addressed and improved.

Towards better characterisation of atmospheric aerosols

During the last decade there has been a strong interaction between EMEP and several EU infrastructure projects. This has improved the measurement platform particularly for aerosol properties on regional sites in Europe, typically joint EMEP/WMO GAW supersites. Not only have the atmospheric variables and number of instrument types reporting measurements to EMEP and the EBAS database increased, but also the measurement methods and the data reporting formats have been standardized and improved. The improved meta-data description has proven an important documentation of the data quality.

The availability of new observational data for aerosol properties is a prerequisite for further development and improvement of the EMEP/MSC-W model. Recently, a work has been initiated to develop the model towards simulating size-resolved particle number and mass concentrations. For this purpose, aerosol dynamics of the sectional aerosol model MAFOR (Marine Aerosol Formation) have been implemented in the EMEP/MSC-W model. The MAFOR model has been developed for the specific purpose to simulate the formation and evolution of marine aerosols. The MAFOR model has been further extended for use in simulations of particle number concentration (PNC) also in urban environments.

The work is well in progress and the first tests are looking promising. In the present report, a brief summary of the approaches applied and first model results are presented. Model calculated for 2008 total particle number concentrations (PNC) and particle number size distributions are compared to EUSAAR/EMEP data and sensitivity analysis of the result to a series of uncertain model parameters is performed. Further improvement of the model requires extensive use of observational data, and improvement of the model's nucleation parameterisation, VOC condensation and SOA formation. Implementation of size-resolved particle number emissions and size-resolved ammonium nitrate formation will also be needed.

1 Status of emissions

By Katarína Marečková, Robert Wankmüller

1.1 Status of reporting emission data for 2011

Parties to the Convention should submit particulate matter (PM₁₀ and PM_{2.5}) emissions to the Convention annually¹ by 15 February, as a minimum for the years from 2000 and onwards. Data should be reported on sector level (NFR) in standardized formats in accordance with the EMEP Reporting guidelines (UNECE, 2009).

45 Parties (out of 51) to the LRTAP Convention submitted inventories for 2011. Of these, 40 countries provided PM emissions. This represents a slight improvement compared to the year 2008 (Figure 1.1). Submitted data can be accessed via the CEIP website (<http://www.ceip.at/status-of-reporting/2013-submissions>).

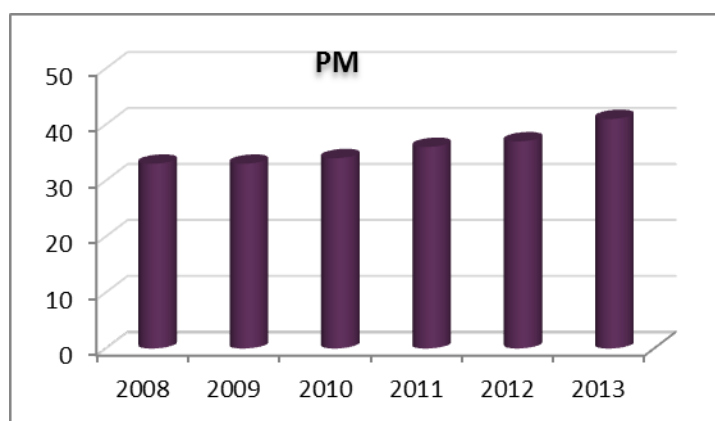


Figure 1.1: Number of Parties reporting since 2008, representing the reporting years. Emission years are two years earlier..

Completeness, consistency, comparability and transparency of reported emissions are analyzed in an annual review process². Feedback is provided to the Parties in the form of individual country reports and summary findings are published in the EEA & CEIP technical report *Inventory Review 2013* (<http://www.ceip.at/review-of-inventories/review-2013>).

1.2 Uncertainty of PM emissions

It is not straight forward to quantify the uncertainty of reported emissions, as countries do not usually provide information on the uncertainties of estimates. Changes in the reporting of the 2005 emissions in subsequent years are therefore regarded as an indicator of uncertainty.

¹ Parties to the LRTAP Convention submit air pollution emissions and projections annually to the EMEP Centre on Emission Inventories and Projections (CEIP) and notify the LRTAP Convention secretariat thereof.

² Methods and Procedures for the Technical Review of Air Pollutant Emission Inventories Reported under the Convention and its Protocols (EB.AIR/GE.1/2007/16).

Figure 1.2 and Figure 1.3 illustrate the variations observed in the 2005 PM emissions reported for individual countries, with 0% corresponding to the latest available 2005 emissions as reported in 2013, and the bars indicating the difference to emissions reported in previous years. Minus values indicate that the 2005 emissions reported in 2013 are higher than the value reported in previous years. Reported 2005 emissions show variations exceeding orders of magnitude for both PM₁₀ and PM_{2.5}. Such differences may indicate errors or incomplete data in some submissions.

No deviation from the value reported in 2013 does not necessarily mean accurate 2005 emissions; this rather implies that there is only one submission for 2005 data from this Party, i.e. that the Party has not updated its historical emissions as recommended by the EMEP Reporting Guidelines.

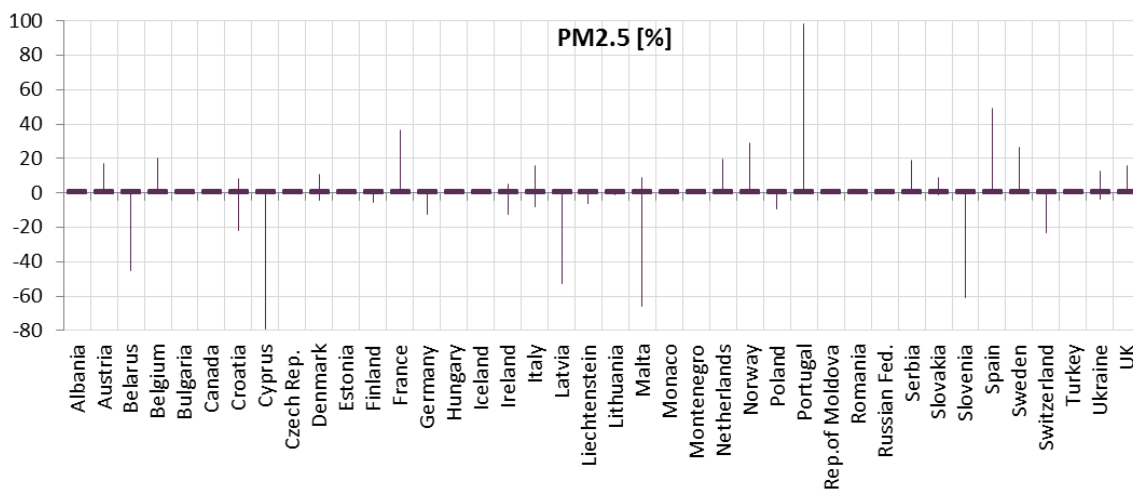


Figure 1.2: Fluctuations of PM_{2.5} 2005 emissions reported in subsequent years (2007-2013).

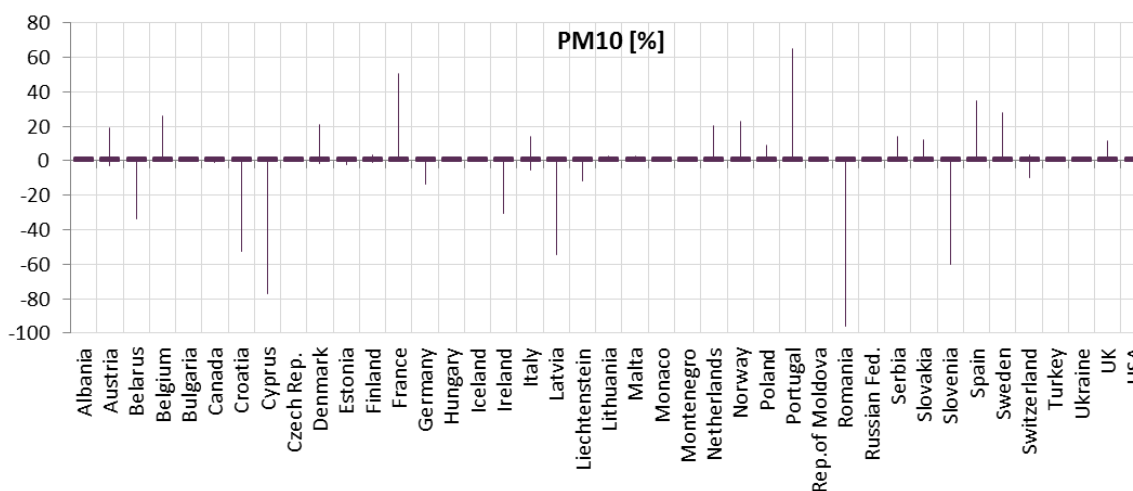


Figure 1.3: Fluctuations of PM₁₀ 2005 emissions reported in subsequent years (2007-2013).

1.3 PM emission per capita and per GDP

In spite of the fact that PM emissions measured as per capita/ gross domestic product (GDP) depend on the structure of national economies, the differences of a few orders of magnitude (see Table 1.1) cannot be explained by this. Such variations of PM emissions per capita and per GDP might be another indicator of a high uncertainty of reported data.

Per country data can be downloaded from <http://www.ceip.at/review-results/review-results-2013>.

Table 1.1: Range of 2011 PM emissions per capita and per GDP.

Pollutant	Emissions in kg per capita in 2011			Pollutant	Emissions in g per GDP in 2011		
	min	middle 50% of the countries (25%-75% quartiles)	max		min	middle 50% of the countries (25%-75% quartiles)	max
PM _{2.5}	0.03	1 - 4	32	PM _{2.5}	0.02	0.06 - 0.2	1
PM ₁₀	0.3	3 - 5	171	PM ₁₀	0.05	0.1 - 0.4	5

1.4 Contribution of key categories to total PM emissions

Key categories are considered those which, when summed up in descending order of magnitude, cumulatively add up to 80% of the national total level. In order to further improve air monitoring and modelling under the Convention, it is important to identify GNFR³ categories that have a significant influence on total emissions.

The most significant source of primary PM emissions is stationary combustion of fossil fuels, producing more than 40% of PM₁₀ and more than 50% of PM_{2.5} emissions (see Figure 1.4 and Figure 1.5). The different distribution of GNFR sectors between EU/EFTA/HR and “Other countries⁴”, and especially the relatively low contribution of “*Small Combustion*” and missing “*Agriculture*” in “Other countries” indicate that emissions from these sectors are potentially underestimated.

Natural emissions (“S_Natural”) are not included in the analysis because Iceland reported a huge amount of PM emissions from volcanic activities for 2011 (13,184 Gg for PM_{2.5} and 40,039 Gg for PM₁₀) which would account for more than 90% of total emissions in Figure A.5 and Figure A.5.

³ 21 GNFR categories are aggregated NFR09 categories (see UNECE 2009 - Annex IV at <http://www.ceip.at/reporting-instructions/annexes-to-the-reporting-guidelines>). GNFR categories should be used for reporting of gridded emissions from 2012 onwards.

⁴ ‘Other countries’ in this chapter refer only to 5 countries, namely Belarus, FYR of Macedonia, the Russian Federation, Serbia, Ukraine, and Turkey (just for PM₁₀). The remaining Parties did not report PM emissions at all. Canada and the USA cannot be included in the KCA since their emissions are not provided in NFR categories.

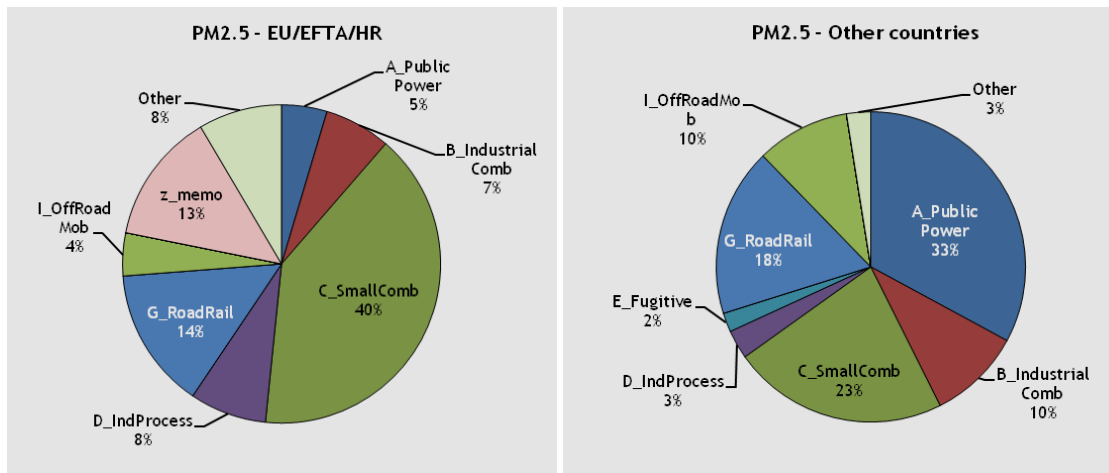


Figure 1.4: Top seven GNFR categories contributing to PM_{2.5} 2011 emissions.

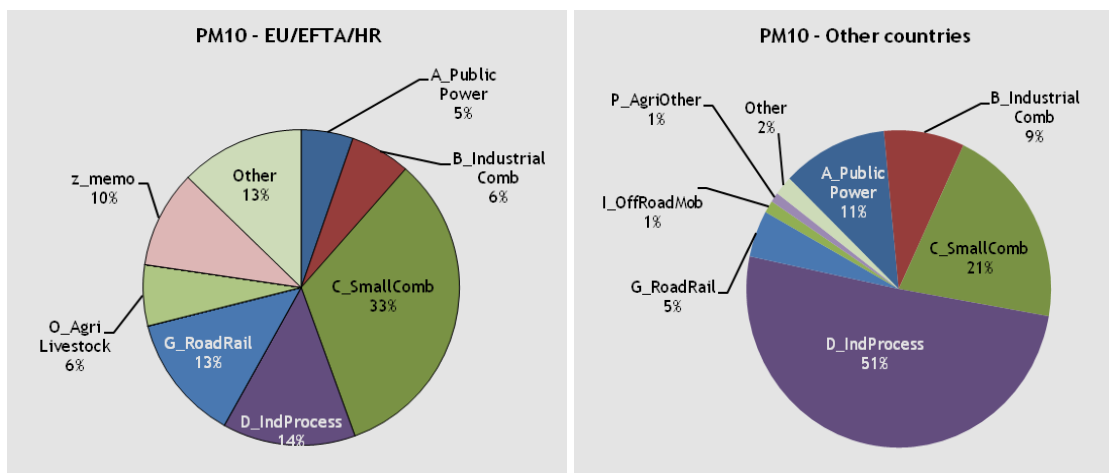


Figure 1.5: Top seven GNFR categories contributing to PM₁₀ 2011 emissions.

Note: Where the total number of categories for a particular pollutant is more than seven or the contribution of a particular sector is < 2%, emissions have been summed up in the category 'Other'

'Memo items' represent emissions reported as international maritime navigation

1.5 PM emission trends

According to the data submitted by countries and gap-filled by expert estimates, PM emissions in the EMEP area are found to gradually decrease (Figure 1.7), but for individual Parties to the CLRTAP emission trends vary quite considerably (see examples in Figure 1.6). For the 38 countries which reported full PM₁₀ and/or PM_{2.5} time series for 2000-2011, emissions increased for 18 of them (see Table 1.2 and Table 1.3).

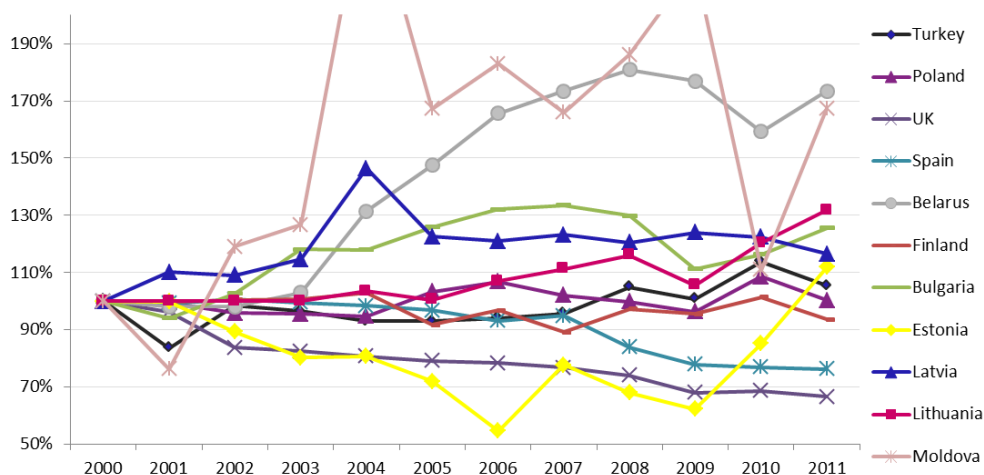


Figure 1.6: Time series of PM_{10} emissions as reported by a selection of countries for the time period (2000-2011).

$PM_{2.5}$ emissions increased for fourteen Parties when comparing 2011 to 2000. The most substantial increases were reported by the Republic of Moldova (+126%) and Belarus (+99%). Bulgaria, Lithuania and Slovakia reported an increase for 2011 compared to 2000. A more than 40% decrease was reported by Belgium, Cyprus, France and the Netherlands (see Table 1.2).

PM_{10} emissions for 2011 was found to increase when compared to 2000 with the most pronounced increases reported by Belarus (+73%) and Moldova (+67%). An increase of more than 25% was observed for Bulgaria, Iceland and Lithuania. A significant reduction of PM_{10} (> 40%) was reported by Belgium and Cyprus (see Table 1.3).

Table 1.2: *PM_{2.5} emission trends (2000-2011) as reported by Parties.*

Country / PM _{2.5} [Gg]	2000	2001	2002	2003	2004	2005	2006	2007	2008	2009	2010	2011	Change 2010 - 2011	Change 2000 - 2011
Albania	9	9	10	13	14	13	14	13	13	11				
Armenia								0						
Austria	23	23	22	22	22	22	21	20	20	19	20	19	-4%	-16%
Azerbaijan														
Belarus	25	25	26	28	36	46	52	51	53	52	45	49	+10%	+99%
Belgium	33	30	30	29	28	24	24	22	21	16	17	17	-2%	-48%
BiH														
Bulgaria	22	21	25	28	27	27	28	26	27	25	27	29	+7%	+30%
Canada	1,014	1,034	997	1,035	1,047	1,088	1,097	1,107	1,118	1,105	1,113	1,113	+0%	+10%
Croatia	9	9	10	11	11	12	11	10	10	10	10	10	+2%	+5%
Cyprus	4	4	4	4	3	3	3	3	3	2	2	2	-12%	-50%
Czech Rep.		0	NE	38	35	21	22	21	21	20	20	17	-16%	
Denmark	23	23	23	24	24	26	27	30	28	26	26	23	-11%	+2%
Estonia	21	22	23	21	22	20	15	20	20	19	23	26	+14%	+25%
Finland	39	40	40	40	40	36	37	34	38	38	41	37	-9%	-5%
France	309	298	274	275	262	242	225	209	204	194	198	173	-13%	-44%
Georgia														
Germany	148	145	138	134	130	125	123	117	113	109	117	111	-5%	-25%
Greece														
Hungary	26	24	25	27	27	31	29	21	23	28	32	31	-3%	+21%
Iceland	0.3	0.3	0.2	0.3	0.3	0.2	0.5	0.3	0.5	0.3	0.3	0.3	-19%	+1%
Ireland	11	11	11	10	11	11	10	10	10	9	8	8	-8%	-31%
Italy	170	167	154	151	155	143	140	140	137	129	131	128	-2%	-24%
Kazakhstan														
Kyrgyzstan											IE	IE		
Latvia	23	26	25	26	28	27	27	26	26	28	27	25	-10%	+6%
Liechtenstein	0.04	0.03	0.03	0.03	0.03	0.03	0.03	0.03	0.03	0.04	0.04	0.04	+4%	+2%
Lithuania	9		NE	NE	9	9	9	10	9	9	10	11	+11%	+26%
Luxembourg	NR													
Macedonia, FYR	NE			NE	7									
Malta	1	1	1	1	1	1	1	1	1	1	1	1	+12%	-15%
Moldova	2	2	1	3	6	6	7	3	5	6	3	5	+47%	+126%
Monaco	0.001	0.001	0.001	0.001	0.001	0.001	0.001	0.001	0.001	0.001	0.001	0.001	0%	0%
Montenegro	4	4	5	5	5	5	5	5	6	4	4			
Netherlands	24	23	22	21	20	19	18	18	17	16	15	14	-6%	-42%
Norway	43	43	44	41	40	40	38	39	38	36	40	37	-8%	-15%
Poland	142	137	133	135	135	146	147	141	135	130	146	139	-5%	-2%
Portugal	71	69	56	54	56	55	51	50	48	46	45	44	-1%	-38%
Romania	NE	NE	NE	NE	NE	106	101	107	123	117	120	109	-9%	
Russia			376	341	383	350	409	348	316	312	367			
Serbia	20	16	19	20	19	21	20	20	21	19	20	20	+2%	+2%
Slovakia	23	33	29	28	28	37	32	28	28	27	27	29	+7%	+26%
Slovenia	15	15	15	15	15	15	16	16	15	16	17	15	-8%	+4%
Spain	98	97	97	98	96	96	92	94	85	79	77	76	-2%	-22%
<i>Spain (grid domain)</i>	93	92	92	92	91	90	87	89	79	73	72	71	-2%	-24%
Sweden	28	28	28	29	29	29	29	29	28	27	28	29	+1%	+2%
Switzerland	12	12	12	11	11	11	11	11	11	10	10	10	-6%	-23%
Turkey									0.0					
Ukraine		NO	0.01		15	125	NE	0.0	NA	NO	41	41	0%	
UK	103	100	90	88	85	84	82	80	76	70	70	67	-5%	-35%
USA	6,061	6,154	5,059	5,048	5,036	4,336	4,419	4,502	4,585	4,564	4,523	4,469	-1%	-26%
EU27	1,510	1,504	1,438	1,416	1,404	1,365	1,322	1,303	1,279	1,233	1,279	1,218	-5%	-19%

Notes: A blank cell indicates that no data have been reported to EMEP
 Shaded cells (red) indicate increased emissions for the given period
 "Emissions shown in the line "Russian Federation" correspond only to the "Russian Federation in the former official EMEP domain"

Table 1.3: PM₁₀ emission trends (2000 - 2011) as reported by Parties.

Party / PM10 [Gg]	2000	2001	2002	2003	2004	2005	2006	2007	2008	2009	2010	2011	Change 2010 - 2011	Change 2000 - 2011
Albania	12	13	14	17	18	17	18	17	17	15				
Armenia								1						
Austria	39	39	38	38	38	38	36	36	36	35	35	35	-2%	-11%
Azerbaijan														
Belarus	37	36	36	38	48	54	60	63	66	65	58	63	+9%	+73%
Belgium	45	45	44	44	42	34	33	30	29	23	24	24	-2%	-47%
Bosnia &														
Bulgaria	35	33	36	42	42	45	47	47	46	39	41	45	+8%	+26%
Canada	4,975	5,151	5,071	5,332	5,474	5,705	5,798	5,922	6,024	5,824	5,856	5,902	+1%	+19%
Croatia	14	14	15	18	19	19	18	17	17	16	15	15	-0%	+8%
Cyprus	6	6	6	6	5	5	4	4	4	4	4	3	-12%	-48%
Czech Rep.		43	51	51	47	34	35	35	35	36	37	32	-12%	
Denmark	29	30	29	31	31	32	33	37	34	32	32	29	-9%	+1%
Estonia	37	37	33	30	30	27	20	29	25	23	32	42	+31%	+12%
Finland	54	54	54	54	56	50	52	48	52	52	55	51	-8%	-6%
France	414	401	374	377	363	338	319	301	294	280	284	260	-8%	-37%
Georgia														
Germany	261	254	244	237	232	224	223	218	212	203	211	209	-1%	-20%
Greece														
Hungary	47	43	44	48	47	52	48	36	38	48	46	44	-4%	-6%
Iceland	0.4	0.4	0.4	0.4	0.5	0.4	0.7	0.6	0.8	0.6	0.6	0.5	-15%	+33%
Ireland	17	18	17	16	16	17	16	16	15	13	13	12	-6%	-30%
Italy	199	198	185	182	186	173	169	171	166	156	159	156	-2%	-22%
Kazakhstan														
Kyrgyzstan											16	20	+23%	
Latvia	27	29	29	30	39	33	32	33	32	33	33	31	-5%	+17%
Liechtenstein	0.05	0.04	0.04	0.04	0.04	0.04	0.04	0.04	0.04	0.04	0.04	0.05	+3%	-1%
Lithuania	10	1	NE	NE	11	10	11	12	12	11	13	14	+10%	+32%
Luxembourg	NR													
Macedonia, FYR	NE		NE	11										
Malta	1.4	2.0	1.9	2.0	2.0	2.1	2.1	2.2	2.2	2.2	1.3	1.4	+9%	-1%
Moldova, Rep. of	5	3	5	6	11	8	8	7	8	10	5	8	+51%	+67%
Monaco	0.01	0.01	0.01	0.01	0.01	0.01	0.01	0.01	0.01	0.01	0.01	0.01	0%	0%
Montenegro	8	7	9	10	10	8	9	8	10	7	7			
Netherlands	39	37	37	35	34	33	32	32	31	29	29	29	-0%	-27%
Norway	50	50	51	48	47	48	46	47	45	43	46	44	-6%	-13%
Poland	257	256	246	245	243	265	274	262	256	247	279	257	-8%	+0.2%
Portugal	98	103	83	76	83	85	76	73	73	70	65	63	-4%	-35%
Romania	NE	NE	NE	NE	NE	126	117	128	138	132	134	124	-8%	
Russia			561	576	647	591	613	522	475	484	569			
Serbia	33	29	32	33	33	35	35	35	36	34	34	35	+2%	+6%
Slovakia	45	47	40	36	32	42	37	32	31	31	30	32	+6%	-28%
Slovenia	20	20	19	19	19	20	20	20	18	19	20	19	-7%	-6%
Spain	141	139	141	140	138	136	131	133	118	110	108	107	-1%	-24%
Spain (grid)	135	134	136	134	132	130	125	127	112	104	102	101	-1%	-25%
Sweden	40	40	40	41	41	42	41	41	40	39	40	40	-0%	+2%
Switzerland	22	22	21	21	21	21	21	21	21	20	20	20	-3%	-11%
Turkey	691	577	680	667	642	643	651	661	725	696	786	728	-7%	+5%
Ukraine		NO	3		119	131	NE	0	NA	NO	133	133	0%	
UK	170	164	142	140	137	134	133	130	126	115	116	113	-3%	-33%
USA	20,901	21,266	19,346	19,335	19,322	18,451	18,475	18,500	18,524	18,506	18,471	18,426	-0%	-12%
EU27	2,218	2,217	2,138	2,101	1,840	2,044	1,984	1,949	1,893	1,824	1,873	1,808	-3%	-18%

Notes: A blank cell indicates that no data have been reported to EMEP
Shaded cells (red) indicate increased emissions for the given period
Emissions shown in the line "Russian Federation" correspond only to the "Russian Federation in the former official EMEP domain"

SNAP National Total
N01 National Total

1.6 Emission data prepared for modellers

Modellers use PM_{2.5} and PM_{coarse}⁵ emissions distributed in a 50 x 50 km² PS EMEP grid⁶. The extended EMEP domain comprises approximately 21,000 grid cells, but PM sectoral data has been reported for less than 50% of this area. More or less complete emission data is available for Europe, except for some of the Balkan countries. No PM emissions were reported by a number of EECCA countries and for the “Russian Federation extended EMEP domain”. Turkey reported only PM₁₀ emissions.

To make submitted emission data usable for modellers, emissions reported in NFR09 categories were converted to 10 SNAP sectors, whereas missing information (i.e. not reported by Parties) had to be added (gap filling)⁷.

In 2013 gridded emissions were reported in GNFR sectors but for the modellers CEIP converted the reported GNFR sectors to SNAP sectors using the reported NFR sector distribution for weighting. This converted grid was then used to distribute the SNAP sector emissions which had been converted from NFR09.

Gap-filled and gridded data can be accessed via the CEIP homepage at <http://www.ceip.at/webdab-emission-database/emissions-as-used-in-emeep-models> and gridded data can also be visualized in Google Maps/Earth at <http://www.ceip.at/webdab-emission-database/gridded-emissions-in-google-maps>.

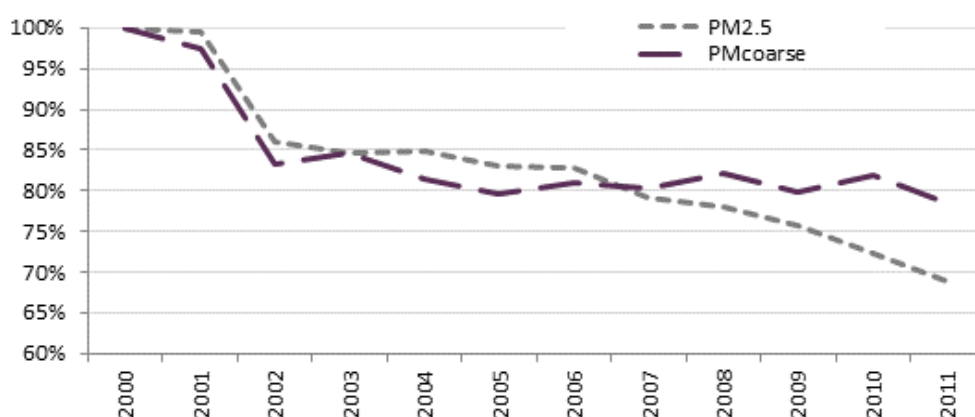


Figure 1.7: PM emission trends (gap filled data) in the EMEP area, 2000-2011.

Emission trends in the EMEP area are significantly influenced by big countries such as Ukraine, Turkey, Belarus and the Russian Federation, for which consistent time series are not available and trends are rather often based on expert estimates.

⁵ PM_{coarse} emissions are not reported but estimated as the difference between PM₁₀ and PM_{2.5}

⁶ Information regarding the gridding procedure can be downloaded from http://www.ceip.at/fileadmin/inhalte/emeep/pdf/gridding_process.pdf

⁷ Basic principles for expert estimates are described in the EEA (2009) ‘proposed gap-filling procedure for the European Community LRTAP Convention emission inventory’.

2 Global emission data set developed with the GAINS model for the period 2005 to 2050

by Zbigniew Klimont, Chris Heyes, Andreas Stohl, Karl Espen Yttri

In the course of 2012-2013 a global emission data set for anthropogenic sources has been developed with the GAINS model (Amann et al., 2011) as part of the activities of the UNECE Task Force on Hemispheric Transport of Air Pollutants (HTAP – <http://www.htap.org>) and within European Commission 7th Framework funded projects ECLIPSE and PEGASOS. Key elements of this dataset, referred to as ECLIPSE V4a, are presented in Table 2.1.

Table 2.1: Key features of the global emission dataset **ECLIPSE V4**.

Parameter	Description
Coverage:	Global
Emission sources:	Anthropogenic sources excluding international shipping and aviation. The following sector-layers are available: energy, industry, solvent use, transport, domestic combustion, agriculture, open burning of agricultural waste, waste treatment.
Pollutants (units):	All outputs in thousand tons of pollutant per year/grid Sulphur dioxide (as SO ₂) Nitrogen oxides (as NO ₂) Non-methane volatile organic compounds Ammonia (as NH ₃) Carbon monoxide (as CO) Methane (as CH ₄) Primary fine particulate matter distinguishing the following components: PM2.5, PM10, black carbon (BC), organic carbon (OC), and organic matter (OM)
Scenarios:	Baseline 2005-2050 (current legislation – CLE), Maximum technically feasible reductions for 2030 and 2050 (MTR)
Temporal distribution:	Total annual values for 2005, 2010, 2030, 2050
Spatial distribution:	0.5°x0.5° longitude-latitude
File location:	Available from the GEIA web site: http://www.geiacenter.org , and for a limited time from anonymous ftp: ftp.iiasa.ac.at/outgoing/mag/ECLIPSE-V4a and then upon request from: http://eclipse.nilu.no
Format:	NetCDF (Network Common Data Form) http://www.unidata.ucar.edu/software/netcdf/
How to reference?	The full documentation is under preparation and currently the link to the web-sites listed above and acknowledgment of the ECLIPSE project should be made; e.g., the European Commission 7 th Framework funded project ECLIPSE (Evaluating the Climate and Air Quality Impacts of Short-Lived Pollutants) Project no. 282688, development of the MTR scenario was supported by PEGASOS (Pan-European Gas-Aerosols-Climate Interaction Study) Project no. 282688 and 'Assessment of hemispheric air pollution on EU air policy' contract no. 07.0307/2011/605671/SER/C3 projects.

The emission calculation for historical years relies on the experience of IIASA in various regional and global projects where respective information on activity data, environmental legislation, production and abatement technology characteristics, etc. have been collected and implemented in the GAINS model (<http://gains.iiasa.ac.at>). For example:

- For Asia recent work on the GAINS-Asia model (Amann et al., 2008; Klimont et al., 2009; Purohit et al., 2010) and results of other related projects (e.g., Klimont et al., 2002; Wei et al., 2008; Zhang et al., 2009) were used;
- At a global level key experience is summarized in (Cofala et al., 2007; Klimont and Streets, 2007; Isaksen et al., 2009; UNEP, 2011; UNEP/WMO, 2011; Höglund-Isaksson, 2012; Klimont et al., 2013). The emissions of black carbon currently calculated in GAINS are also largely consistent with the GAINS dataset used for the ‘Bounding BC’ study (Bond et al., 2013);
- For Europe, the results of the national consultations within the work for the UNECE Convention on Long-Range Transboundary Air Pollution (CLRTAP) in 2011-2012 undertaken prior to the revision of the Gothenburg Protocol and further work towards revision of the EU Thematic Strategy on Air Pollution (TSAP) (Amann et al., 2012) were implemented.

The global energy database in GAINS has been updated for 2005 and 2010 using most recent IEA (International Energy Agency) statistics and for agriculture data from FAO (UN Food and Agriculture Organization). For Europe, the statistical data for energy, production, and agricultural activities from EUROSTAT were also used. For methane, we have made use of the latest GAINS assessment (Höglund-Isaksson, 2012).

One of the important extensions is inclusion of emissions from gas flaring in oil and gas industry and their explicit spatial allocation; it is the first time emissions from this source are integrated in the global emission dataset (Klimont et al., in preparation). These emissions were calculated using data on activities available from the World Bank initiative on Global Gas Flaring Reduction initiative (GGFR) (Elvidge et al., 2007, 2011). The global and regional data were downloaded from the NGDC website http://www.ngdc.noaa.gov/dmsp/interest/gas_flares.html. The potential importance of considering this source in the analysis is illustrated in the recent paper by Stohl et al. (2013) and briefly discussed in the last section.

2.1 Emission scenarios

Two principal emission scenarios extending until 2050 were developed: the current legislation case (CLE) and the maximum technically feasible reduction case (MTFR_{ult}). Both scenarios rely on the baseline energy projections from the PRIMES model for EU-27 (as used in the work on revision of the EU Thematic Strategy for Air Pollution – (Amann et al., 2012)). For the rest of the world the combination of the IEA World Energy Outlook 2011 reference scenario [IEA, 2011] up to 2035 and the results of the POLES model developed at the EU Joint Research Center (JRC, Sevilla) up to 2050 were used. For agriculture, the CAPRI

model baseline, as developed for the TSAP strategy, was used for EU-27, while FAO Outlook (Alexandratos and Bruinsma, 2012) was used for the rest of the world.

The reference emission scenario, **current legislation case (CLE)**, assumes that existing legislation is implemented but there is no assumptions made as to how such legislation can develop further in the coming decades. From that perspective, one can see this as a rather conservative case but on the other hand it assumes that control technologies deliver expected reductions and that perfect enforcement of the laws is implemented in the modelling time horizon; both of the latter assumption appear fairly optimistic considering experience in the last decades of, for example, achieving NO_x reductions in transport sector in Europe and Asia (e.g., Huo et al., 2012) or SO_2 control power sector in China (Xu et al., 2009; Xu, 2011). The calculation was performed with the IIASA GAINS model and the evolution of global emissions in the period from 2000 to 2050 is summarized in Figure 2.1. The CO_2 emissions in the period up to 2050 are following a similar trajectory as those estimated in the RCP6.0 (Van Vuuren et al., 2011) and a discussion of recent global air pollutant scenarios and their comparison to Representative Concentration Pathways (RCP) will be soon available from (Amann et al., in press).

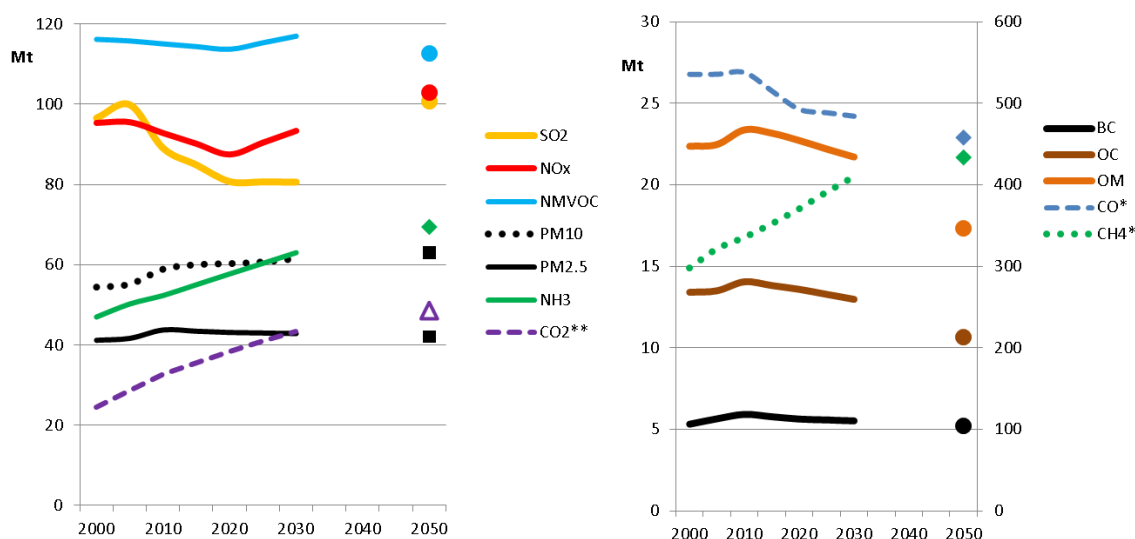


Figure 2.1: Global emissions of air pollutants and methane in the baseline scenario (CLE). (*) For CO and CH_4 the right hand scale is used, (**) for CO_2 the units are Gt.

Compared to the recently used IIASA scenarios, e.g., (UNEP, 2011; UNEP/WMO, 2011), we have updated information on the implementation of the current legislation in several regions and key sectors. At the same time, recent data from source measurement campaigns was used to update emission factors for major sources, considering specifically impact of control measures on co-emitted species. Key sectors include combustion of solid fuels in the residential sector for heating and cooking, transportation with specific focus on high-emitting diesel vehicles and off-road machinery, open burning of agricultural residue, and selected industrial processes in the developing world, e.g., coke ovens, brick kilns.

A more detailed discussion of the recent developments of the GAINS database and these scenarios will be presented in Klimont et al. (in preparation).

The **maximum technically feasible reduction (ultimate) (MTFR_{ult})** scenario considers best available technology applied to all source sectors in 2030 and 2050, i.e., it assumes unconditional implementation of technologies with lowest emission factors in GAINS but no introduction of non-technical measures that would improve resource efficiency and lead to a significant change of energy balance. The scenario ignores possible constraints, either of technical, institutional, or cultural nature that would be still in place by 2030 or 2050 in some regions. Analysis of such constraints is underway within the Task Force on Hemispheric Transport of Air Pollution (HTAP) and will result in development of a scenario, which will consider possible limitation for implementation of measures within different timeframes.

The calculated emissions were distributed into RCP sectors (energy, industry, solvent use, transport, agriculture, open burning of agricultural waste, residential combustion, and waste treatment) and spatially allocated into 0.5°x0.5° longitude-latitude using RCP consistent proxies as used and further developed within Global Energy Assessment project (GEA, 2012). These are consistent with proxies applied within the RCP projections as described in (Lamarque et al., 2010) and were modified to accommodate for more recent information where available, e.g., population distribution, open biomass burning, effectively making them year specific (Riahi et al., 2012; Klimont et al., 2013).

The developed emission data sets **do not include** emissions from international shipping and aviation, biogenic VOC emissions, and forest and savannah fires (emissions from open burning of agricultural residue **are included**). We recommend using the following sources for these emissions:

- International shipping (Buhaug et al., 2009; Eyring et al., 2010) and aviation (Lee et al., 2009) as developed for the work on Representative Concentration Pathways (RCP) (Van Vuuren et al., 2011),
- Biogenic emissions (<http://acd.ucar.edu/~guenther/MEGAN/MEGAN.htm>) (Guenther et al., 2012)
- Biomass burning emissions for other sectors than open burning of agricultural residue (included in the GAINS calculation) can be obtained from the GFEDv3.1 global database, including gridded dataset (<http://www.globalfiredata.org/Data/index.html>).

2.2 Example of findings using the ECLIPSE dataset

One of the novelties of the actual emission data set is that it includes emissions from gas flaring. Although gas flaring is estimated to account for less than 3% of the global BC emissions in the current data set, this source is found to dominate the estimated BC emissions in the Arctic (i.e. north of 66°N), accounting for 42% of the annual mean BC surface concentrations in the Arctic (Stohl et al., 2013).

By accounting for gas flaring in the emission inventories and by improving time resolution of domestic combustion emissions (DCE), as well as applying the

concept of heating degree day in DCE, substantial improvements of the simulated Arctic BC mean concentration and its seasonality were demonstrated. This suggests that missing emissions and lacking time resolution of the emissions data may explain why models struggle to capture Arctic Haze (see Figure 2.2). Even including the gas flaring emissions, BC concentrations were underestimated by model calculations, compared to shipboard measurements in the White, Kara and Barents Seas, downwind of the main gas flaring region in northern Russia. This suggests that the gas flaring emissions are not overestimated in the emission data set.

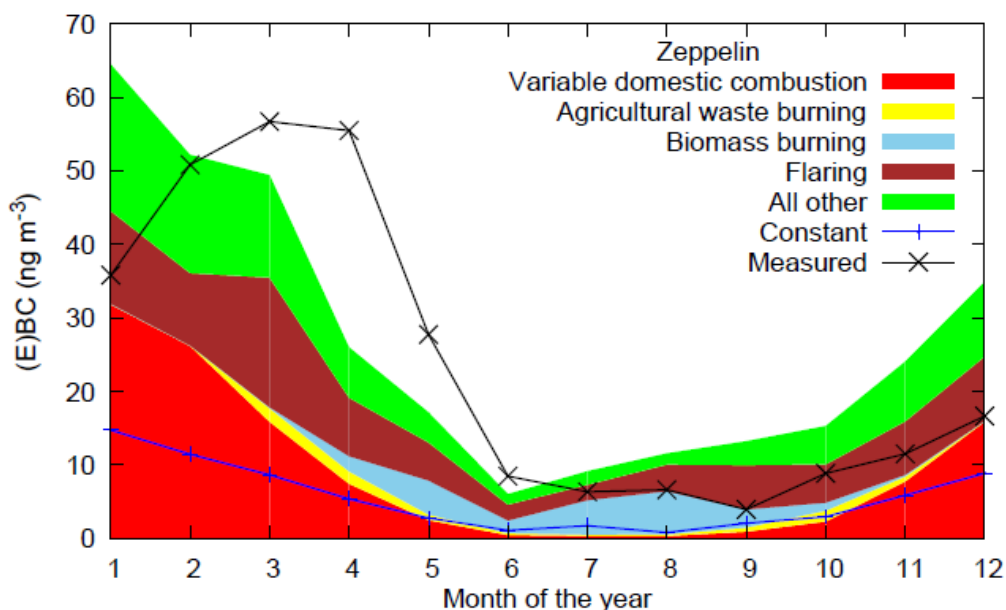


Figure 2.2: Comparison of monthly mean modelled BC and measured EBC concentrations at Zeppelin. The measurements are shown with a black line with crosses, whereas the model results are split into contributions from different sources according to the colour legend. Also shown are the results for the domestic combustion tracer with constant emission rate throughout the year (blue line with pluses), which can be compared directly with the variable emission tracer (red area). Data shown is the average for the years 2008–2010. Figure and figure caption taken from Stohl et al. (2013).

3 Measurement and model assessment of particulate matter in Europe in 2011

By Svetlana Tsyro and Wenche Aas

3.1 Introduction

The current assessment of the concentration levels of regional background PM₁₀ and PM_{2.5} in 2011 has been made based on EMEP model calculations and data from the EMEP monitoring network. The main changes in calculated PM₁₀ and PM_{2.5} levels from 2010 to 2011 are documented. Calculated mean concentrations of the individual aerosol pollutants are also included. The mass distribution between the PM₁₀, PM_{2.5} and PM₁ size fractions based on model and observational data is briefly discussed. Further, calculated regional background concentrations of PM₁₀ and PM_{2.5} exceeding EU limits and WHO Air Quality Guidelines in 2011 are presented. We evaluate the model's ability to reproduce observed exceedances of PM₁₀ and PM_{2.5} EU limit values and WHO Air Quality Guidelines at the individual stations. Finally, we make a closer look at two high pollution periods in central Europe in February and November 2011.

3.2 The measurement network

The observed annual mean concentrations of PM₁₀, PM_{2.5} and PM₁ for 2011 at European rural background sites can be found in Hjellbrekke and Fjæraa (2012). For 2011, mass concentrations of PM are reported for 65 regional or global background sites (55 for PM₁₀ and 44 for PM_{2.5}); four less than in 2010. There are five new sites in 2011 compared to 2010: DE0043, FI009, FI0017, FR0014 and GR0001. However, nine of the sites for which data was reported in 2010 did not report for 2011; i.e. DK0005, ES0017, GB0006, GR0002, HU0002, LV0016 and the three Slovakian sites. For Slovakia, the sites are still measuring particulate matter, but data has not been reported in time. Several sites have stopped measuring PM₁₀ and only measure PM_{2.5}, i.e. six of the Spanish sites. The number of Parties which reported aerosol mass data in 2011 was 21. It is worth noting that even though the spatial distribution of sites with mass measurements in Europe has become improved, several sites have unsatisfactory data coverage. For 2011, 47 of the 55 sites measuring PM₁₀ had data completeness higher than 75%. For PM_{2.5}, 38 of the 44 sites had satisfactory data coverage. PM₁ was reported for 5 sites in 2011, one less than for 2010.

3.3 The EMEP model and runs setup for 2011

The calculations presented in the current report have been performed with the EMEP/MS-CW model, version rv.4.4. The main developments of the model since reporting in 2012 mainly aimed at improving its technical features and robustness, whereas the descriptions of physical and chemical processes have not changed significantly (Simpson et al., 2012). The model version used for this report corresponds to the EMEP/MS-CW Open Source model (http://emep.int/mscw/index_mscw.html).

The meteorological data used in the model simulations for 2011 is from the ECMWF-IFS meteorological model. The national emissions of SO_x, NO_x, NH₃, NMVOC, PM₁₀ and PM_{2.5} for the year 2011 were prepared by EMEP/CEIP (see

Chapter 1). The emissions of primary PM₁₀ and PM_{2.5} have been disaggregated to elemental carbon (EC), primary organic aerosol (POA) and remaining inorganic dust using the latest information from IIASA.

The modelled PM₁₀ and PM_{2.5} concentrations include secondary inorganic aerosols (SIA = SO₄²⁻ + NO₃⁻ + NH₄⁺), organic aerosols (both primary and secondary), elemental carbon, sea-salt, mineral dust and water. The aerosol water content is calculated for a temperature of 20 °C and a relative humidity of 50%, which corresponds to required standardized conditions for equilibration of PM samples.

The following procedure has been used to generate the combined maps presented in Figure 3.2. For each measurement site with PM data in 2011, the difference between the observed value and the modelled value in the corresponding grid cell has been calculated. The differences for all sites have been interpolated spatially using radial base functions, which provide a continuous 2-dimensional function describing the difference in any cell within the modelled grid. The combined maps have been constructed by adjusting the model results with the interpolated differences, giving larger weight to the observed values close to the measurement site, and using the model values in areas with no observations. The range of influence of the measured values has been set to 500 km.

3.4 Annual PM₁₀, PM_{2.5} and PM₁ concentrations in 2011

Annual mean concentration fields of regional background PM₁₀ and PM_{2.5} in 2011, based on EMEP/MSC-W model calculations and measurements from the EMEP monitoring network, are presented in Figure 3.2. According to the concentration maps, the annual mean PM₁₀ concentration in 2011 typically varied from 2-5 µg/m³ in Northern Europe to 15-25 µg/m³ in Southern Europe. The corresponding range for PM_{2.5} was from 1-3 µg/m³ to 5-20 µg/m³ (Northern Europe) to 5-20 µg/m³ (Southern Europe). The enhanced PM_{2.5} and PM₁₀ levels in Southern Europe are associated with large emissions in major cities, industrial and agricultural regions and also with windblown dust generation in arid regions.

The lowest concentrations of PM₁₀ were observed in the northern and north-western parts of Europe, i.e. the Nordic countries, the British Isles, and for high altitude sites (> 800 masl) on the European mainland. The average observed annual mean PM₁₀ concentration for all sites was 16.1±7.1 µg/m³. The highest annual mean was recorded at Montelibretti in Italy (IT0001, 29.2 µg/m³). High levels were also observed in Greece and The Netherlands. The lowest annual means were recorded at the high altitude global site Jungfrauoch in Switzerland (3.0 µg/m³) closely followed by the Norwegian site Kårvatn (NO0039, 3.6 µg/m³). The average observed annual mean PM_{2.5} concentration for all sites was 10.1±4.9 µg/m³. The lowest annual mean was recorded at the Swedish site Breckälven (SE0005, 1.9 µg/m³), whereas the highest annual mean was recorded at Ispra in Northern Italy (IT0004, 22.2 µg/m³).

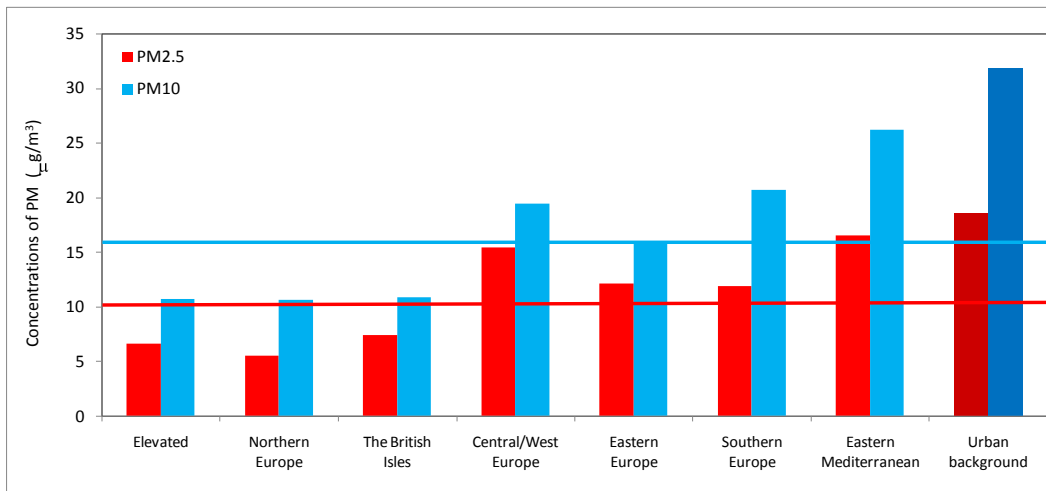


Figure 3.1: Annual mean concentrations of PM_{10} and $PM_{2.5}$ for various regions of the EMEP domain in 2011 ($\mu\text{g m}^{-3}$). Solid blue and red lines denote the average concentrations for all sites. Annual mean concentrations for European urban background sites (from AirBase) are included for comparison.

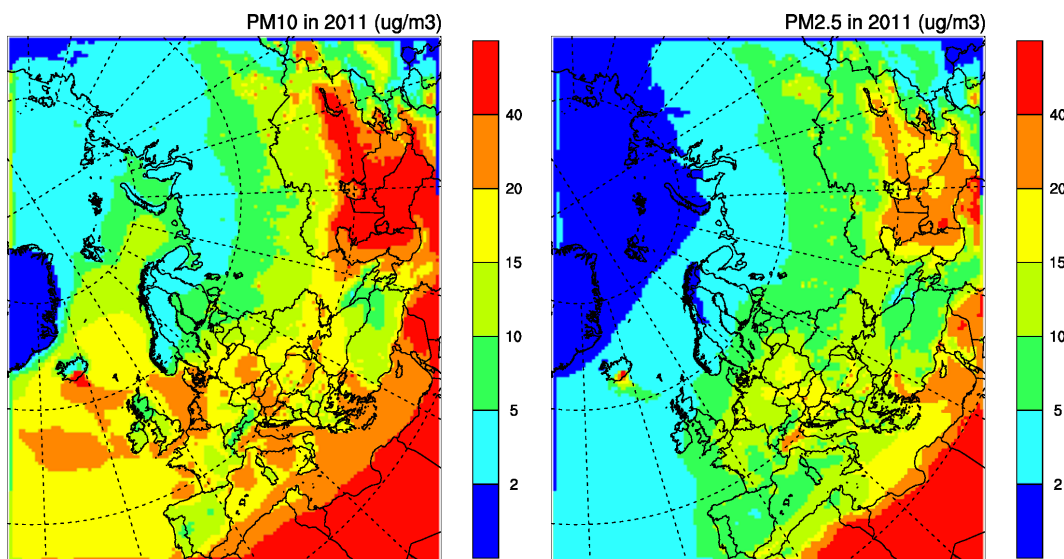


Figure 3.2: Annual mean concentrations of PM_{10} (left) and $PM_{2.5}$ (right) in 2011 based on EMEP/MSC-W model calculations and EMEP observation data.

The mean European urban background concentration of PM_{10} and $PM_{2.5}$ has been included in Figure 3.1 to give an idea of the rural background influence. Close to 50% of the urban background concentration is likely to be attributed to the mean rural background concentration for both size fractions.

3.4.1 *PM₁₀ and PM_{2.5} in 2011 compared to 2010*

75% of the sites which reported concentrations of PM₁₀ both for 2010 and 2011 had higher annual means in 2011 compared to the previous year. For all sites it was an average 7% increase going from 2010 to 2011. However, there were large variations between sites, e.g. the annual mean decreased from 40.4 µg/m³ in 2010 to 23.3 µg/m³ in 2011 at Ayia Marina in Cyprus (CY0002), whereas it increased from 11.7 to 17.0 µg/m³ at Råö in Sweden (SE0014). For PM_{2.5} there was an average increase of 2%.

The observed increase in concentration is confirmed by the EMEP model. Calculated with the same model version (rv. 4.4) and updated emission data, the results show that annual mean PM₁₀ levels were 0.5-2 µg/m³ higher in 2011 than in 2010 in Western, Central and Southern Europe, and as much as 2-5 µg/m³ higher in the northern of Italy, South-eastern Europe, in Denmark and the Netherlands. On the other hand, in the eastern part of the EMEP domain (east for appr. 15°E), i.e. in Finland, the Baltic countries, Eastern Europe, Greece, Malta and Turkey, the mean PM₁₀ levels were 1-5 µg/m³ lower in 2011 than in 2010 (in fact it was more than 10 µg/m³ lower in parts of the southern region). The pattern seen for PM_{2.5} generally reflects that described for PM₁₀.

These differences in calculated PM concentrations between 2010 and 2011 are most likely due to the differences in precipitation amounts. According to ECMWF_IFS meteorology used in the EMEP/MSC-W model, 2011 was drier in Western/Central/Southern Europe and wetter in the most of the other regions when compared to 2010. Changes in PM₁₀ and PM_{2.5} concentrations due to anthropogenic emissions were minor for most of the EMEP domain going from 2010 to 2011. The exception was the 1-5 µg/m³ concentration increase in the east of Turkey and on Malta caused by increased Turkish emissions of SO₂ and NO_x, and the 1-3 µg/m³ decrease in the Po Valley. Concerning PM from natural sources, the model calculates higher sea salt concentrations in the North Sea and lower levels of African dust in 2011 than in 2010. The latter is probably due to more precipitation and smaller surface stress in North-African and Central Asian deserts which inhibited dust generation.

3.4.2 *PM size fractions*

Table 3.1 shows the annual mean PM_{2.5} to PM₁₀ ratio at EMEP sites based on observational data and model calculations for 2011. The ratios have been calculated for common days, i.e. when both observational and modelled concentrations of PM_{2.5} and PM₁₀ were available. Further, only sites with similar methods for both size fractions have been used, i.e. sites with e.g. TEOM for one size fraction and gravimetric for the other has not been included in order to avoid inconsistencies due to different methodologies. Notice that some of the sites have data capture with less than 75% coverage. These are denoted in the table.

Table 3.1: Observed and model calculated annual mean PM ratios at EMEP sites in 2011.

	Site		PM _{2.5} /PM ₁₀		PM ₁ /PM ₁₀		PM ₁ /PM _{2.5}	
			Obs	Mod	Obs	Mod		
Northern Europe	Norway	NO002 ¹⁾	0.55	0.65				
		NO0039 ¹⁾	0.73	0.78				
		NO0056 ¹⁾	0.71	0.77				
	Sweden	SE0005	0.46	0.74				
		SE0014	0.46	0.55				
	Finland	FI0050	0.78	0.78	0.60		0.75	
The British isles	Great Britain	GB0036	0.61	0.59				
		GB0048	0.55	0.58				
Central/ Western Europe	Austria	AT0002	0.75	0.82	0.58		0.78	
	Switzerland	CH0002 ³⁾	0.67	0.78	0.52		0.78	
		CH0005 ³⁾	0.74	0.78				
	Czech Rep.	CZ0003 ^{2,3)}	0.70	0.80				
	Germany	DE0002	0.71	0.73	0.47		0.66	
		DE0003	0.74	0.77				
		DE0007	0.71	0.73				
		DE0008	0.71	0.77				
	France	DE0044	0.80	0.77				
		FR0009 ²⁾	0.53	0.74				
		FR0013 ²⁾	0.66	0.62				
	FR0015 ²⁾	0.57	0.67					
Eastern Europe	Latvia	LV0010 ³⁾	0.73	0.70				
	Poland	PL0005	0.74	0.76				
Southern Europe	Spain	ES0007	0.55	0.59				
		ES0008	0.42	0.69				
		ES0010	0.47	0.58				
		ES1778 ³⁾	0.67	0.81	-		-	
	Slovenia	SI08	0.83	0.82				
Eastern Mediterranean	Cyprus	CY0002	0.73	0.73				
Average			0.65	0.72	0.54		0.74	

1) Estimated based on weekly data; 2) Based on hourly data; 3) Less than 75% data coverage

The fractions of PM_{2.5} in PM₁₀ from the model correspond quite well with the observed ones at most of the sites. However, the model tends to calculate somewhat higher PM_{2.5} to PM₁₀ ratios compared to measurements. Averaged over all sites, the observed and calculated PM_{2.5} to PM₁₀ ratios are quite close, namely 0.65 and 0.72, respectively. However, there are larger geographical differences, where the measurements tend to show higher spatial variability than the model.

The mean observed ratios for Northern, Central/Western, Eastern and Southern Europe are 0.62, 0.69, 0.74 and 0.59 respectively, whereas the correspondent numbers from the model are 0.71, 0.75, 0.73 and 0.70. For Cyprus, PM_{2.5} fraction in PM₁₀ is 0.73 according to both measurements and the model. The observational and model data agree that the fine fraction of PM₁₀ accounts for a larger fraction of PM₁₀ in Eastern, Central and Western Europe, where anthropogenic emissions dominate, compared to southern Europe, where windblown dust has a large influence. Lower PM_{2.5} to PM₁₀ ratios are observed at French, British and Swedish sites located relatively close to the coast and thus influenced by sea salt aerosols. For those sites, there is a large disagreement between the model and measurements, with the model allocating a larger portion of aerosol mass to PM_{2.5} fraction compared to the observations.

3.5 Exceedances of EU limit values and WHO Air Quality Guidelines in the regional background environment in 2011

Here, PM₁₀ and PM_{2.5} concentrations calculated with the EMEP/MSW model are compared to EU critical limits and WHO recommended AQ Guidelines. The EU limit values for PM₁₀ entered in force 1.1.2005 (Council Directive 1999/30/EC) are 40 µg/m³ for the annual mean and 50 µg/m³ for the daily mean, with the daily limit not to be exceeded more than 35 times per calendar year. For annual mean PM_{2.5}, the target value of 25 µg/m³ entered into force 1.1.2010.

The WHO AQGs (WHO, 2005) are:

for PM₁₀: < 20 µg/m³ annually, 50 µg/m³ 24-hour (99th perc. or 3 days per year)

for PM_{2.5}: < 10 µg/m³ annually, 25 µg/m³ 24-hour (99th perc. or 3 days per year).

The EU PM limit values for protection of human health and WHO Air Quality Guidelines (AQGs) for PM should apply to concentrations for so-called zones, or agglomerations, in rural and urban areas, which are representative of the exposure of the general population. The EMEP model is designed to calculate regional background PM concentrations. Clearly, the rural and urban PM levels are higher than those at the background sites due to the influence of local sources. However, comparison of model calculated PM₁₀ and PM_{2.5} with EU limit values and WHO AQGs can provide an initial assessment of air quality with respect to PM pollution, flagging the regions where already the regional background PM is in excess of the critical values.

The combined model and observation maps show that the annual mean regional background PM₁₀ concentrations were below the EU limit value of 40 µg/m³ over all of Europe in 2011, with the exception of Central Asian area affected by desert dust (Figure 3.1). However, the annual mean PM₁₀ concentrations calculated by the model exceed the WHO recommended AQG of 20 µg/m³ in Benelux, parts of Central Europe, in the Po Valley (the Caucasus and Central Asia). The regional background annual mean PM_{2.5} concentrations were above EU target value and the WHO recommended AQG value in the Po Valley and Central Asia in 2011.

The maps in Figure 3.3 show the model calculated number of days exceeding 50 µg/m³ for PM₁₀ and 25 µg/m³ for PM_{2.5} in 2011. To illustrate the relative importance of man-made and natural particulates in the deterioration of air

quality, Figure 3.4 shows the correspondent exceedance maps for anthropogenic PM_{10} and $PM_{2.5}$ (i.e. excluding sea salt, windblown dust and biogenic organic aerosols).

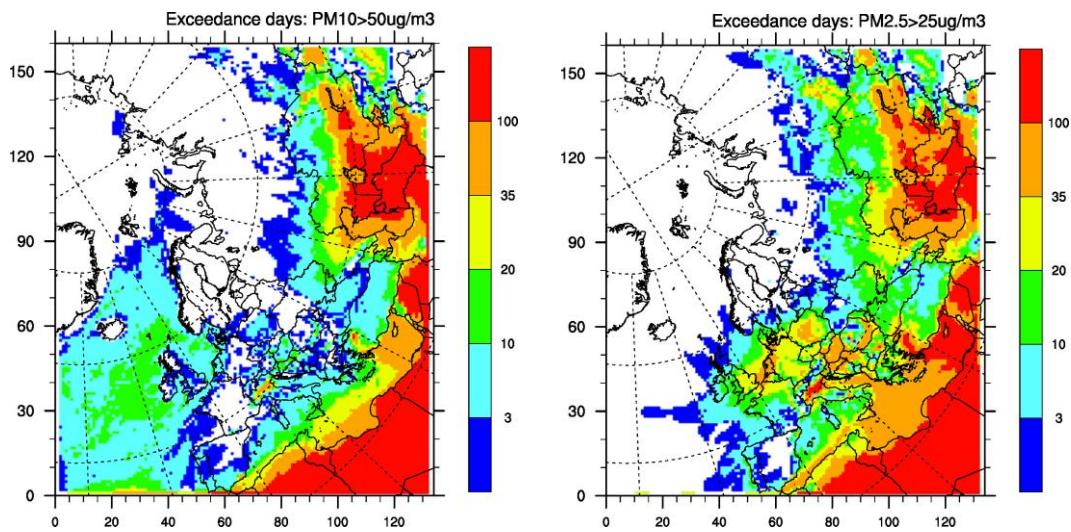


Figure 3.3: Calculated number of days exceeding the WHO AQG in 2011: PM_{10} exceeding $50 \mu\text{g}/\text{m}^3$ (left) and $PM_{2.5}$ exceeding $25 \mu\text{g}/\text{m}^3$ (right). Note: EU Directive requires that no more than 35 days exceed the limit value, while the WHO AQG recommendation is not to be exceeded more than 3 days.

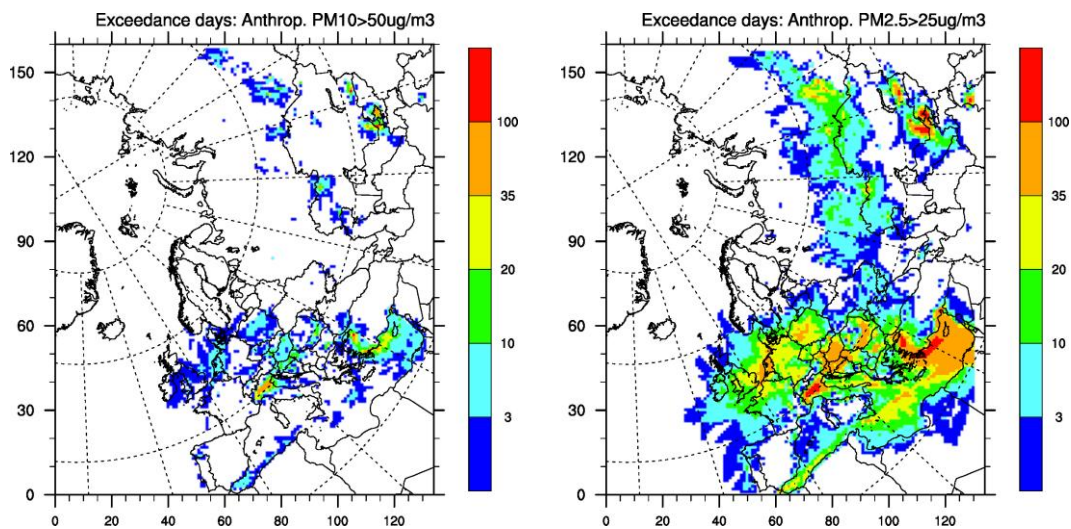


Figure 3.4: Calculated number of days exceeding the WHO AQG in 2011: same as Figure 3.3, but for anthropogenic PM_{10} (left) and anthropogenic $PM_{2.5}$ (right).

Based on the model and measurements data, a number of days with exceedances of the WHO AQGs at EMEP sites have been calculated for 2011. The observed and calculated numbers of exceedance days, as well as the number of common exceedance days, i.e. the days for which observed PM exceedances are also predicted by the model, are presented in Table 3.2.

Table 3.2: Number calculated and observed days exceeding the WHO AQGs ($50 \mu\text{g m}^{-3}$ for PM_{10} and $25 \mu\text{g m}^{-3}$ for $\text{PM}_{2.5}$) at EMEP sites in 2011

Site	PM_{10}				PM_{25}			
	Obs	Model	Common	Hit ratio,%	Obs	Model	Common	Hit ratio,%
AT0002	37	5	0	0	92	31	27	29
AT0005	0	3	0					
AT0048	1	0	0	0				
CH0001	0	2	0					
CH0002	9	1	0	0	9	2	1	11
CH0003	4	5	0	0				
CH0004	1	1	0	0				
CH0005	0	2	0		1	3	0	0
CY0002	13	31	4	31	37	85	19	51
CZ0001	1	1	0	0				
CZ0003	4	0	0	0	21	10	6	29
DE0001	15	5	1	7				
DE0002	15	0	0	0	48	26	13	27
DE0003	0	0	0		4	6	0	0
DE0007	15	0	0	0	49	23	15	31
DE0008	2	0	0	0	14	16	1	7
DE0009	17	2	0	0				
DE0044	26	0	0	0	81	33	23	28
DK0012	28	1	0	0				
ES0005	1	1	1	100				
ES0006	0	3	0					
ES0007	6	6	2	33	1	1	0	0
ES0008	3	0	0	0	3	1	0	0
ES0009					0	0	0	
ES0010	1	0	0	0	6	7	0	0
ES0011					5	2	0	0
ES0012					0	2	0	
ES0013					0	1	0	
ES0014					7	13	3	43
ES0016					6	4	1	17
ES1778	0	0	0		0	7	0	
FI0009					5	0	0	0
FI0017	2	0	0	0	3	0	0	0
FI0050	0	0	0		0	0	0	
FR0009	17	0	0	0	44	24	14	32
FR0013	4	0	0	0	26	7	3	12
FR0014	1	0	0	0				
FR0015	12	1	0	0	33	29	13	39
FR0018	0	0	0					
GB0006	0	0	0					
GB0036	5	1	1	20	22	21	11	50
GB0043	3	1	0					
GB0048	0	0	0		2	3	0	0
GR0001	5	0	0	0				
IT0001	31	2	1	3				
IT0004					94	67	30	32
LV0010	1	0	0	0	24	2	1	4
MD0013	22	1	0	0				
MK0007	0	2	0					
NL0007	25	8	3	12				
NL0009	25	8	3	12	44	37	20	45
NL0010	18	4	1	6	63	45	34	54
NL0011	34	5	4	12	29	26	19	66
NL0091	19	13	2	11	47	46	28	60
PL0005	6	0	0	0	35	10	4	11
RO0008	0	0	0					
SE0005	0	0	0		0	0	0	
SE0011	5	1	0	0	21	15	7	33
SE0012	0	0	0					
SE0014	2	3	0	0	10	10	2	20
SI0008	5	4	0	0	38	19	11	29

Hit ratio (%) shows the percentage of observed exceedance days correctly predicted by the model ($\text{common_days/obs_days} \times 100\%$). Cursive font is used for sites for which hourly measured PM concentrations were averaged to obtain daily values. Cell in grey are sites with less than 75% data coverage.

For most of the sites, where observed concentrations of PM₁₀ and PM_{2.5} exceeded the WHO recommended limits in 2011, the model also calculated exceedances. However, the model tends to under-predict the total number of exceedance days for PM₁₀ and to some smaller degree for PM_{2.5} with the exception of Cypriote site (CY02).

The “Hit ratio” in Table 3.2 shows the percentage of observed exceedance days correctly predicted by the model. The hit ratios vary substantially between the sites, ranging from 0 to 100%. More non-zero hit ratios were achieved for PM_{2.5} than for PM₁₀.

The exceedance days for the Central European sites were mainly seen in February and November. These episodes will be further discussed in Chapter 4.

3.6 Evaluation of the model performance for PM in 2011

The ability of the EMEP model to reproduce PM concentrations measured at EMEP monitoring sites in 2011 has been evaluated. The model performance has been evaluated for PM₁₀, PM_{2.5} and for individual aerosol components. The main result of this work is summarised in the current section and in the Appendix.

3.6.1 Overall statistical analysis

Table 3.3 provides a summary of annual and seasonal statistical analysis of the comparison of model results with EMEP monitoring data for 2011. Note that only measurement data obtained from 24-hourly sampling have been included in this comparison. The statistical parameters shown are the observed and modelled means, the Relative Bias, the Root Mean Square Error, the Correlation coefficient and the Index of Agreement (IOA). The IOA quantifies the degree to which the model predictions are error free and varies from 0.0 (theoretical minimum) to 1.0 (perfect agreement).

On the annual basis, calculated PM₁₀ and PM_{2.5} are respectively 17% and 13% lower than measured concentrations. The negative bias for both PM₁₀ and PM_{2.5} is larger in winter-spring (also in summer for PM₁₀), whereas for the autumn (and summer for PM_{2.5}) the model results are quite close to the observations. The model underestimation in cold months is probably related to underestimated emissions from wood burning for residential heating. The annual mean spatial correlation between calculations and measurements is 0.73 for PM₁₀ and 0.85 for PM_{2.5}.

Measured SO₄²⁻ is underestimated by 24% and NH₄⁺ by 18% on average. The model under predicts those components in all seasons, performing best during autumn. Note that calculated SO₄²⁻ is in a better agreement with SO₄²⁻ measurements corrected for sea salt. The annual mean bias for NO₃⁻ is only 3%, but the model’s seasonal performance varies significantly.

The annual mean spatial correlations are quite good, being 0.85, 0.91 and 0.75 for SO₄²⁻, NO₃⁻ and NH₄⁺ respectively. Overall correlation between daily calculated and measured concentrations for SO₄²⁻, NO₃⁻ and NH₄⁺ are 0.64, 0.67 and 0.65. Modelled sodium from sea spray is on average 37% higher than measured Na⁺

concentrations, which is a somewhat larger overestimation compared to previous years. Comparison of ECMWF_IFS wind fields shows that wind speed at 10 m height (which is driving the sea salt emissions in the model) in 2011 is higher than in 2010 over vast areas of the North Atlantic. Consequently, that resulted in greater sea spray generation by the model in 2011 compared to 2010, which appears far more efficient than in reality. This may be an indication that the sea spray source function implemented in the model is too sensitive to wind speed. Further, the rate of sea salt wet scavenging is rather uncertain, as the dry deposition rates (especially for the coarse fraction) which depend on the assumed aerosol diameter in the model. By increasing the scavenging ratio and the median aerosol diameter, the bias was reduced to only 2%. The correlation for Na^+ is, however, very good in both calculations, notably 0.92.

The parameter IOA for PM_{10} , $\text{PM}_{2.5}$ and the individual components varies between 0.73 and 0.92, which is considered to be fairly good results (Elbir, 2003).

Table 3.4 provides additional insight in the model performance with respect to secondary inorganic components in different size fractions. Note that the number of measurement sites is rather limited. The model performs rather well with respect to reproducing the observed SO_4^{2-} in both PM_{10} and $\text{PM}_{2.5}$ on annual basis, as well as for the four seasons (a slightly lower correlation was observed in spring though).

For NO_3^- , the model shows positive biases, larger for nitrate in $\text{PM}_{2.5}$ compared to PM_{10} . In particular, NO_3^- in $\text{PM}_{2.5}$ is severely overestimated in summer and autumn at all sites. This is explained by the equilibrium parameterisation of the gas/aerosol partitioning tends to calculate too efficient evaporation of ammonium nitrate aerosol at higher temperatures. Thus, too much coarse NO_3^- is formed from the ample nitric acid (at present the reaction rate solely depends on relative humidity, and not on the availability of sea salt and dust for formation of sodium nitrate and calcium nitrate). In the EMEP/MSC-W model, 27% of coarse NO_3^- is assumed to have the median diameter of 3 μm . Assuming log-normal distribution with standard deviation 2.0, we calculate that about 27% of coarse NO_3^- mass is associated with aerosols smaller than 2.5 μm in diameters. Therefore, 27% of coarse NO_3^- mass contributes to $\text{PM}_{2.5}$ mass in the model results. The correlation is fair for NO_3^- in $\text{PM}_{2.5}$, but very poor for NO_3^- in PM_{10} (for which data from only five Spanish sites were available). Among those sites, Montseny is an outlier with very low measured concentrations in all seasons, except in winter. These differences might be due to uncertainties in measurements as well as bias in the model. For Montseny, the model tends to exaggerate observed concentrations of all aerosol components; this might partly be due problems with representativity within the EMEP grid cell since this site is situated in a grid-cell adjacent to the cell hosting Barcelona city. For more robust estimate of the model performance for the SIA components, it is referred to the EMEP status report 1/2013 where a larger dataset from the EMEP network is used, including the filter pack measurements.

Table 3.3: Annual and seasonal comparison statistics between EMEP model calculated and EMEP observed concentrations of PM_{10} , $PM_{2.5}$, SO_4^{2-} , NO_3^- , NH_4^+ and Na^+ for 2011.

Period	N sites	Obs ($\mu\text{g}/\text{m}^3$)	Mod ($\mu\text{g}/\text{m}^3$)	Rel.Bias, %	RMSE	R	IOA
PM_{10}							
Annual mean	36	15.20	12.64	-17	5.32	0.67	0.73
Daily mean	36	15.27	12.63	-17	11.18	0.54	0.70
Jan-Feb	36	17.26	13.19	-24	8.68	0.62	0.59
Spring	36	17.38	13.3	-23	6.26	0.65	0.69
Summer	36	12.67	9.90	-22	5.20	0.70	0.78
Autumn	36	16.09	15.48	-4	5.70	0.69	0.77
$PM_{2.5}$							
Annual mean	33	10.84	9.48	-13	3.09	0.83	0.85
Daily mean	33	10.88	9.42	-13	8.67	0.61	0.75
Jan-Feb	33	13.93	9.52	-32	8.11	0.83	0.63
Spring	33	12.42	9.81	-21	4.28	0.76	0.78
Summer	33	8.16	7.71	-5	2.75	0.76	0.86
Autumn	33	11.20	11.81	5	2.98	0.86	0.92
SO_4^{2-}							
Annual mean	43	1.88	1.36	-27	0.75	0.85	0.84
Daily mean	43	1.89	1.36	-28	1.66	0.64	0.77
Jan-Feb	43	2.27	1.72	-24	1.00	0.81	0.84
Spring	43	1.99	1.25	-37	0.96	0.85	0.74
Summer	43	1.59	0.95	-40	0.81	0.76	0.73
Autumn	43	2.06	1.78	-13	0.75	0.84	0.90
SO_4^{2-} SScorr							
Annual mean	33	1.45	1.18	-19	0.47	0.88	0.91
Daily mean	33	1.44	1.16	-20	1.43	0.67	0.79
Jan-Feb	33	1.72	1.42	-18	0.64	0.90	0.90
Spring	33	1.58	1.13	-29	0.66	0.88	0.84
Summer	33	1.29	0.85	-34	0.63	0.77	0.79
Autumn	33	1.61	1.58	-2	0.55	0.87	0.93
NO_3^-							
Annual mean	18	2.62	2.70	3	0.76	0.91	0.92
Daily mean	18	2.66	2.74	3	2.75	0.67	0.81
Jan-Feb	18	3.56	2.63	-26	1.87	0.72	0.71
Spring	18	3.54	2.92	-17	1.41	0.94	0.85
Summer	18	1.29	1.5	16	0.45	0.93	0.95
Autumn	18	2.78	3.96	43	1.51	0.87	0.84
NH_4^+							
Annual mean	24	1.29	1.05	-18	0.48	0.75	0.81
Daily mean	24	1.30	1.06	-19	1.27	0.65	0.78
Jan-Feb	24	1.57	1.15	-27	0.83	0.75	0.73
Spring	24	1.58	1.10	-30	0.72	0.83	0.74
Summer	24	0.83	0.60	-27	0.58	0.24	0.54
Autumn	24	1.52	1.52	0	0.63	0.69	0.83
Na^+							
Annual mean	31	0.77	1.05	37	0.51	0.92	0.91
Daily mean	31	0.76	1.03	35	1.38	0.63	0.77
Jan-Feb	31	0.84	1.13	35	0.58	0.89	0.90
Spring	31	0.79	1.16	47	0.60	0.86	0.87
Summer	31	0.49	0.62	25	0.40	0.80	0.86
Autumn	31	0.77	1.11	43	0.67	0.89	0.88

Here, Ns – the number of stations, Obs – the measured mean, Mod – the calculated mean, Bias is calculated as $\Sigma(\text{Mod}-\text{Obs})/\text{Obs} \times 100$, RMSE – the Root mean Square Error= $[1/\text{Ns}\Sigma(\text{Mod}-\text{Obs})^2]^{1/2}$, R – the tempo-spatial correlation coefficient between modelled and measured daily concentrations and spatial correlation for seasonal mean concentrations. IOA= $1-\Sigma(\text{Mod}-\text{Obs})^2 / \Sigma(|\text{Mod}-\text{Obs}|+\Sigma|\text{Obs}-\text{Obs}|)^2$.

Table 3.4: Annual and seasonal comparison statistics between EMEP model calculated and EMEP observed concentrations of SO_4^{2-} , NO_3^- , NH_4^+ , EC, OC, and TC in PM_{10} and $PM_{2.5}$, for 2011. Note: only sites with daily measurements are included.

Period	N sites	Obs ($\mu\text{g}/\text{m}^3$)	Mod ($\mu\text{g}/\text{m}^3$)	Rel.Bias, %	RMSE	R	IOA
SO_4^{2-} in PM_{10}							
Annual mean	7	2.35	1.90	-19	0.68	0.50	0.61
Daily mean	7	2.35	1.75	-25	1.51	0.65	0.76
Jan-Feb	7	1.86	1.52	-18	0.74	0.74	0.80
Spring	7	2.59	1.90	-27	1.02	0.22	0.54
Summer	7	2.66	2.15	-19	0.59	0.94	0.85
Autumn	7	2.55	2.14	-16	0.78	0.47	0.59
SO_4^{2-} in $PM_{2.5}$							
Annual mean	10	2.57	2.16	-16	1.93	0.35	0.49
Daily mean	10	2.77	2.10	-24	3.94	0.41	0.53
Jan-Feb	10	2.92	2.09	-28	2.98	0.60	0.34
Spring	10	2.91	1.98	-32	2.39	0.18	0.39
Summer	10	2.45	2.14	-12	1.90	0.64	0.75
Autumn	10	2.70	2.70	0	1.87	0.56	0.66
NO_3^- in PM_{10}							
Annual mean	5	1.59	1.96	23	1.06	-0.16	0.19
Daily mean	5	1.64	1.67	1	1.74	0.49	0.68
Jan-Feb	5	2.36	1.82	-23	0.95	0.63	0.72
Spring	5	1.88	2.37	26	1.59	-0.14	0.25
Summer	5	1.26	1.67	32	0.97	-0.50	0.12
Autumn	5	1.33	2.25	69	1.41	-0.33	0.19
NO_3^- in $PM_{2.5}$							
Annual mean	10	1.70	2.51	48	1.22	0.88	0.84
Daily mean	10	2.49	2.96	19	4.73	0.48	0.65
Jan-Feb	10	3.61	2.72	-25	3.76	0.77	0.53
Spring	10	2.10	2.79	32	1.77	0.54	0.72
Summer	10	0.20	1.08	443	1.00	0.37	0.17
Autumn	10	1.67	3.86	132	2.40	0.86	0.72
NH_4^+ in $PM_{2.5}$							
Annual mean	9	1.24	1.29	4	0.77	0.48	0.56
Daily mean	9	1.76	1.44	-19	2.36	0.47	0.59
Jan-Feb	9	1.90	1.34	-29	1.71	0.75	0.48
Spring	9	1.63	1.38	-15	1.27	0.15	0.39
Summer	9	0.62	0.79	26	0.48	0.39	0.63
Autumn	9	1.22	1.79	47	0.86	0.74	0.72
EC in $PM_{2.5}$							
Annual mean	13	0.50	0.39	-22	0.38	0.50	0.61
Daily mean	13	0.77	0.43	-44	1.04	0.47	0.47
Jan-Feb	13	0.78	0.54	-31	0.78	0.50	0.49
Spring	13	0.42	0.33	-21	0.32	0.32	0.55
Summer	13	0.25	0.24	-1	0.14	0.56	0.73
Autumn	13	0.63	0.50	-20	0.45	0.56	0.64
OC in $PM_{2.5}$							
Annual mean	13	2.83	1.41	-50	1.93	0.66	0.46
Daily mean	13	3.53	1.54	-56	4.46	0.3	0.39
Jan-Feb	13	4.04	1.17	-71	4.61	0.81	0.41
Spring	13	2.71	1.31	-52	1.61	0.48	0.47
Summer	13	1.88	1.70	-10	0.61	0.48	0.65
Autumn	13	3.24	1.57	-52	2.32	0.66	0.5
TC in $PM_{2.5}$							
Annual mean	8	3.50	1.90	-46	2.50	0.64	0.44
Daily mean	8	5.34	2.31	-57	6.99	0.37	0.41
Jan-Feb	8	5.24	1.83	-65	6.19	0.77	0.41
Spring	8	3.23	1.77	-45	1.83	0.28	0.41
Summer	8	2.01	1.94	-3	0.47	0.76	0.83
Autumn	8	4.23	2.24	-47	3.11	0.63	0.49

The carbonaceous aerosols in $PM_{2.5}$ are on average underestimated by 22% with respect to EC and by 50% for OC. For both EC and OC, calculated concentrations are closer to measured values in the summer period, whereas larger underestimation during the cold period probably is due to large uncertainties in residential heating emissions, especially from residential wood burning. The same is seen for total carbon (TC), which measurements are less artefact-prone. The annual correlation is 0.50 for EC, 0.66 for OC and 0.64 for TC, showing significant seasonal variations.

3.6.2 Individual stations.

Statistical analysis of model calculated PM_{10} and $PM_{2.5}$ versus daily observations at individual sites are summarised in Tables A.1 and A.2 in the Appendix. All measurements of PM_{10} and $PM_{2.5}$ from the EMEP monitoring network in 2011, available to MSC-W by June 2013, have been made use of, including daily, hourly and weekly time resolved measurements. The hourly concentrations have been averaged to 24-hourly concentrations.

The model performance is fairly robust for most of the sites. Model calculated PM_{10} is within 30% of observed value at about 70% of the sites and within 50% at 91% of the sites on an annual basis. For $PM_{2.5}$, all but one calculated annual concentrations are within 50% of measurements and at 84% sites the calculations differ from measurements by less than 30%.

The largest positive bias between calculated PM levels and observations is for the high-mountain Jungfraujoch, for which the model largely exaggerates pollution in the cold seasons. For several of the central European sites, e.g. AT0002, CH0002, CH0003, CZ0001, CZ0003, DK0012, underestimation of annual mean PM is partly due to models failure to reproduce a pollution episode in the end-February – beginning of March period (see Chapter 4).

The correlation (in r^2) between calculated and measured PM_{10} and $PM_{2.5}$ ranges mostly between 0.4 and 0.7 for the individual sites, with correlation coefficients below 0.45 being mostly for elevated sites.

4 A closer look at episodes of high PM₁₀ concentration in Central Europe

4.1 EMEP observations and model

By Svetlana Tyro and Wenche Aas

Observational data shows that in Central Europe, most of the days with exceedances of the PM₁₀ EU limit value in 2011 occurred during two periods with enhanced pollution levels, notably in February and November. Quite often, pollution periods are associated with stagnant meteorological conditions, which suppressed the dispersion of local pollution and favour the accumulation of regional scale pollution. The November 2011 pollution episode is documented in Pfeffer et al. (2013) and presented in chapter 4.2 in the present report, where concurrent measurements of PM₁₀ and levoglucosan demonstrated that residential wood burning contributed substantially to the elevated PM₁₀ levels due to unfavourable meteorology in North Rhine-Westphalia (NRW).

The elevated levels of PM air pollution in the NRW region was part of a regional scale air pollution episode, as seen from time-series of PM and PM species at sites in Germany, the Czech Republic, Switzerland, Austria, Poland, Holland and Denmark. The EMEP/MSC-W model manages quite well to reproduce the November pollution period, whereas it is not so successful in calculating that for February 2011 (see examples for PM₁₀ in Figure 4.1). Here, we take a closer look at these two periods from monitoring and modelling perspective, trying to understand the reasons for discrepancies which can have implications for models capability to predict PM exceedances.

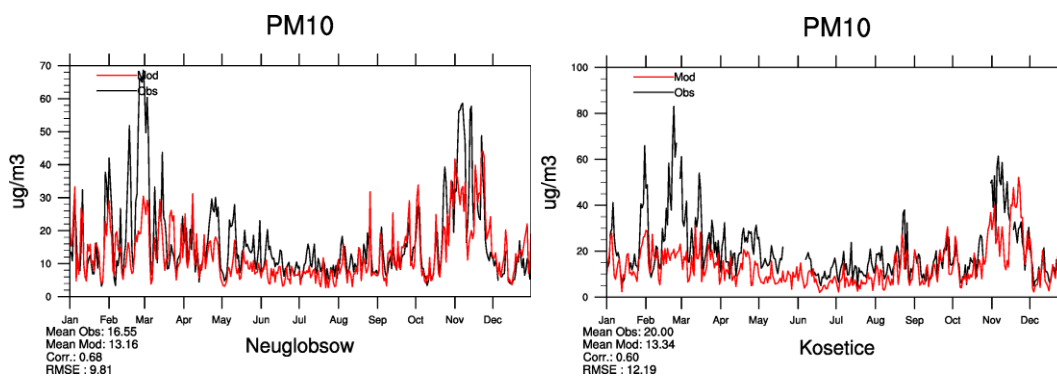


Figure 4.1: Measured and calculated daily time-series of PM₁₀ at Neuglobsow (DE0007) and Košetice (CZ0003) in 2011.

Figure 4.3 shows averaged meteorological fields of mixing height and wind speed at 10-m height for the time period 1-20 November 2011, taken from the ECWMF-IFS model which drives the pollution calculations with the EMEP/MSC-W model. During the actual period, a vast area in the Central Europe was characterized by a shallow boundary layer with low wind speeds and turbulent mixing, causing stagnant air mass. Relatively cold weather was likely to cause extensive wood

burning in stoves and fireplaces for residential heating, similar to that documented in Pfeffer et al. (2013).

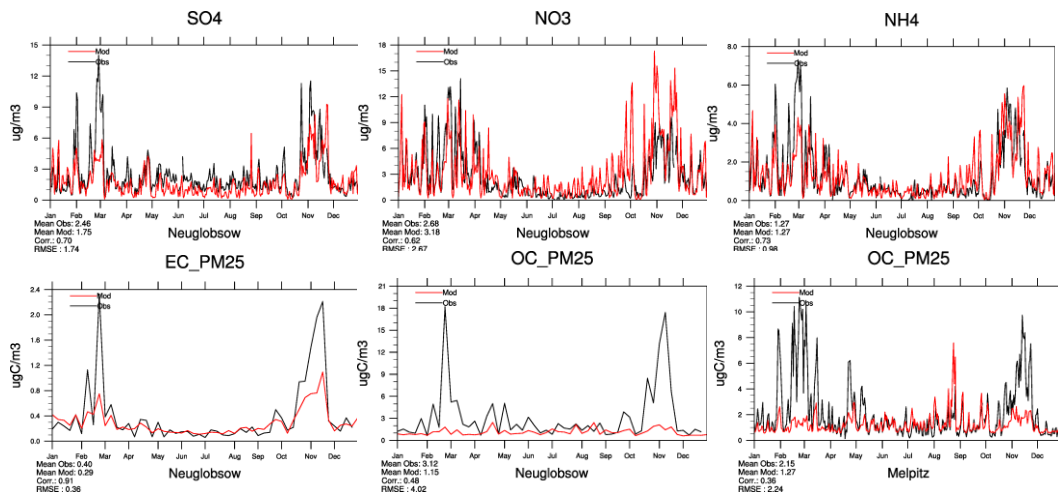


Figure 4.2: Measured and calculated time-series at Neuglobsow (DE0007) in 2011: sulphate, nitrate and ammonium (daily), elemental and organic carbon (plotted as weekly series due to measurements' time resolution). Also shown is OC time-series at Melpitz (DE0044).

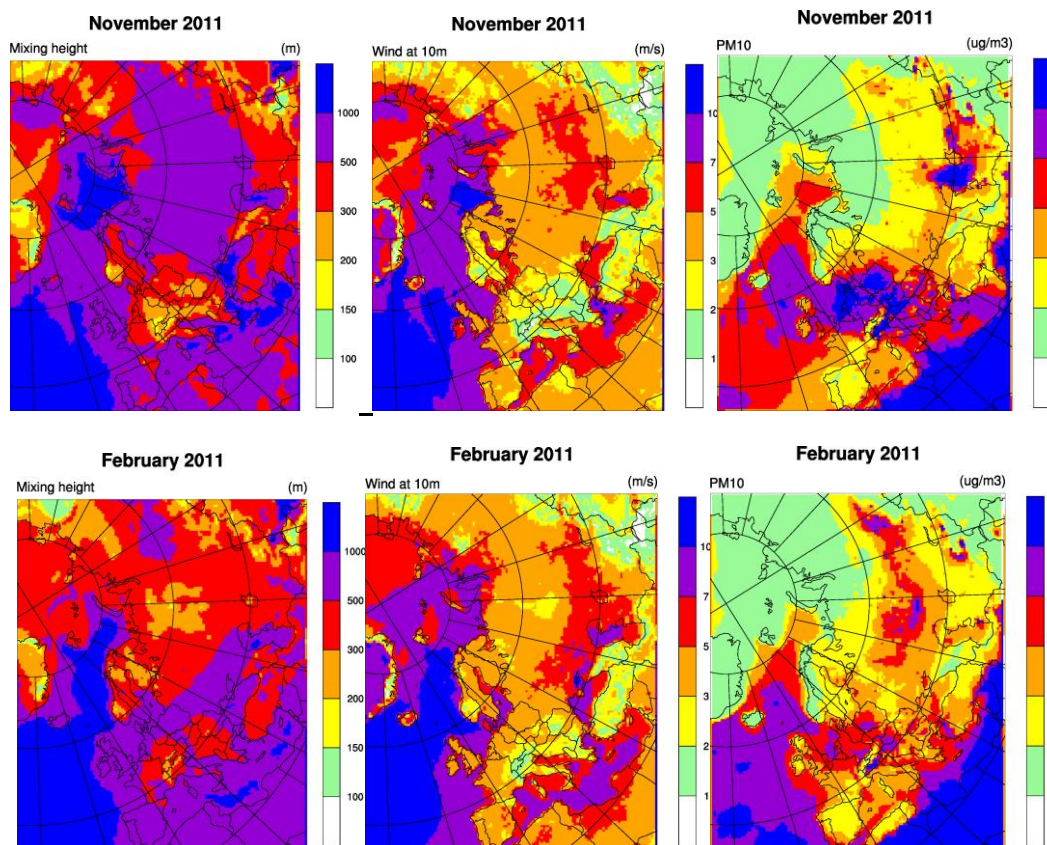


Figure 4.3: Average fields of mixing height (left) and 10-m wind speed (middle), input to the EMEP/MSC-W model, and calculated PM_{10} concentrations (right) for November and February 2011.

For the actual period, the model calculates enhanced levels of PM (Figure 4.1 and Figure 4.3) resulting from increased concentrations of both secondary (regional pollution) and primary particulate matter. As shown in Figure 4.2, the calculated levels of all SIA components (especially NO_3^-) are all very high at DE0007. The levels of calculated EC are also enhanced, though they are not as high as seen for the observations. Modelled concentrations of OC did not deviate from that of the average level. This finding strongly suggests that wood burning emissions are severely underestimated. It should be pointed out that the model tries to account for the air temperature when making temporal profiles of emissions from residential and commercial combustion (SNAP2) (the reported annual total SNAP-2 emissions are, however, conserved).

It should also be noted that the model predict the major episode to start about 7-10 days later than that observed. This is particularly pronounced in western parts of Central Europe. This is because the most stable conditions in the very shallow boundary layer (mixing heights less than 150 m) occurred there after 10-15 November, as calculated with the ECMWF model.

In February, the meteorological situation according to ECMWF-IFS calculations was far from being as stagnant as in November. Driven by the ECMWF-IFS meteorological fields, the EMEP/MSC-W model calculates somewhat elevated pollution levels in Central Europe, but the calculated concentrations of PM_{10} did not exceed the limit value, as shown by the observations (Figure 4.3, low right map). Figure 4.4 and Figure 4.5 show the daily averages of PM_{10} for measurements and model for the central European sites which do experience the high episodes in February and November.

In the spring episode, the measurements show that PM_{10} daily concentrations exceeded $50 \mu\text{g}/\text{m}^3$ on between four (DE01) to twenty (AT02) days above $50 \mu\text{g}/\text{m}^3$. In other words, during this period alone the WHO recommended AQG of less than 3 days of PM_{10} above $50 \mu\text{g}/\text{m}^3$ per year was already breached. The model does not manage to produce these high levels as discussed above, no exceedance days are recorded for the calculated results. In the November period, the model manage to reproduce the episode better and exceedance days are seen at two of the sites (DK12 and AT02). For the measured daily mean there are four (DE02) to twelve (AT02) days above $50 \mu\text{g}/\text{m}^3$. These two periods contributes to most of the exceedance days for the whole year for these seven selected sites. On average 80% of the exceedance days shown in Table 3.2 in Chapter 3 are from these periods.

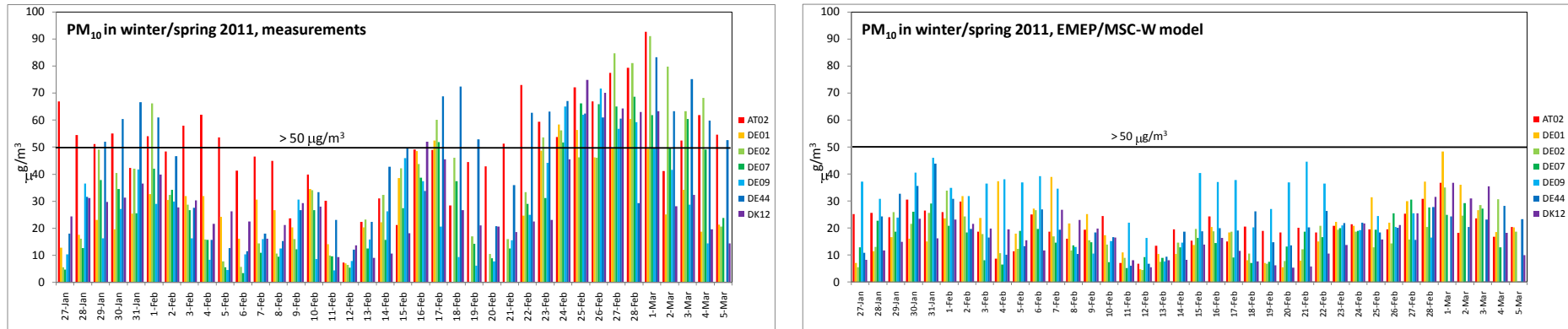


Figure 4.4: Measured (left) and calculated (right) of the daily PM₁₀ averages at selected sites for the period 27 Jan. – 5 March 2011. Solid black line indicates which days exceed the limit value of 50 µg/m³.

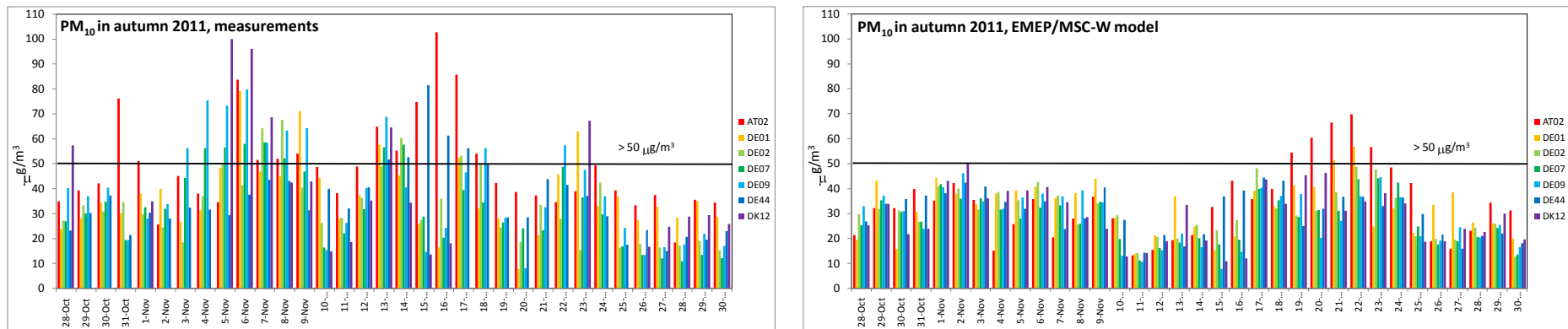


Figure 4.5: Measured (left) and calculated (right) of the daily PM₁₀ averages at selected sites for the period 28 Oct. - 20 Nov. 2011. Solid black line indicates which days exceed the limit value of 50 µg/m³.

Summarizing, in several sites in Central Europe the number of days with PM₁₀ exceedance of 50 µg/m³ were the greatest in 2011 compared to at least 5 years before. On average 80% of the exceedance days took place during two pollution episodes caused by unfavorable meteorological situation and probably enhanced local emissions from residential heating in February and November 2011. Model investigation of those episodes shows that accurate meteorological input (presently from the ECMWF model) is a prerequisite for successful prediction of the occurrence of pollution episodes by the EMEP/MSC-W model. Furthermore, in order to correctly represent the pollution levels and the exceedances of limit values, good quality emission data is crucial. Particularly, information on local emissions becomes very important during stagnant meteorological conditions.

4.2 High PM₁₀-episodes in Germany in November 2011

By Tanja Schuck, Ulrich Pfeffer, Ludger Breuer, Dorothee Adolfs

In November 2011, elevated PM₁₀-concentrations was observed in Germany for a prolonged time period. The actual period started November 2 in the northeastern part of Germany, from where high PM₁₀ concentrations spread southwards, and persisted until November 24 (Umweltbundesamt, 2012). During this period, the weather conditions over Germany were influenced by a high pressure system causing a stable inversion and low boundary layer heights. Vertical transport of air was suppressed and air pollutants accumulated in the boundary layer. This led to daily averages of the PM₁₀ concentration above the European limit value of 50 µg/m³.

Two distinct PM₁₀-episodes occurred in Germany, November 3 through 9 and November 12 through 24. In the state of North Rhine-Westphalia, actually three episodes could be distinguished: Nov. 6-10, Nov. 14-17, and Nov. 20-24. Figure 4.6 (top) shows PM₁₀ concentrations measured in November 2011 for selected stations of the state's air quality monitoring network LUQS (Landesamt für Natur, Umwelt und Verbraucherschutz NRW, 2007). For the majority of stations, represented by grey symbols, the three periods of elevated PM₁₀ concentrations, often above 50 µg/m³, are apparent. Also PM_{2,5} concentrations were elevated during these episodes (not shown).

One station, marked by red symbols, stands out by showing lower PM₁₀ concentrations. This is the station EIFE, located at 6.28 E, 50.65 N, at an altitude of 572 m in a rural and forested area, outside a small town. For comparison, a second rural background station BORG, is highlighted by blue symbols. This station is situated at 6.87 E, 51.86 N, at an altitude of only 45 m. During the PM₁₀ episodes, boundary layer heights derived from soundings were low, often less than 500 m. In consequence, station EIFE was frequently outside the boundary layer and “missed” the high PM₁₀ concentrations, while the second background station BORG was inside the boundary layer, experiencing as high concentrations as stations influenced by industry or traffic.

For a more detailed analysis of different sources contributing to the elevated PM₁₀ concentrations, several anhydrosugars, products of combustion of cellulose containing biofuels, e.g. wood, were measured at 25 stations of the LUQS network (Pfeffer et al., 2013). Of these, in particular levoglucosan is a common

tracer for wood burning (Puxbaum et al., 2007; Piazzalunga et al., 2011; Maenhaut et al., 2012; Schmidl et al., 2008; Schmidl et al., 2011). Figure 4.6 (middle panel) shows the levoglucosan concentration, Figure 4.6 (bottom) depicts its mass contribution to PM_{10} . Both quantities are enhanced during the PM_{10} episodes. Three high concentrations episodes are distinguishable, with the highest levels occurring from November 20-23. The higher share of levoglucosan in PM_{10} indicates an increased contribution of wood burning emissions to the total PM_{10} burden. Following a temperature decrease on November 6, ambient temperatures ranged between 1°C and 10°C. Thus, while the dispersion of pollutants was suppressed by the inversion, increased emissions from domestic heating occurred due to the lower temperatures, enhancing the adverse effect of the meteorological conditions.

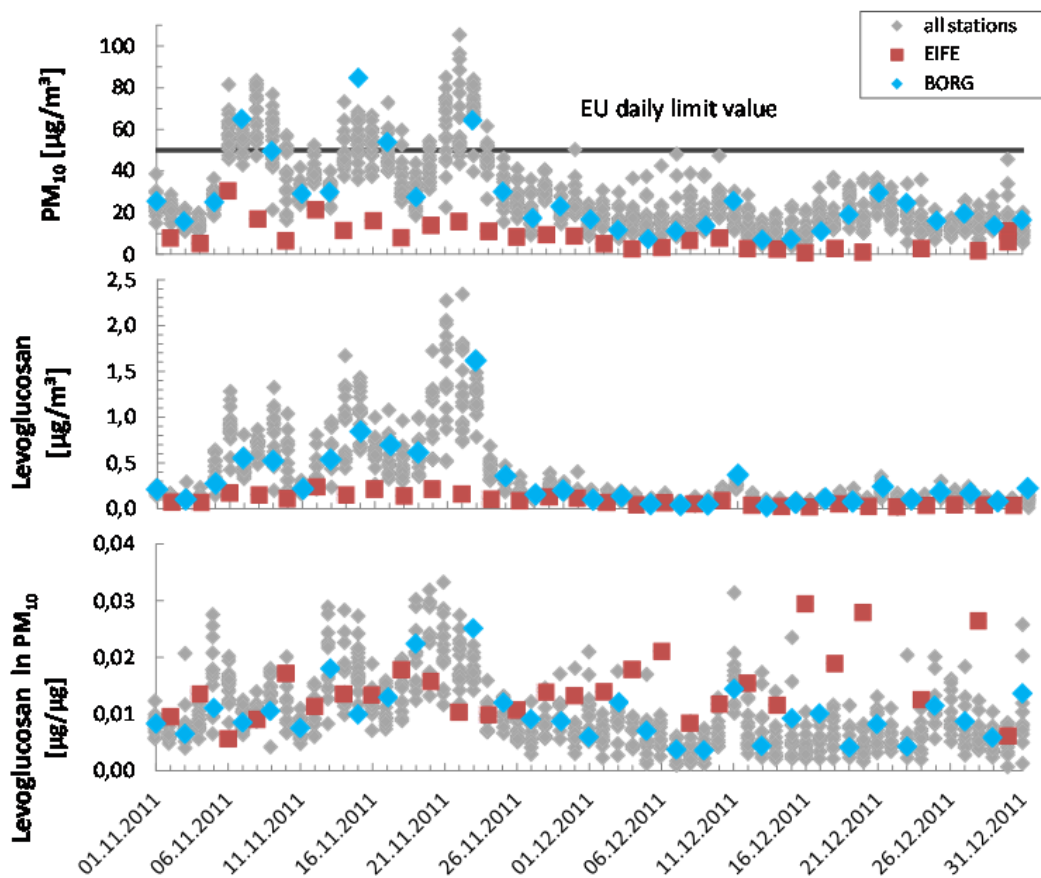


Figure 4.6: Measurements at selected stations of the air quality monitoring network LUQS in NRW in November and December 2011. Top: PM_{10} concentrations, middle: levoglucosan concentration, bottom: mass contribution of levoglucosan to PM_{10} .

At EIFE lower concentrations were measured, but also at this site PM_{10} and levoglucosan time series correlate. The relative share of levoglucosan in PM_{10} , however, shows a different behavior. During the PM_{10} episodes, values at EIFE are comparable to those at other sites with a monthly average of 0.011 $\mu\text{g}/\mu\text{g}$ (0.013 $\mu\text{g}/\mu\text{g}$ for all stations). But at EIFE, the ratio of levoglucosan mass to PM_{10} remains high, even after the PM_{10} episode ended on November 24, although pronounced day-to-day variations occur. Maximum values are observed at the end

of December when absolute levels of both, levoglucosan and PM_{10} were moderate. Owing to its altitude, EIFE is less affected by the inversion, but, related to the absence of other major sources, the contribution of wood burning to the PM_{10} concentration is often higher at this site, as wood combustion for domestic heating purposes is common in the Eifel region. E.g. in December, when no PM_{10} episode took place, the monthly mean mass ratio of levoglucosan to PM_{10} was $0.017 \mu\text{g}/\mu\text{g}$ at EIFE, which is relatively high compared to that of other stations ($0.007 \mu\text{g}/\mu\text{g}$).

In a more detailed analysis, levoglucosan has been used to quantify the influence of wood burning on the number of days on which the EU daily limit of $50 \mu\text{g}/\text{m}^3$ was exceeded in North Rhine Westphalia (Pfeffer et al., 2013). It was found that wood burning may cause up to 10-13 exceedance days for individual sites, and on some days up to 40 % of the PM_{10} burden may be related to wood burning. During the third phase of the November PM_{10} episode, 10 to $30 \mu\text{g}/\text{m}^3$ of PM_{10} were estimated to originate from wood burning. While this is certainly to some extent due to local sources, also long-range transport from other regions may contribute. Since wood burning has become more and more popular for domestic heating over the last decade, PM_{10} emissions from single stoves operated in households have become a concern.

5 Time series of PM₁₀ and PM_{2.5} and their chemical composition

By Svetlana Tsyro, Wenche Aas

5.1 Time series of PM₁₀ and PM_{2.5}

The longest time series of PM data reported to EMEP goes back to 1996-1997; i.e. for four Swiss sites, one Czech and one British. Significant inter-annual variations in the PM concentrations are observed, of which those associated with the peak in 2003 is the most pronounced (Figure 5.1). However, despite large inter-annual variations, there is a relatively clear general decrease in the observed mass concentration in Europe the last decade (Tørseth et al., 2012; Barmpadimos et al., 2012). Trend analysis, using the Mann Kendall test, of PM₁₀ mass measurements from sixteen sites, with measurements from 2000 to 2011 show an average decrease of 18% ±13%, which corresponds to an annual loss in average mass of 0.29 µg/m³ pr year. 56% of the sites show a significant decrease, non with significant increase. Similar numbers are observed for PM_{2.5}; an average decrease of 26 ±16%, at 13 sites with measurements from 2000 or 2001. 46% of the sites have a significant downward trend, non with positive trend. The downward tendency in the observed annual mean concentration of PM, corresponds to a rather broad reduction in the emissions of primary PM and secondary PM precursors in Europe in the actual period (Tørseth et al., 2012; Barmpadimos et al., 2012).

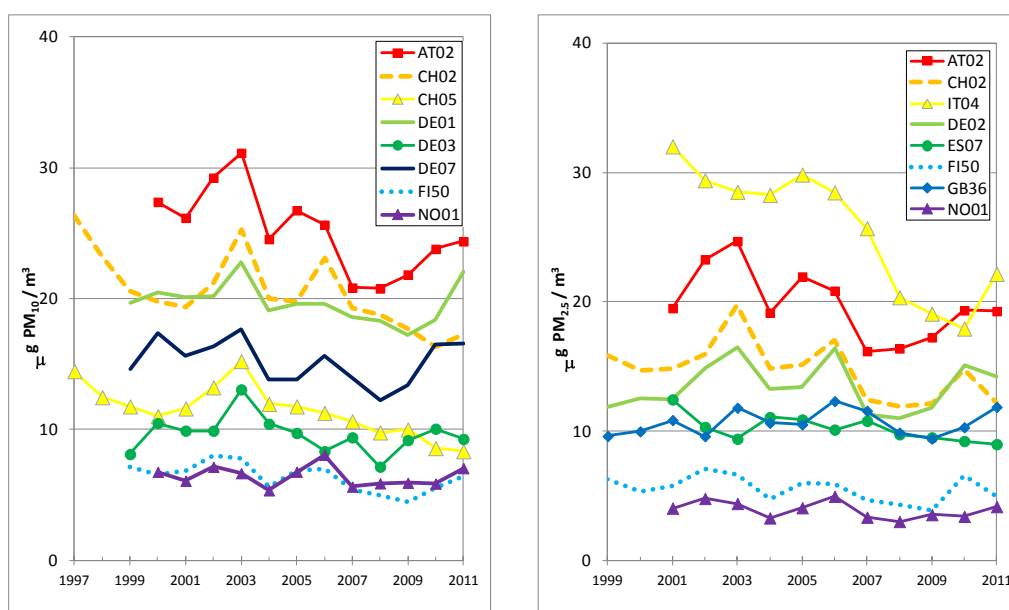


Figure 5.1: Time series from 1997 (1999) to 2011 of PM₁₀ (left) and PM_{2.5} (right) at selected EMEP sites.

Figure 5.2 shows model calculated and observed 12-year trends of annual mean PM₁₀ and PM_{2.5} concentrations in the period 2000-2011. The calculated trends have been obtained using the same EMEP/MSC-W model version (rv. 4.4), driven

with ECMWF-IFS meteorology, and emission trend data prepared by CEIP in 2012.

Shown are both trend plots, for the sites with measurements in all of these twelve years (left panels) and for all EMEP sites with PM measurements (right panels). The sites with at least 75% data coverage for each of the years are included. The consistent 12-year trends are based on eleven sites for PM_{10} and only two sites (DE0002 and DE0003) for $PM_{2.5}$. Those PM_{10} sites are located in Germany, Switzerland and Austria and thus the trends are representative for Central Europe. For those sites, a slight downward trend in annual mean PM_{10} and $PM_{2.5}$ levels from 2000 to 2011 is seen in observational and model data. When all sites with PM measurements are included, the trends get disturbed by the inconsistency in data sets due to inter-annual changes in the number and suit of sites (see Figure 5.2, lower panels), in particular in the beginning of the period (and in the end for PM_{10}).

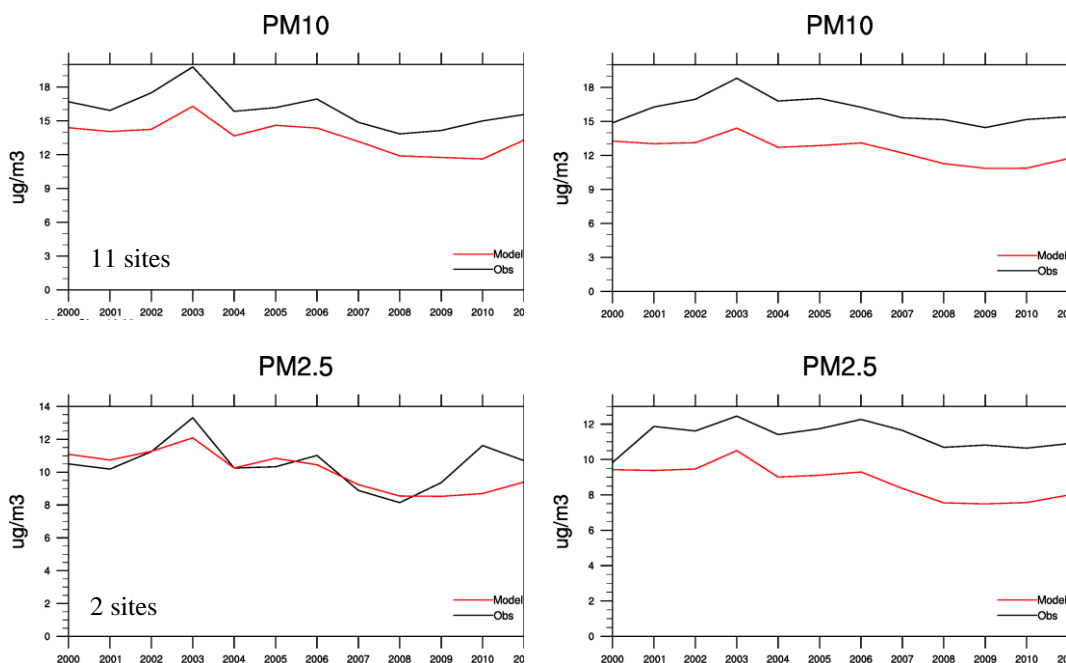


Figure 5.2: Calculated and observed 12-year time series in annual mean PM_{10} and $PM_{2.5}$ concentrations from 2000 to 2011: left – only for the EMEP sites with measurements during the whole 12-year period; right – all EMEP sites with PM measurements.

In both observational and model data, elevated PM levels occurred in 2003 due to unfavourable meteorological situation, namely the heat wave in Europe in summer 2003. Somewhat smaller PM peak is seen for 2006. If we zoom in at the period 2005-2011 (Figure 5.3), for which continuous observations at more sites are available, we find a very good agreement between modelled and observed PM trends (with the model underestimating by 18-20% the measured PM). For both PM_{10} and $PM_{2.5}$, the mean concentrations drop from 2006 to 2008-09 and then somewhat increase to 2010-11.

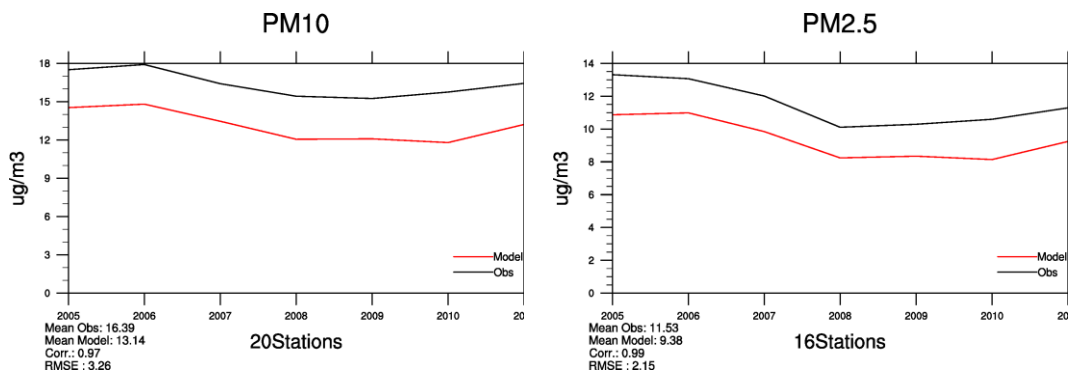


Figure 5.3: Calculated and observed 7-year time series in annual mean PM_{10} and $PM_{2.5}$ concentrations (only EMEP sites with measurements during the whole period from 2005 to 2011 are included).

Figure 5.4 summarises evaluation of model performance in terms of bias (upper panel) and spatial correlation (middle panel) for PM_{10} and $PM_{2.5}$ for the considered 12-year period. The performance of the latest model version rv.4.4 is also compared with performance with earlier model versions used for reporting for the correspondent years (for which the statistics are taken from EMEP Status Reports 4/2002 – 4/2012). The lower panel provides information on the number of sites with PM_{10} and $PM_{2.5}$ measurements for each of the year, available for model verification at present (2012 update, denoted “Ns_new”) and previously (“Ns_old”). Note that the number of PM measurement sites varies from year to year and that it is different in the old and new dataset.

The statistic plots convincingly show quite a significant improvement in model performance the last decade. Especially, the model has become much better in reproducing observed levels of PM_{10} and $PM_{2.5}$. Also the model’s ability to calculate PM spatial distribution over Europe has increased. These achievements are due to improvements in both the model formulations, emission inventories and meteorological input.

The other important conclusion from Figure 5.4 is that the model version used for 2000-2011 trend runs shows quite robust performance in the whole period. Some decrease in the model accuracy is seen in 2008 associated with model’s large under-prediction for two new Latvian sites. However for later years, the model accuracy for those sites improved. This can be partly due to still significant uncertainties in East European emission data, but could also be due to a variable quality of measurement data. Measured mean PM_{10} was rather high in 2008, namely 21.5 and 25.9 $\mu\text{g}/\text{m}^3$ respectively at LV0016 and LV0010, whereas the correspondent values were 16.8 and 18.8 $\mu\text{g}/\text{m}^3$ in 2009, 15.8 and 14.6 $\mu\text{g}/\text{m}^3$ in 2010, and 14.4 $\mu\text{g}/\text{m}^3$ at LV0010 in 2011. In summary, the overall results strengthen our confidence in the model’s ability to reproduce regional PM levels with quite good accuracy in variable meteorological conditions and chemical regimes.

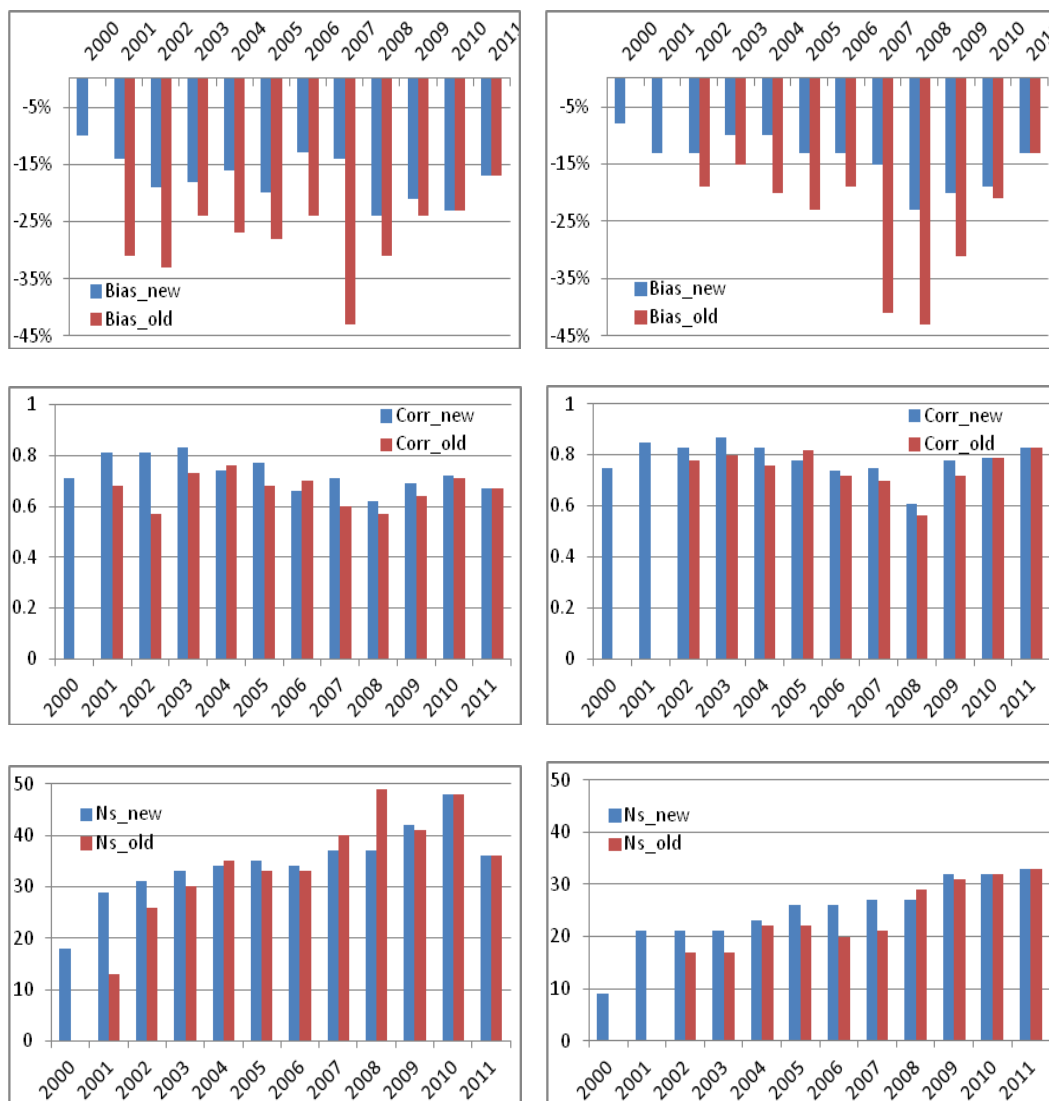


Figure 5.4: Evaluation of model performance with observations for PM_{10} (left) and $PM_{2.5}$ (right) for the 12-year period: yearly mean model bias (upper panels), spatial correlation (middle panels) and the number of measurement sites (lower panels). Blue – the latest model version rv4.4 (or the number of measurement sites presently available); red – earlier model versions (or measurement site number) used for earlier EMEP reporting (see EMEP Status Reports 4/2002 to 4/2012).

5.2 Time series in chemical composition

In addition to trends in the concentrations of PM_{10} and $PM_{2.5}$, it is interesting to see whether and how their chemical composition changed during those 12 years. There are relatively few EMEP sites with concurrent chemical composition measurements of secondary inorganic (SIA), carbonaceous matter (EC/OC), mineral dust in addition to mass measurements. However there are long term measurements of nitrogen and sulphur components which show a significant decrease the last decades (Tørseth et al., 2012). From 2000 to 2009 it has been a reduction in the observed sulphate and ammonium in air of about 10%. No

significant reductions were seen for this period for nitrate in air (Tørseth et al., 2012). These extended SIA measurements together with the EMEP model are included in the EMEP Status Report 1/2013 where trends in main components are also discussed (EMEP, 2013).

In this work, four sites with measurements of SIA and carbonaceous matter (EC/OC) in PM₁₀ and PM_{2.5} for the last decade have been selected for this analysis: Birkenes (NO0001/NO0002), Melpitz (DE0044), Ispra (IT0004) and Montseny (ES1778). The calculated annual mean from each data set were used when there was a sufficient data coverage throughout the year, however it was not taken into account common days of the various measurements since the sampling period differed sometimes (i.e. daily and weekly), and it was assumed that the annual average is representative for the year. This is a bit problematic, especially for ES1778 where the data coverage is about 25% with a sampling frequency of 2-3 days per week, and not necessarily the same days for the different components.

For Birkenes, the filterpack measurements were used to estimate the SIA composition in PM₁₀. There are not regular monitoring of inorganic ions in the fine fraction at this site, and the fine/course fraction measured at campaigns have been used to estimate the contribution in fine fraction for the whole period. At Melpitz total carbon is shown since the split between EC/OC is biased for the first periods when a non reference method was used. The observed OC are multiplied with a factor 1.7 to estimate the organic matter (OM) for all sites, except Ispra where a factor of 1.4 were used, due to the possibly less aged organic at this site. The observed EC was multiplied with a factor 1.1. Only Montseny has regular measurements of mineral dust components. To estimate the total dust fraction at this site, the measurements of Al, Ca and Mg was used, and Al was multiplied with a factor 5.67, Ca with 1.5 and Mg 2.5 (Querol et al, 2001; Van Loy et al., 2000). For the other sites with only Ca measurements a factor 8 is chosen in accordance to what is used in the EURODELTA III exercise (Bertrand Bessagnet, pers. comm.), this is an average value for dust from “local” soils (Guinot et al., 2007) and from desert areas (Putaud et al., 2004).

Figure 5.5 shows trends in the relative contribution of sulphate, total inorganic nitrogen (NO₃+NH₄) and total carbonaceous matter (OM + EC corrected) to PM₁₀ and PM_{2.5} for both measured and calculated estimates. Modelled values are shown for the whole periods (2000-2011), while measured for those years with sufficient data coverage. Even though there are some biases in the absolute value of the relative contribution between the two methods for some sites, the trends seems to follow each other, especially for sulphate. Figure 5.5 shows quite clearly that the relative contribution of sulphate has decreased in both size fractions and in both modelled and measured estimates. Using Mann Kendall test, there are statistically significant decrease at three sites for the modelled estimates and one site for measurements. The average decrease all four sites considered has been 0.3 µgSO₄/year for the modelled estimates, and 0.4 µgSO₄/year for the measurements. For total nitrogen, the relative contributions to neither PM₁₀ nor PM_{2.5} seem to have changed. There is no significant trend at any of the sites, and the average change is small, the exception is for nitrogen in the fine fraction at ES1778, which seems to have decreased. For the total carbonate the picture is

more scattered. The model shows a significant increase in the relative contribution at three of the sites, while for the measurements it was a significant increase at two sites and decrease at one site. One should notice the high uncertainties in both the measured and calculated estimates of the carbonaceous fraction and it is not possible to say anything conclusive on changes in this component.

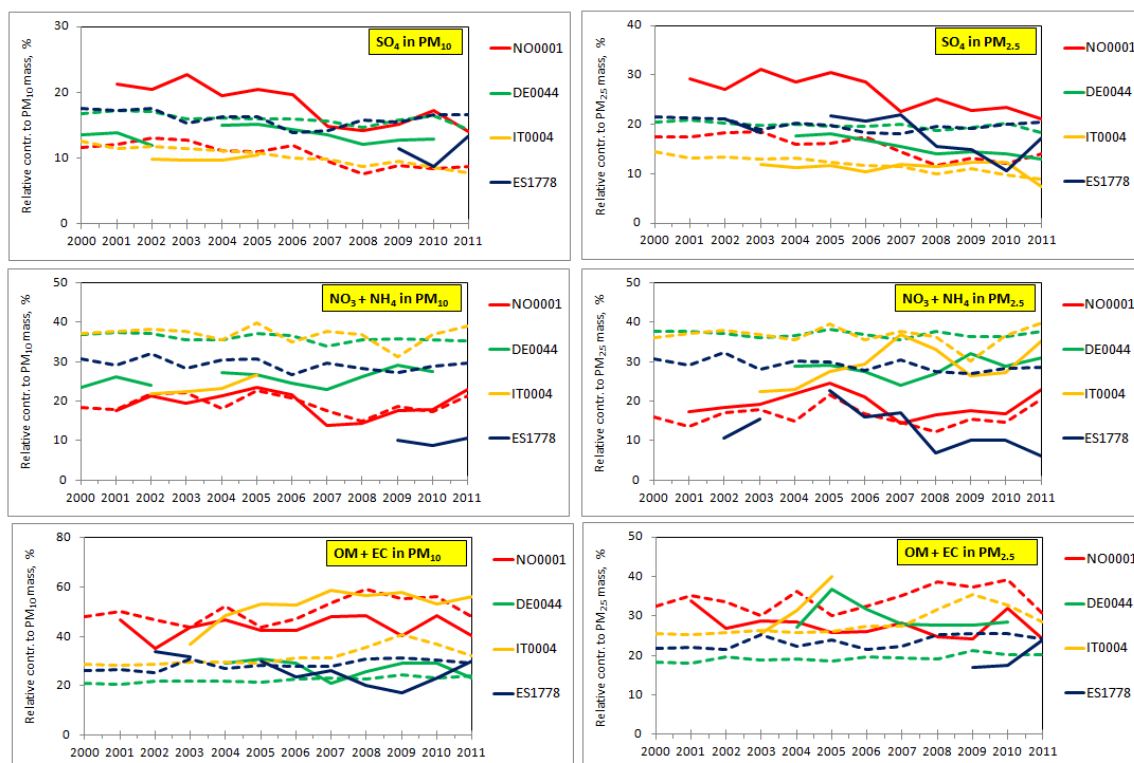


Figure 5.5: Time series in relative contribution of sulphate, nitrogen components and carbonaceous matter in PM_{10} and $PM_{2.5}$ at selected EMEP sites, 2000-2011. Solid lines are measured concentrations while dotted lines are modelled.

The chemical composition has been averages for three three-years time periods and shown in Figure 5.6. For those periods where there has not been measurements for all three years, either two or one year period is used, which is indicated in the figure. For some periods there are no measurements and only modelled estimates are given. Non-determined mass (ND) is for the measurements the difference between the measured mass and the sum of the components measured, while for the model, ND is calculated water. The chemical composition in measurements and model resembles each other quite well. It seems like the modelled manage to reproduce to measured estimates at Birkenes (NO01) the best. A slight underestimation is seen. At Montseny it is a bit more scattered, highest bias for nitrate which is much higher in the modelled than in the measurements in both size fractions.

For Montseny, the model tends to exaggerate observed concentrations of aerosols. On the EMEP grid, Montseny is situated in a grid-cell adjacent to the cell hosting Barcelona city. Thus, the Montseny-cell appears to be heavily affected by

Barcelona's pollution in model calculations. This is especially true for secondary pollutants, such as SO_4 , NO_3 and NH_4 , which concentrations at Montseny are in fact even higher than those in the neighbouring Barcelona-cell. Further information on the station location and local specifics of pollution dispersion would be useful for understanding the model results.

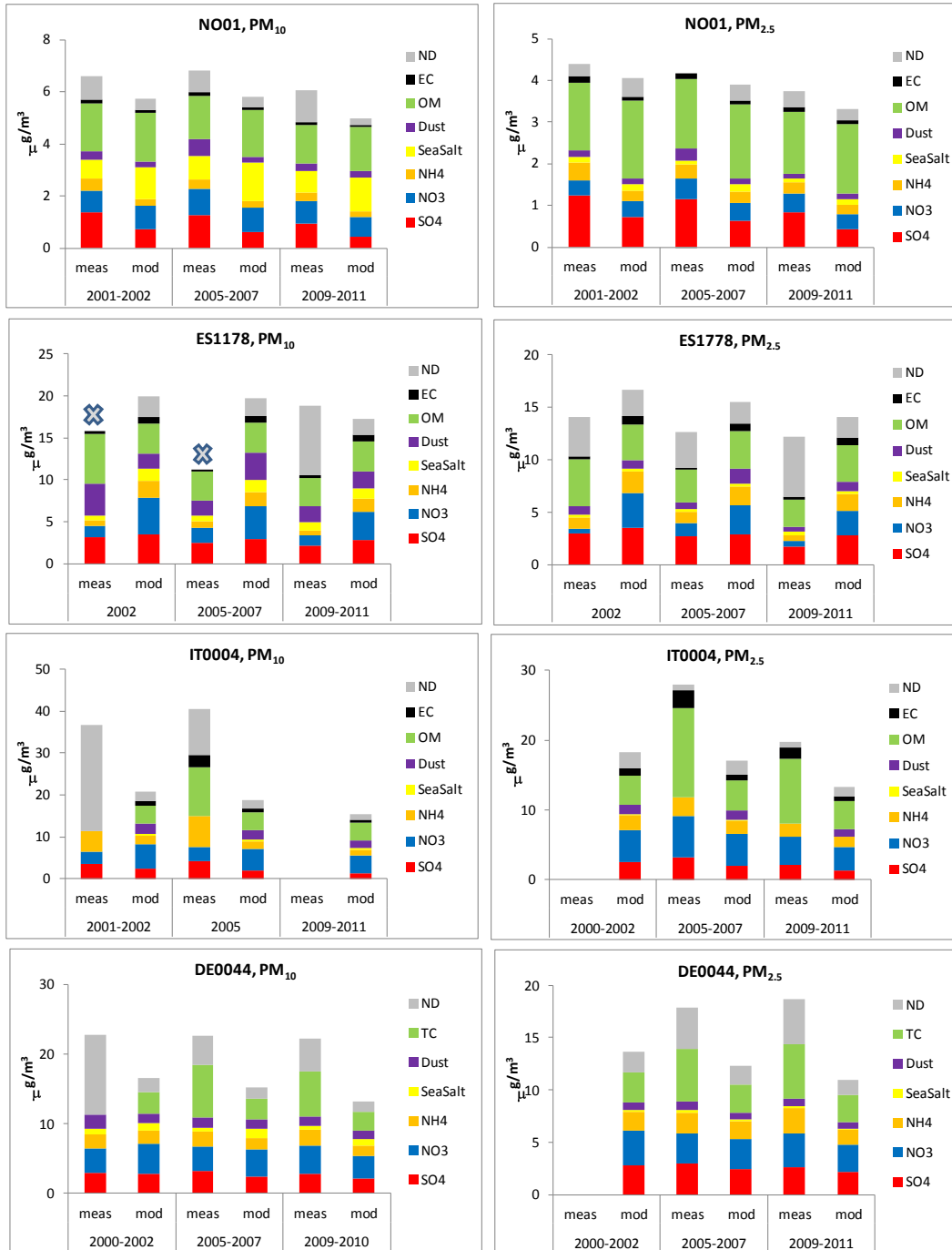


Figure 5.6: Chemical composition in PM_{10} and $\text{PM}_{2.5}$ for the average three year periods (or less if no data). X at ES1178 for two of the periods indicate that PM_{10} mass was not determined.

For Ispra, there is a problem with the carbonaceous fraction, which is very high at this site and the model underestimate this, this can partly be explained by an underestimation of residential wood burning sources (Aas et al., 2012). At Melpitz (DE44), the general pattern correlates well between model and measurements, but the model underestimate the mass significantly. This can be attributed to all species, but most significant for the carbonaceous fraction.

6 The EMEP intensive measurement period in summer 2012 – Mineral dust and trace metals in PM₁₀

By Andres Alastuey, Xavier Querol, Franco Lucarelli, Wenche Aas, Noemí Pérez, Teresa Moreno, Hans Areskou, Violeta Balan, Fabrizia Cavalli, John N. Cape, Maria Catrambone, Darius Ceburnis, Sebastien Conil, Lusine Gevorgyan, Jean Luc Jaffrezo, Christoph Hueglin, Nikos Mihalopoulos, Marta Mitosinkova, Jean-Phillippe Putaud, Véronique Riffault, Karine Sellegri, Gerald Spindler

6.1 Introduction

The EMEP task force of measurement and modelling (TFMM) periodically arrange Intensive Monitoring Periods (IMP) (Aas et al., 2012). The third EMEP IMP took place during the periods 8 June to 12 July in 2012 and 11 January to 8 February in 2013 and was arranged in cooperation with the EU funded projects ACTRIS, ChArMEx and PEGASOS. One of the major aims was to establish the chemical speciation of the PM₁₀ size fraction, focusing particular on the mineral dust and trace metal content.

On a global scale, mineral matter along with sea salt aerosol is the major component of the total PM mass present in the atmosphere (IPCC, 2007), arising mainly from natural sources, such as the transport of dust from arid regions. At a local/regional scale, resuspension of dust from natural sources and anthropogenic dust emissions (by road dust resuspension, demolition/construction activities, etc.) may be important as well.

The composition of mineral dust originating from natural sources at a given site depends on the geology of the source region of the emission. For Europe, and the Mediterranean region in particular, the proximity to the North African deserts is obviously decisive for the composition as well as for the concentration observed (Bergametti et al., 1989; Rodríguez et al., 2001; Escudero et al., 2007; Kallos et al., 2006; Mitsakou et al., 2008; Querol et al., 2009; Pey et al., 2013). Dust transport episodes are frequently observed in European countries and are consistently reported as exceedances of PM limit values caused by natural sources, but these are not considered as violation of the current legislation (EU, 2008).

A number of studies have been conducted concerning the content and speciation of mineral matter in PM in Europe (e.g.: Querol et al., 2001; Moreno et al., 2006; Calzolari et al., 2008; Lucarelli et al., 2011; Alemón et al., 2004; Putaud et al., 2010). However, different sampling techniques and analytical methodologies have hampered the possibility to compare these data.

During the present EMEP IMP, aerosol filter samples was collected at a number of EMEP sites, representing different European rural background environments, using an identical approach both with respect to sampling and subsequent speciation analysis of the mineral dust content. This qualifies for a unique data set, which is comparable beyond any other data set currently available for Europe, and which enables an extensive evaluation of sources, transport, and regional distribution of mineral dust across the European continent.

In the present report the PM₁₀ mineral dust composition across Europe during the June/July part of the IMP is presented and interpreted, a time period which includes the appearance of two African dust outbreaks.

6.2 Methods

6.2.1 Sampling sites

Ambient aerosol filter samples were collected at thirteen EMEP sites located in twelve different countries, covering a wide range of different environments (See Figure 6.1). These sites cover a wide range of environments, such as the Atlantic coastal site Mace Head in Ireland (IE31: “Atlantic” (11)) and the Pyrenean mountain site Montseny in Spain (ES1778: “Southwest Europe” (9)). A group of stations together classified as “Eastern Europe” (AM01: Armenia (1); MD13: Moldova (2); SK06: Slovak Republic (3)). In addition there is a site in Greece (GR02: representing “Southeastern Europe” (7)), two sites in Italy (IT01 and IT04: “South Central Europe” (10 and 8)), one each in Switzerland and Germany (CH02 and DE44: “Central Europe” ((4 and 5)), one in France (FR30: “Western Europe” (6)), the United Kingdom (GB48: “Northwestern Europe (12)”) and one in Sweden (SE12: “Northern Europe” (13)).

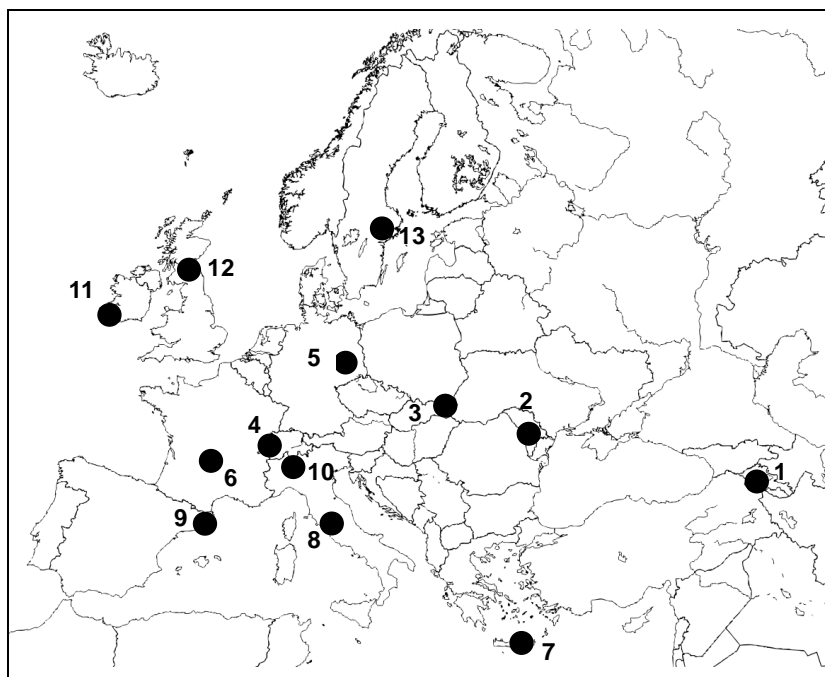


Figure 6.1: Location of sampling sites participating in the EMEP mineral dust campaign in summer 2012.

6.2.2 Sampling and analysis

Ambient aerosol filter samples were collected on Teflon filters (PALLFLEX, Pall Corporation Teflon Membrane Disc Filters cod. R2PJ047, 2 µm, 47 mm) using low volume samplers with a PM₁₀ cut-off size. Daily sampling (24 h) was performed for the time period 8 June - 12 July 2012. One blank and one field blank were collected at each of the sampling sites.

Samples were analyzed by Proton Induced X-ray Emission (PIXE) at the LABEC facilities (Laboratorio di Tecniche Nucleari per i Beni Culturali – Firenze) at the University of Florence. PIXE allows for determination of elemental concentrations for elements with $Z > 10$, with a good sensitivity. The minimum detection limit (MDL) for each element is listed in Table 6.1. It is a nondestructive technique that does not require sample preparation.

PIXE LABEC setup consists of two detectors which do not require any form of pre analysis sample preparation, in contrast to traditional PIXE set ups. At LABEC simultaneous high sensitivity detection of most mineral elements (Na, Mg, Al, Si, K, Ca, Ti, Mn, Fe, Sr, Zr) in a filter sample can be performed within a rather short time frame, ranging from 30 seconds to 3 minutes, depending on the aerosol load.

Table 6.1: Average minimum detection limit (MDL) for the elements analyzed. Units in ng/cm^2 and ng/m^3 .

	MDL				
	ng/cm^2	ng/m^3	ng/cm^2	ng/m^3	
Na	24.8	5.5	Ti	4.8	1.1
Mg	18.9	4.2	V	3.4	0.7
Al	12.7	2.8	Cr	2.1	0.5
Si	10.2	2.3	Mn	1.5	0.3
P	9.3	2.0	Ni	0.6	0.1
S	9.9	2.2	Cu	0.6	0.1
Cl	11.1	2.5	Zn	0.6	0.1
K	11.5	2.5	As	0.8	0.2
Ca	9.2	2.0	Se	0.9	0.2
Fe	1.1	0.2	Br	1.2	0.3
			Rb	1.9	0.4
			Sr	2.5	0.5
			Zr	4.0	0.9
			Mo	7.4	1.6
			Ba	12.8	2.8
			Pb	1.7	0.4

6.3 Levels of PM_{10}

As shown in Figure 6.2 and Figure 6.3, the mean PM_{10} concentrations typically increased along a North to South/South East transect. Mean levels ranging from 20-31 $\mu\text{g}/\text{m}^3$ were recorded, from highest to lowest, at the sites IT01, ES1778, MD13, GR02 and DE44, whereas for the sites IT04, AM01, CH02, SK06, SE12 GB48, IE31 and FR30 the corresponding range was 3-15 $\mu\text{g}/\text{m}^3$. The very low values recorded for the FR30 site (3 $\mu\text{g}/\text{m}^3$) are probably due to problems with the gravimetric measurements. The rather high levels observed at IT01 are probably due to the proximity of the city of Rome, whereas for ES1778, the influence of the two African dust episode seems to have had a substantial influence on the mean concentration for this period.

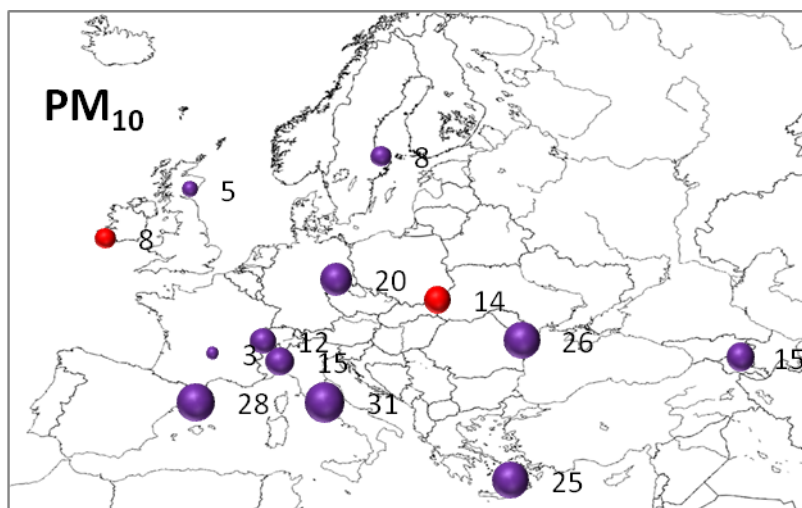


Figure 6.2: Mean PM₁₀ concentrations (µg/m³) recorded during the June/July 2012 EMEP IMP. Red dots indicate estimated PM₁₀ concentrations which are constructed based on the elements analyzed; i.e. no gravimetric data available.

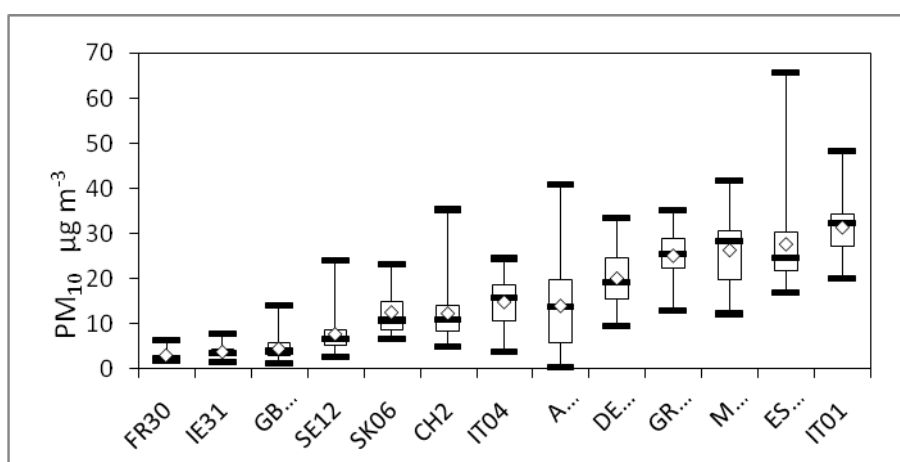


Figure 6.3: Minimum, maximum, 25 percentile, 75 percentile, median and mean daily PM₁₀ concentrations observed during the June/July 2012 EMEP IMP.

6.4 Spatial variation

Mean levels of PM₁₀ (in µg/m³) and of major and trace elements (in ng/m³) determined for the sampling period at each site are presented in Table 6.2. Major elements were grouped according to their major origin, i.e. into mineral dust and sea salt aerosol. Figure 6.4 shows the spatial distribution of the mean concentration of major elements (converted into their major oxides) with a principal mineral affinity (Al, Si, Ca, Fe, K, Mg) for the EMEP IMP in June/July 2012. The highest concentrations of these elements were observed at sites in the Southern and Eastern parts of the sampling domain.

To determine the mineral dust load, major mineral elements have been multiplied by the respective stoichiometry factors to convert them into their respective oxide forms. The mineral loadings of Na₂O, K₂O, CaO and MgO were obtained by subtracting the bulk concentrations of the marine contributions for these components, as calculated from their sea water ratios with respect to bulk Cl concentrations obtained for each sample. This approach may result in an underestimation of the marine aerosol e.g. due to the potential loss of Cl as HCl during sampling (from the reaction between NaCl with HNO₃) and consequently in an overestimation of the mineral load, for elements with a mixed origin. One could speculate that this artefact is more pronounced at sites situated close to the coast such as e.g. GB48 IE31 and SE12).

The spatial distribution of the mean concentrations of mineral dust, sea salt and sulphate aerosols, as well as their relative contribution to the sum of the determined mass (i.e. the sum of mineral dust, sea salt aerosol and SO₄²⁻), are presented in Figure 6.5. From this figure it is apparent that sea salt accounts for a larger part of PM₁₀ at coastal sites with high recorded wind speeds such as IE31 and GR02 (approximately 2 µg/m³). Sea salt levels ranged from 0.2 to 0.7 µg/m³ at sites situated close to the coast such as IT01, GB48, ES1778 and SE12, whereas it was below 0.2 µg/m³ for the remaining sites

Table 6.2: Mean concentrations of PM₁₀ (in µg/m³) and mean concentrations of major and trace elements (in ng/m³) during the June/July 2012 EMEP IMP for each of the participating sites.

	AM01	MD13	SK06	GR02	DE44	IT04	CH02	IE31	SE12	ES1778	GB48	FR30	IT01
ng/m³													
Al ₂ O ₃	938	1792	646	736	242	426	283	70	70	1376	60	135	1168
SiO ₂	2816	5734	1662	2077	644	1085	795	58	208	3267	176	339	2856
Fe ₂ O ₃	413	986	320	423	151	328	183	8	59	608	46	56	688
CaO	972	1184	206	618	114	193	246	40	53	857	44	37	1984
MgO	384	368	131	466	90	124	83	144	102	457	72	34	385
Na ₂ O	75	157	110	1757	195	241	147	786	488	1114	304	54	1078
K ₂ O	233	589	216	302	143	143	140	33	67	334	44	31	426
Cl	18	18	15	1048	41	20	27	1118	75	207	147	3	393
SO ₄ ²⁻	2258	3314	2708	5843	1956	2529	1052	1149	1583	3228	1125	491	3406
ng/m³													
Ti	31.5	56.3	21.9	27.2	8.3	14.6	9.9	3.0	3.0	49.4	2.5	4.8	37.3
P	3.8	14.1	20.7	3.2	31.0	7.4	23.4	3.0	7.6	8.1	5.5	0.8	9.6
V	1.0	1.9	1.0	6.2	1.1	1.7	0.7	1.4	1.0	4.9	0.4	0.2	4.9
Cr	1.4	2.2	5.0	1.1	1.6	1.1	1.0	1.1	0.3	2.6	0.3	0.2	2.7
Mn	9.3	16.9	4.9	6.8	3.0	4.2	2.8	0.8	1.2	8.0	0.9	0.9	10.0
Ni	1.3	1.1	2.2	2.5	0.8	1.3	0.5	0.6	0.9	2.4	0.6	0.2	2.3
Cu	1.5	2.5	2.2	2.0	2.7	8.3	2.8	0.7	0.8	4.0	0.8	0.5	11.4
Zn	16.1	18.0	19.3	21.9	14.3	14.4	7.5	12.0	4.5	17.2	8.4	5.4	19.4
As	1.6	0.6	0.7	0.6	0.6	0.2	0.2	0.3	0.3	0.2	0.2	0.1	0.1
Se	0.7	1.1	0.5	0.6	0.6	0.4	0.2	0.4	0.2	0.3	0.1	0.0	0.5
Br	2.4	3.3	1.9	8.4	2.3	2.8	1.4	3.3	1.9	3.7	1.3	0.5	5.1
Rb	1.7	3.0	0.9	1.3	0.6	0.9	0.8	0.8	0.2	1.1	0.0	0.0	4.2
Sr	2.5	3.5	1.1	2.8	0.9	4.2	0.6	1.2	0.4	1.6	0.1	0.2	6.2
Zr	1.7	2.0	1.2	1.4	1.2	1.1	0.7	1.8	0.5	0.8	0.0	0.1	2.4
Mo	3.3	2.3	2.0	2.1	2.1	1.5	0.9	3.2	0.9	0.4	0.0	0.0	0.2
Ba	4.7	6.5	4.2	4.4	3.5	16.0	1.8	5.1	1.6	0.0	0.0	0.0	7.6
Pb	8.3	5.8	2.4	15.2	2.3	3.8	1.2	0.8	1.2	1.3	1.4	0.2	4.2
ng/m³													
Mineral	5889	10954	3370	5533	1633	2567	1926	183	1005	7944	637	693	8341
Sea salt	33	33	28	1954	76	38	51	2085	575	386	475	6	733
µg/m³													
PM ₁₀	15	26	14	25	20	15	12	8	8	28	5	3	31
Total det.	8.2	14.3	6.1	13.3	3.7	5.1	3.0	3.4	2.7	11.5	2.0	1.2	12.5
% det.	54	56	44	53	18	35	25	43	35	42	45	42	40

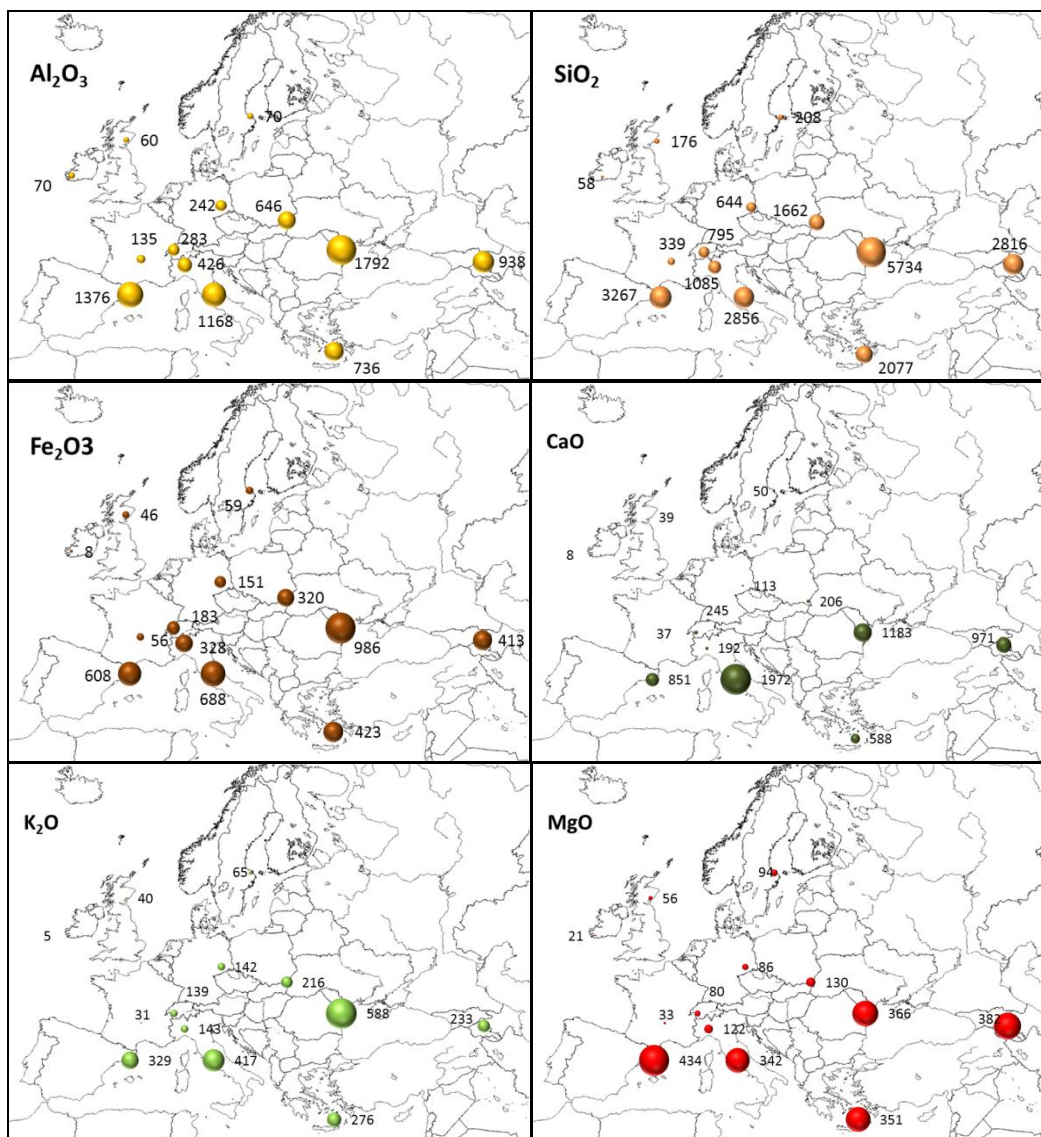


Figure 6.4: Spatial distribution of the mean concentrations of Al_2O_3 , SiO_2 , Fe_2O_3 , CaO , K_2O and MgO (in ng/m^3) determined for each site during the June/July 2012 EMEP IMP.

Figure 6.5 shows that mineral dust concentrations followed a similar pattern as that described for PM_{10} ; i.e. with a high dust load (5.5 to $11 \mu g/m^3$) at the sites MD13, IT01, ES1778, AM01 and GR02, intermediate levels (1.5 - $3.5 \mu g/m^3$) at SK06, IT04, CH02 and DE44, and low levels at GB48, FR30 and SE12 (0.6 - $1.0 \mu g/m^3$) and IE31 ($0.2 \mu g/m^3$).

The highest mean sulphate concentration was observed at the Southeastern site GR02 ($5.8 \mu g/m^3$). Relatively high concentrations were also determined for the eastern (AM01, MD13 and SK06) and the South Central and Southwestern sites, ranging from 2.6 - $3.4 \mu g/m^3$. Lower levels were measured at the Central and Northern sites (0.5 - $1.1 \mu g/m^3$) with an intermediate concentration for DE44 ($2.0 \mu g/m^3$).

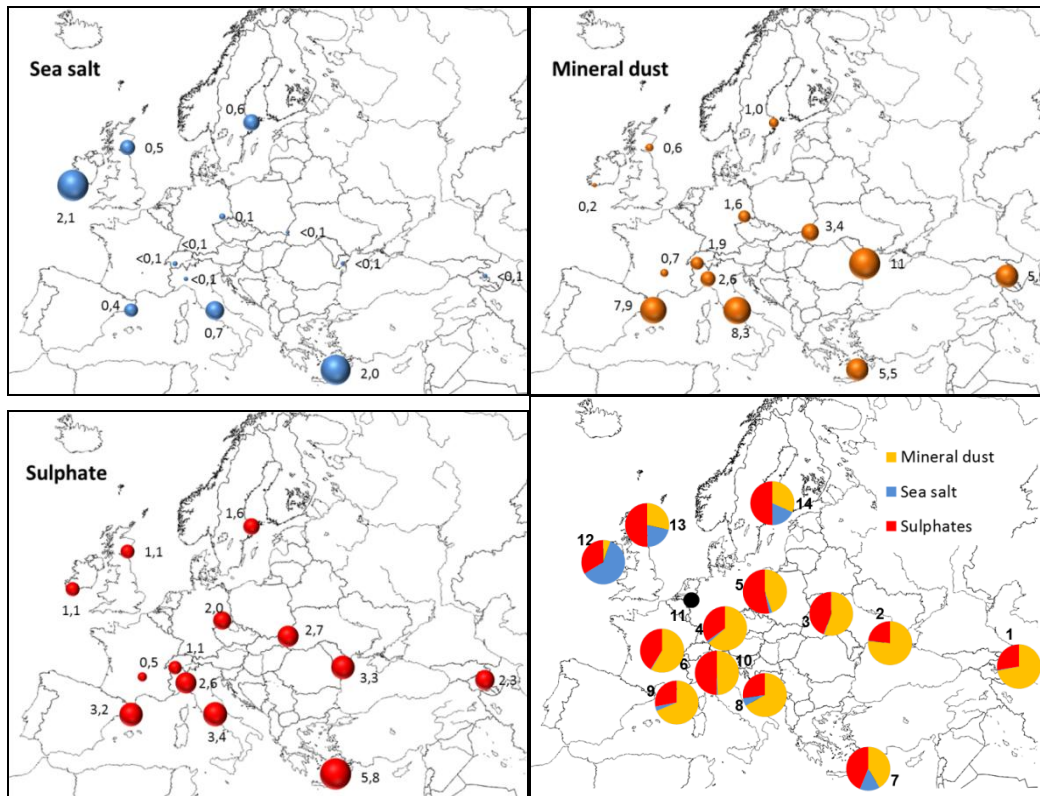


Figure 6.5: Spatial distribution of the mean sea salt, mineral dust and sulphate concentration (in $\mu\text{g}/\text{m}^3$), as well as their relative contribution to the sum of the determined mass (i.e. the sum of mineral dust, sea salt and SO_4^{2-}) for each of the sites participating in the June/July 2012 EMEP IMP.

The high mineral load at Southern- and some Central European sites during the June/July EMEP IMP are mainly attributed to African dust episodes. However, there is also a noticeable regional contribution (soil wind resuspension) for the southernmost sites caused by resuspension of soil and mineral dust from e.g. semis arid land. In addition, an anthropogenic source causing increased levels of Ca containing minerals (from construction and road dust) is evident for the two Italian sites (IT01 and IT04), most likely being road dust and dust originating from construction sites.

As shown in the next sub chapter 6.5, the African dust outbreaks did not affect Eastern Europe. Thus, the mineral dust observed for this region should be related to the influence of local and/or regional sources. Certain geochemical ratios (e.g. Si/Al and Mg/Al) are characteristic for this region and the data provided by the present study confirms this, and thus the local/regional source. Indeed, the present study has allowed us to demonstrate the importance of crustal sources in the eastern European region. More detailed research is needed to identify the sources in more detail, e.g. to establish emission factors, and to quantify their impact on the ambient PM level.

The high concentrations of sulphate are related to the impact of SO_2 emissions, mainly originating from fuel oil and coal combustion. A major origin of sulphates

in the Mediterranean can be related to shipping (heavy oil) emissions, whereas in Central- and Eastern Europe high levels are more often related to stationary sources, such as e.g. coal power plants.

As shown in Figure 6.6, mineral dust is the major component of the determined mass of PM_{10} at the eastern (AM01, MD13), Southwestern and South Central sites (ES1778 and IT01), as well as for some of the Central sites (CH02 and FR30). An equally large contribution of mineral dust and sulphate was seen for some of the Central European sites (IT04, DE44 and SK06), and for the Southwestern site (GR02). Sulphate was the major component at the Northwestern sites GB48 and SE12, whereas sea salt dominated at the Irish coastal site IE31. Note that a substantial fraction of the PM_{10} mass concentration is not accounted for by the species analyzed. E.g. more than 60% was not accounted for at the DE44 site, of which OC and NO_3^- are likely to account for the majority of the unaccounted mass.

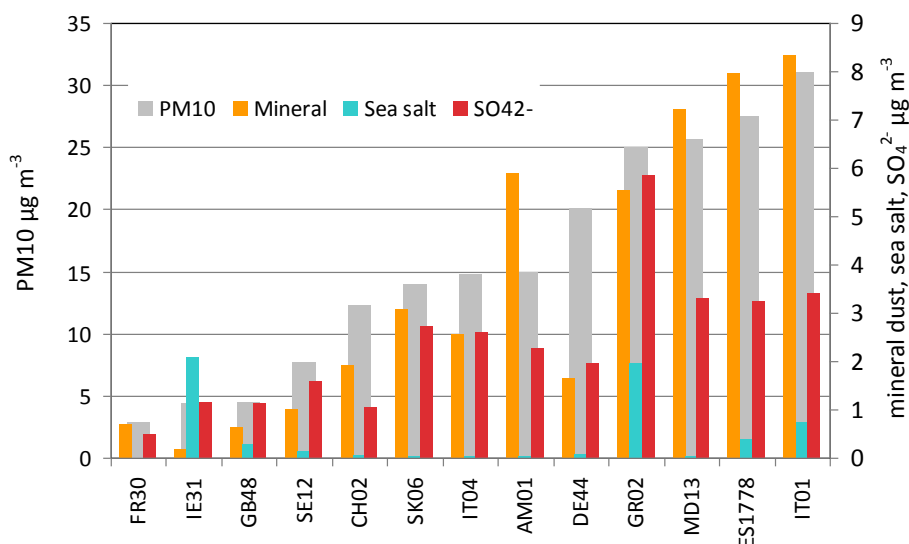


Figure 6.6: Mean PM_{10} , mineral dust, sea salt and SO_4^{2-} concentrations recorded at each site during the June/July 2012 EMEP IMP. Note that PM_{10} concentrations at IE31 and SK06 were estimated based on the elements and species analyzed.

6.5 African dust outbreaks: time evolution and spatial influence

Two African dust outbreaks occurred during the June/July 2012 EMEP IMP: the first from the 17th until the 23rd of June and the second one from the 28th of June until the 7th of July. The two episodes were initiated by the development of a thermal low south of the Atlas Mountains. During such conditions cyclones travel eastward, crossing the Mediterranean Basin. As shown by the NAAPS model (Figure 6.7) the plume first hit the Iberian Peninsula, moving north and eastwards successively affecting parts of Central, South Central, and Southeastern Europe. The mineral dust analyses performed allowed studying the influence of the two African dust outbreaks occurring during the study period on the levels and composition of PM_{10} across large parts of Europe.

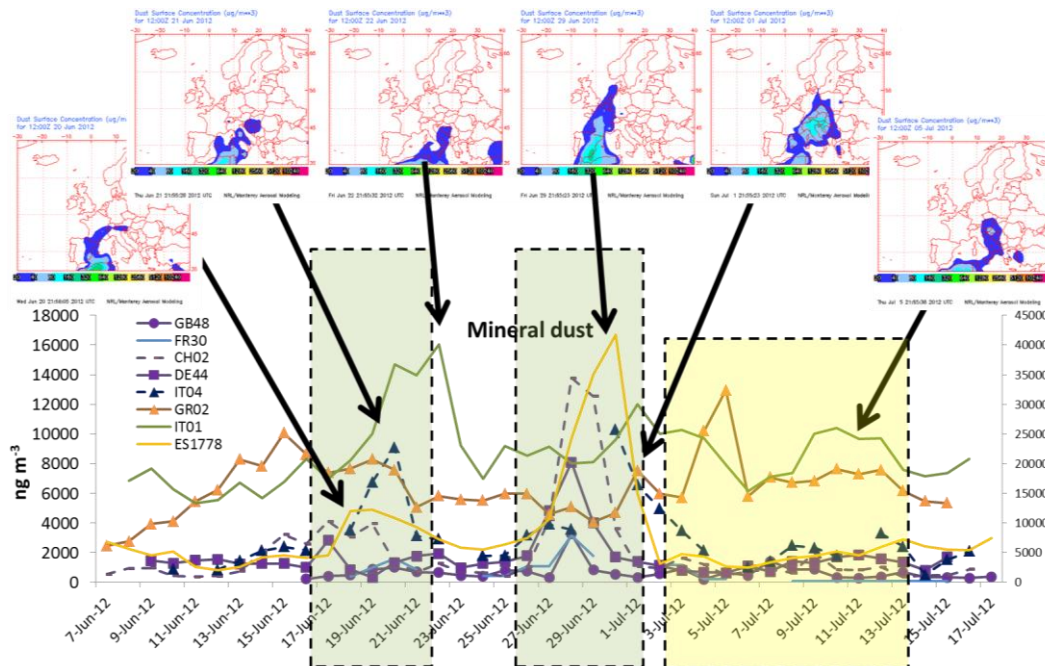


Figure 6.7: Time series of mineral dust concentrations during the June/July 2012 EMEP IMP at sites affected by the Saharan dust outbreak. Levels at ES1778 referred to the right axis. Aerosol maps from NAAPS show the dust distribution during selected days. The two dust episodes are highlighted. In both cases, the dust outbreak is displaced eastwards subsequently impacting the different sites. Finally, the dust remains in the eastern Mediterranean basin from the beginning to the fifteenth of July. NAAPS Navy Aerosol Analysis Prediction System from the Marine Meteorology Division of the Naval research Laboratory, USA (NRL) (<http://www.nrlmry.navy.mil/aerosol>).

The first episode was less intense and did not affect such a large part of the European continent as the second one. As shown in Figure 6.7, concentrations of mineral dust first increased at ES1778, reaching $12 \mu\text{g}/\text{m}^3$ on the 17th of June. As the plume moved eastward, levels increased at IT04 and IT01, reaching $15 \mu\text{g}/\text{m}^3$ at IT01 on the 22nd of June.

On the 26th of June a second plume was observed over the European continent, initially affecting ES1778, at which daily concentrations reached $45 \mu\text{g}/\text{m}^3$ on the 28th. Increased levels were also observed at FR30, CH02 ($15 \mu\text{g}/\text{m}^3$), DE44 ($10 \mu\text{g}/\text{m}^3$) and GB48 ($5 \mu\text{g}/\text{m}^3$), reaching their maximum on the 29th. The mineral load subsequently decreased at these sites, but increased at IT04 and IT01 reaching 5 and $10 \mu\text{g}/\text{m}^3$ on the 2nd of July, respectively. On the 5th of July the mineral load peaked at GRO2, reaching $15 \mu\text{g}/\text{m}^3$. From the first of July and until the end of the June/July 2012 EMEP IMP, levels remained relatively high in the central and eastern parts of the Mediterranean basin.

The time evolution of the mineral dust is based on that of the time evolution of the major mineral components. The mean concentration and the mean relative

contribution of the various mineral components seen during the 2nd African dust episode are presented in Figure 6.8 (left graphs) for a selection of sites. Higher concentrations of mineral components were seen at all sites. Further, the relative contribution (Figure 6.8, left-bottom graph) shows that the mineral dust composition was rather similar at the sites affected by the African dust outbreak, despite being situated in different parts of Europe. This finding is not surprising given the source strength of the actual African dust episode, and indicates that other local/regional sources of mineral dust is of minor importance during such events.

During non-African dust episodes the PM mineral load (Figure 6.8, right graphs) was higher at ES1778 and GR02 compared to CH02 and DE44 showing a more substantial influence of regional and local dust emissions at these sites than in Central Europe. The relative contribution of mineral components during non-African dust episodes shows that the mineral dust composition has certain specific features for each site. At ES1778 and GR02 the mineral dust has a higher content of Mg. However, it cannot be excluded that this is due to an influence by marine Mg. At DE44 and CH02 there is a higher contribution of K and Fe. The high K content could potentially be related to biomass emissions.

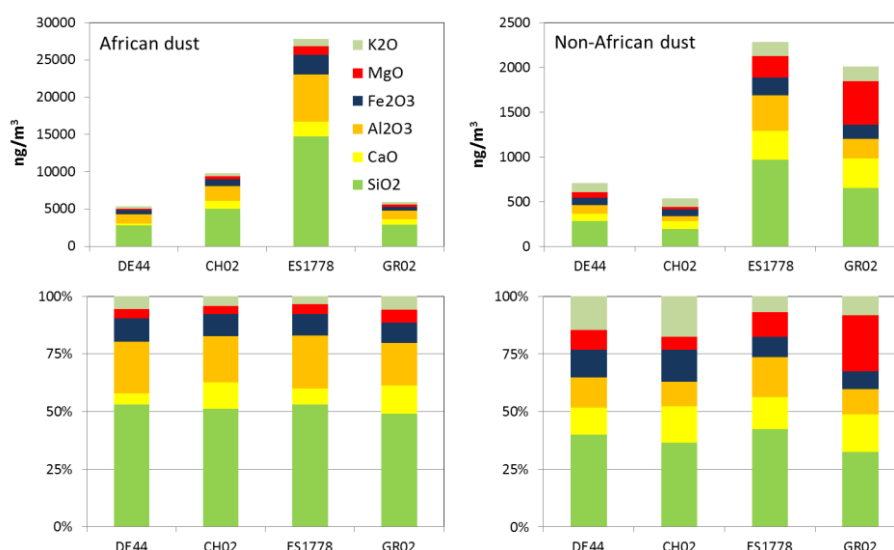


Figure 6.8: Average composition (absolute values – ng/m^3 , top- and relative contribution –%, bottom) of mineral dust at selected sites affected by the African dust episodes, during the second African dust outbreak (left) and during days not influenced by African dust (right).

6.6 Trace metals

The observed concentrations of trace metals at EMEP sites during the June/July 2012 EMEP IMP varied substantially between sites. I.e. average concentrations of metals were comparatively higher for Zn (SK06), Pb (AM01, MD13), Cr (SK06, MD13), As (AM01) and Mn (MD13, AM01) in Eastern Europe; for Pb, V and Ni (GR02) in Southeastern Europe and for Ba (IT04), Mn (IT01), and Cu (IT01 and IT04) in South Central Europe.

Certain metals, such as Ti, Sr and Rb, were highly correlated with major mineral elements owing to their major crustal origin. Consequently, these elements showed a spatial distribution similar to that of mineral dust, with higher mean concentrations in the Southern and Eastern European sites (See Figure 6.9). For some mineral related elements with a major carbonate affinity, such as Sr, the highest mean concentrations were observed at IT01, reflecting the spatial distribution of Ca, probably as a consequence of the influence of the anthropogenic emissions from Rome.

Higher concentrations of V were recorded at the Mediterranean sites (ES1778, GR02, IT01); i.e. ranging from 5 - 6 ng/m³. At the remaining sites, mean V concentrations ranged from 1-2 ng/m³, whereas particularly lower concentrations were observed at FR30 and GB48 (0.2-0.4 ng/m³). V is typically considered a tracer of fuel oil combustion emissions (Viana et al., 2008).

Ni is commonly found to be associated with V tracing fuel oil combustion emissions; however it can also be emitted from metallurgical processes (Viana et al., 2008; Pandolfi et al., 2011). The highest levels of Ni were recorded at Southern (2.3-2.5 ng/m³) and Eastern European sites (1-2 ng/m³). In the present study, V-Ni showed a high correlation for the Mediterranean sites (Figure 6.10, R²=0.72), especially for GR02 and ES1778, confirming a major common source likely related to fuel oil combustion emissions. At these sites the V/Ni ratio was 2.5, which is similar to the one obtained for shipping emissions at Southeastern Spain (Pandolfi et al., 2011), corroborating to the theory that the high levels of V and Ni recorded at the Mediterranean sites are mainly related to shipping emissions (harbours and maritime traffic). By contrast Ni does not correlate with V at the Eastern sites (AM01, MD13 and SK06), but rather with Cr (R²=0.93), indicating a major metallurgical origin for these elements in this region (Figure 6.10). At the sites MD13 and AM01, high correlations of Cr and Ni with Mn and Cu, underpin the influence of metallurgical activities.

Other elements tracing metallurgical activities such as Mn was found to have higher concentration in Eastern Europe, underlining the importance of such emission sources in this region.

Tracers of coal emissions, such as As, were more concentrated (0.6-0.7 ng/m³) at Southeastern and Central European sites (DE44, MD13, GR02 and SK06) with the most elevated levels at AM01 (1.6 ng/m³). Concentrations of As was substantially less for the Western European sites, for which average concentrations ranged from 0.1 to 0.3 ng/m³.

Cu could be considered a tracer of traffic emissions (Schauer et al., 2006; Amato et al., 2009) and was found to be present in higher concentrations at the Southern and Central European sites with average concentrations of 11 ng/m³ at IT01 and 8 ng/m³ at IT04. At the remaining sites mean Cu concentrations range from 1 to 4 ng/m³.

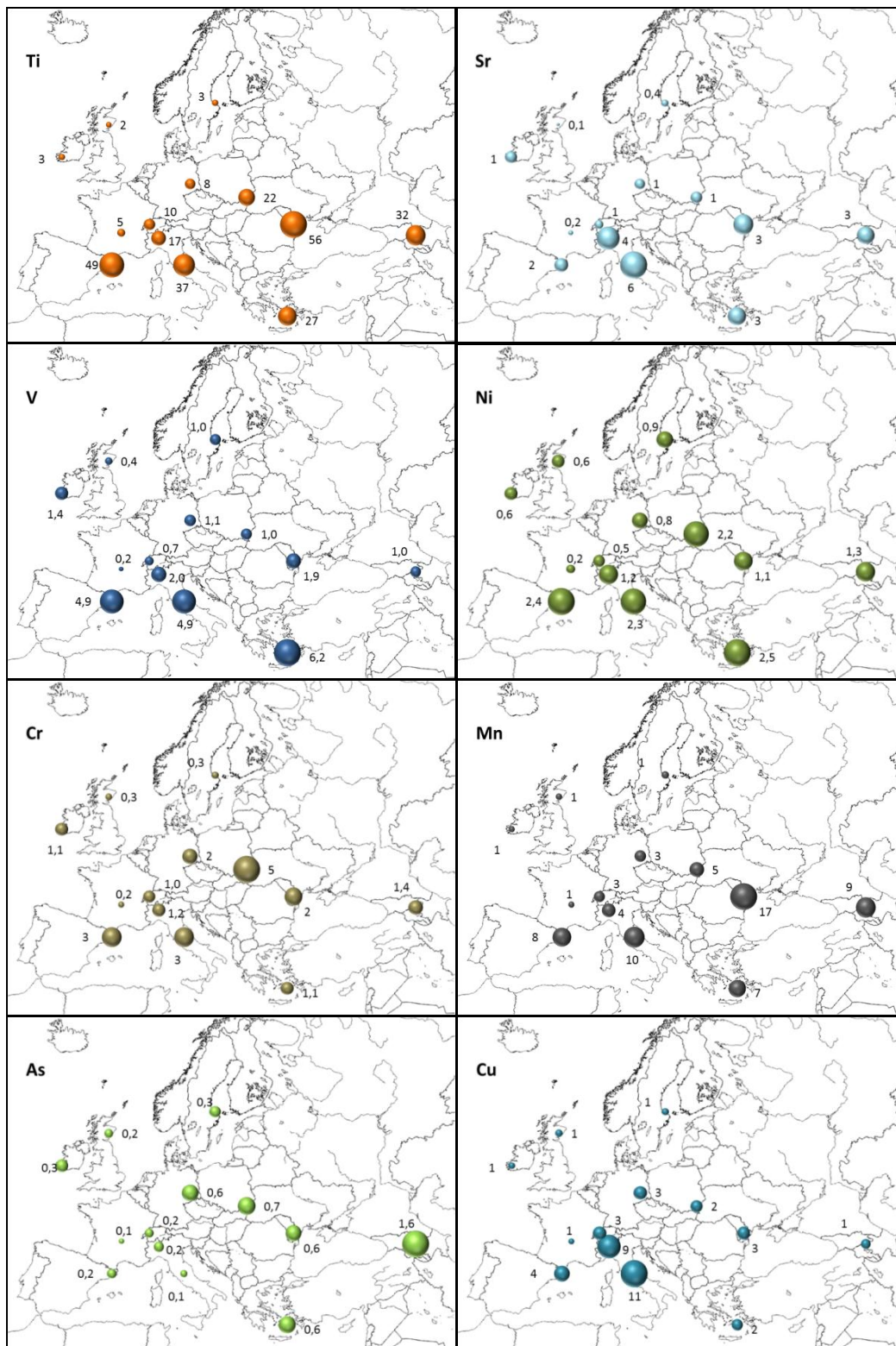


Figure 6.9: Spatial distributions of the mean concentrations (in ng/m^3) of selected trace elements determined at each site during the June/July 2012 EMEP IMP.

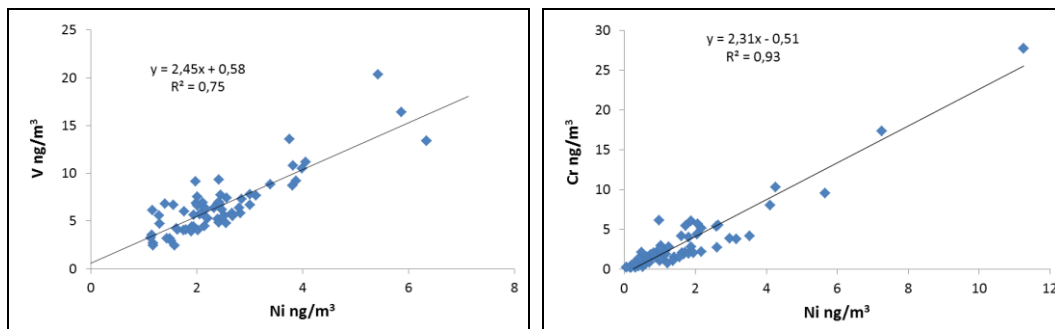


Figure 6.10: Left: scatter plot for V and Ni concentrations observed at the in the Southern Mediterranean sites GR02 and ES1778. Right: scatter plot for Cr and Ni concentrations at the Eastern sites AM01, MD13 and SK06.

To investigate differences in metalliferous tracers of emissions from main sources such as traffic, mineral dust and industry, a triangular diagram has been employed to compare the sites. Thus, Ti, Sr and Rb were considered as mineral tracers, Cu, Pb and Ba as at least partly influenced by traffic, and V, Cr and Ni as industrial or shipping (Figure 6.11). The resulting concentration fields have been plotted based on all samples for each of the different European regions. The relative proportions of these three possible sources indicate similar values for samples from the Atlantic coast, Northern and Eastern Europe; although in the latter case, MD01 samples have a higher proportion of mineral elements, whereas SK06 samples are richer in industrial tracers. Central European sites show different behaviours, with FR30 samples being more influenced by mineral elements, DE44 by traffic, and CH02 by industry. Samples from South Central and Southeastern Europe have quite similar features, although the latter region is more influenced by industrial sources. Finally, samples from the Southwestern Europe are the ones most

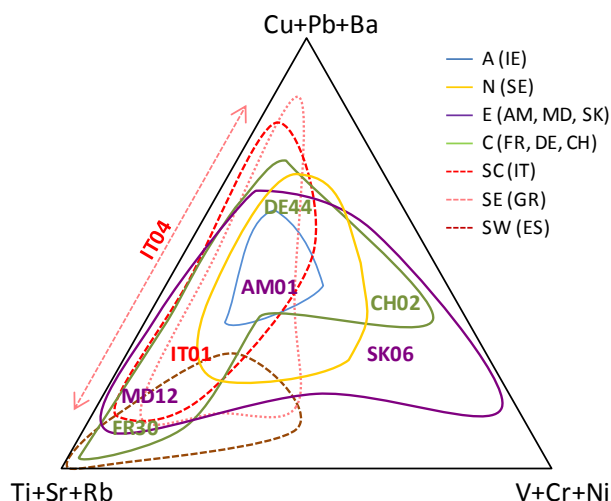


Figure 6.11: Triangular diagram for mineral dust, traffic and industrial trace metal tracers for all sampling days during the June/July 2012 EMEP IMP. Letters indicate main areas where samples for each site plot.

affected by mineral dust tracers, presumably due to the greater influence of Saharan dust intrusions. They also show rather similar features with respect to traffic and industrial elements.

6.7 Factor analysis

A simple source apportionment study was performed by applying a Principal Component Analysis (PCA). All the samples analyzed and 25 elements were considered for the analysis. The PCA analysis permitted the identification of four major sources explaining 76% of the total variance (Table 6.3): mineral matter; sea salt + shipping emissions; urban + industrial pollution; and coal combustion.

Table 6.3: Factor loadings results of the factor analysis carried out with the daily concentrations of 25 elements present in PM_{10} .

	Factor 1	Factor 2	Factor 3	Factor 4
Na	0.02	0.95	0.17	-0.05
Mg	0.77	0.47	0.11	0.19
Al	0.97	0.02	0.11	0.10
Si	0.97	0.01	0.05	0.14
S	0.60	0.30	0.37	0.39
Cl	-0.10	0.91	-0.09	-0.08
K	0.91	0.14	0.22	0.16
Ca	0.81	0.17	0.35	0.09
Ti	0.97	0.03	0.07	0.11
V	0.52	0.42	0.43	0.04
Cr	0.53	-0.08	0.34	0.07
Mn	0.93	0.02	0.11	0.22
Fe	0.95	0.05	0.24	0.13
Ni	0.55	0.25	0.48	0.16
Cu	0.32	0.13	0.87	0.01
Zn	0.61	0.16	0.47	0.33
As	0.03	-0.02	-0.08	0.78
Se	0.55	0.06	0.08	0.41
Br	0.45	0.70	0.34	0.23
Rb	0.90	0.10	0.26	0.00
Sr	0.53	0.20	0.68	0.07
Zr	0.77	-0.01	0.28	-0.08
Mo	0.02	-0.07	0.03	0.63
Ba	0.00	-0.01	0.87	-0.01
Pb	0.30	0.11	0.15	0.60
% Variance	53	11	7	6
Eigenval	13	3	3	2

The first source, mineral matter, explaining 53% of the variance, is characterized by the association of the typical mineral related elements (Al, Si, Ca, K, Ti, Mn, Rb, Fe) along with those with a mixed mineral affinity (Mg, S, V, Cr, Ni, Zn, Se).

The second source (11% of the variance) groups elements with a major marine origin (Na, Cl, Mg) and those tracing oil combustion sources such as S, V and Ni. Thus, this source has been labelled as sea salt and shipping emissions.

The third source (11% of the variance) is represented by the association of typical industrial/traffic related metals (Cu, Ba, V, Cr, Ni, Zn, V) and other elements partially anthropogenic such as Ca and Sr (related to construction/demolition activities and road dust). This component is regarded as reflecting an urban-industrial emission source.

Finally, the fourth source (6% of the variance) is related to coal combustion and is characterized by the presence of As, Pb, Mo, Zn, Se, and S. The results of this preliminary source apportionment analysis confirm the previous interpretation of spatial variation of the PM components.

6.8 Conclusions

One of the major aims of the third EMEP intensive measurement period (IMP) of summer 2012 and winter 2013 was to measure the chemical speciation of the PM₁₀ size fraction, focusing in particular on mineral dust and trace metals. During the June/July 2012 EMEP IMP, mineral dust was simultaneously determined, for the first time, using the same sampling and analytical methodology at a number of regional background sites representative of different European regions.

The highest PM mineral load was measured in Southern and Eastern European countries. The origin of the mineral dust was found to be attributed to different source regions. Saharan dust outbreaks were responsible for increased concentration of mineral matter in Southern and some Central European sites, whereas high levels of mineral dust in Eastern Europe was attributed to regional sources, such as wind suspension of soil or agricultural emissions.

Two African dust outbreaks occurred during the study period affecting the levels and composition of PM₁₀ across Southwestern and Central Europe. The impact of Saharan dust results in a relative increase of SiO_2 and Al_2O_3 and a relative decrease of CaO , K_2O and MgO . The composition of African dust affecting different regions of Europe was compared in order to study changes during transport, showing that the composition of the Saharan dust was quite homogeneous over the different areas.

The spatial distribution of metals allowed tracing the influence of specific anthropogenic sources at a regional scale. The importance of shipping emissions in the Mediterranean region (traced by V, Ni, and SO_4^{2-}), metallurgic industry (Cr, Ni, and Mn) in Central and Eastern Europe, and coal combustion (As, Se, and SO_4^{2-}) in Eastern European countries were predicted.

7 Measurements of particulate matter in the EECCA countries

By Karl Espen Yttri, Wenche, Aas, Emil Abdulazizov, Marine Arabidze, Violeta Balan, Lusine Gevorgyan, Lyudmila Chuntanova

7.1 Introduction

The number of sites which report mass concentration of particulate matter (PM) to EMEP has increased steadily since this parameter was implemented to the EMEP monitoring program in 1999. However, the sites measuring PM are not uniformly distributed throughout the EMEP monitoring network. Amongst those particularly poorly represented with respect to PM measurements are the Eastern European, the Caucasian and the Central Asian (EECCA) countries.

The EECCA countries host a number of anthropogenic and natural sources which have the potential to cause both severe local and regional PM air pollution. E.g. the European countries bordering the Black Sea have particularly high SO₂ emissions, accounting for more than one third of the total SO₂ emissions reported over Europe in 2004 (Vestreng et al., 2007). According to Sciare et al. (2008), it is likely that levels of carbonaceous aerosol having the same origin as SO₂ in this region will remain high the coming years. Further, some of Europe's largest agricultural land areas can be found in the EECCA countries, and agricultural activity, e.g. emissions from ploughing and off-road vehicles, is a well known source of ambient PM. While agricultural waste burning is banned in most western European countries, it is common practice in large parts of the world including the EECCA countries, thus this is likely to represent a substantial source of combustion aerosol. Indeed, several studies have shown how such emissions can substantially deteriorate the air-quality in Europe ranging from the Eastern-Mediterranean (Sciare et al., 2008) to the European Arctic (Stohl et al., 2007). Large areas of the EECCA countries are semi-arid land, which is subject to erosion. Subsequently the eroded material, i.e. mineral and soil dust, can be entrained into the atmosphere and thus contribute to PM air pollution both on the local and regional scale.

To help implement the obligations under the EMEP protocol in the EECCA region, the work plan of EMEP (ECE/EB.AIR/WG.5/2010/16) particularly support enhanced cooperation between the EMEP centres, Task Forces and the countries in the actual region to improve the emissions reporting, as well as establishing monitoring and modelling activities. Thus, in order to improve our current understanding of PM pollution in the EECCA region a one year measurement program, funded by the Norwegian Ministry of Foreign Affairs was initiated to determine the ambient mass concentration of PM₁₀. Ambient PM₁₀ mass concentration levels were established based on ambient aerosol filter samples collected at five sites in Armenia, Azerbaijan, Georgia, Kazakhstan and Moldova. The same filters were subjected to analyses of total (TC), elemental (EC) and organic carbon (OC), as well as the biomass burning tracer levoglucosan in order to learn more about the relative contribution of carbonaceous aerosol sources, and biomass burning sources in particular, to PM₁₀. Furthermore these sites do have regular EMEP level one measurements where inorganic ions are determined with filterpack measurements using a PM₁₀ inlet. These data are not

presented here due to comparability issues, but they are available from <http://ebas.nilu.no/>.

Although the EECCA countries are defined as one region it is a region of great diversity and which is reflected in the five measurement sites addressed; Leovo II in the agricultural low land region in the south of Moldova, the high altitude sites Abastumani in Georgia and Amberd in Armenia, both situated in the Lesser Caucasus mountain range, and Borovoe in a low land forested region of the otherwise typically non-forested Eurasian plains. The Xizi site in Azerbaijan is located North of Baku in a forested area close to the Altyaghach National Park. See Table 7.1 and Figure 7.1 for location of the actual sites. Here we present selected results based on PM₁₀ mass concentration, total carbon (TC), elemental carbon (EC), organic carbon (OC) and levoglucosan measurements performed at the sites in Armenia, Georgia, Kazakhstan and Moldova. We have chosen not to include the preliminary data from Azerbaijan here due to quality assurance and data completeness issues.



Figure 7.1: Location of the five EECCA countries sampling sites discussed in the current text; Amberd in Armenia (AR), Abastumani in Georgia, Borovoe in Kazakhstan (KZ), Leovo II in Moldova (MD) and Xizi in Azerbaijan (AZ). The measurements from the station in Azerbaijan (AZ) are not included.

Table 7.1: Location of the five EECCA rural background sites and the duration of the sampling period. The inlet cut-off size of the aerosol sampler and the number of samples are also provided.

Sampling site	Location	Height (masl)	Sampling period	Number of samples	Cut-off size
Amberd (Armenia)	40°23'4"N 44°15'38"E	2080	26.06.2010 – 23.12.2011	56	PM ₁₀
Abastumani (Georgia)	41°45'18"N 42°49'31"E	1650	24.09.2010 – 14.11.2011	47	PM ₁₀
Xizi (Azerbaijan)	40°54'26"N 49°2'20"E	639	29.01.2012 – January 2013	50	PM ₁₀
Borovoe Kazakhstan	53°00'17"N 70°36'24"E	334	29.04.2010 – 29.08.2011	47	PM ₁₀
Leovo II (Moldova)	46°29'18"N 28°17' 0"E	166	15.10.2010 – 18.11.2011	47	PM ₁₀

7.2 Mass concentration of PM₁₀

The annual mean PM₁₀ concentration varied from $12 \pm 7.0 \mu\text{g m}^{-3}$ at the Armenian site Amberd and $12 \pm 9.7 \mu\text{g m}^{-3}$ at the Georgian site Abastumani to $23 \pm 8.6 \mu\text{g m}^{-3}$ at the Moldovan site Leovo II (see Figure 7.2). The annual mean concentration observed at the Borovoe site in Kazakhstan ($14 \pm 5.0 \mu\text{g m}^{-3}$) was slightly higher than for the Abastumani and Amberd sites but substantial lower than that observed for Leovo II.

The annual mean PM₁₀ concentration observed for the Amberd and Abastumani sites was slightly higher than the levels observed at EMEP sites in Northern Europe ($9.0 \pm 5.0 \mu\text{g m}^{-3}$) and at the British Isles ($9.6 \pm 2.2 \mu\text{g m}^{-3}$) for 2010, which typically are the lowest within the EMEP monitoring network. It should be noted though that the true PM cut-off size for the sampler operating at the Amberd site was less than 10 μm equivalent aerodynamic diameter (EAD) for 60% of the samples, as the sampler was operated at a too high flow rate from the start of the sampling period.

For Borovoe, the annual mean PM₁₀ concentration was somewhat higher than for EMEP sites in Northern Europe and at the British Isles but less than that observed for EMEP sites in Eastern ($17 \pm 7.5 \mu\text{g m}^{-3}$) and Southern Europe ($17 \pm 5.0 \mu\text{g m}^{-3}$). The annual mean PM₁₀ concentration at Leovo II was somewhat higher than that observed for Central/Western Europe ($20 \pm 3.7 \mu\text{g m}^{-3}$), but still less than the rather high levels observed for the Eastern Mediterranean region ($30 \mu\text{g m}^{-3}$). The Abastumani (1650 m.a.s.l.) and Amberd (2080 m.a.s.l.) sites are both high altitude sites situated in the lesser Caucasus mountain range. The observed annual mean concentrations of PM₁₀ at these two sites were slightly higher than the mean level observed for high altitude EMEP sites situated in Continental Europe ($11 \pm 3.9 \mu\text{g m}^{-3}$), which all except one are situated at altitudes less than 1360 m.a.s.l.

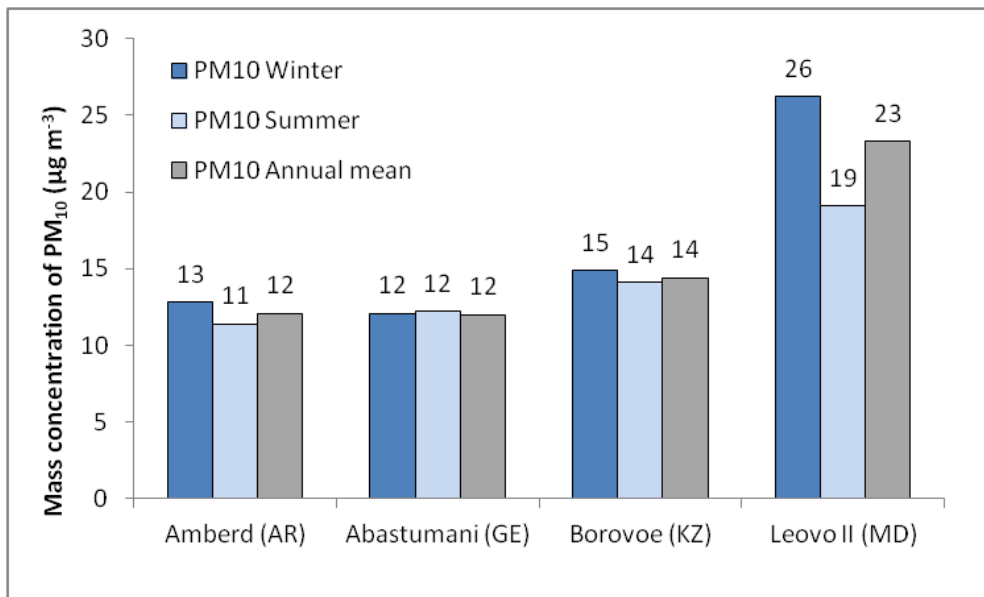


Figure 7.2: Annual and seasonal (i.e. winter and summer) mean concentration of PM_{10} at the four EECCA sites Amberd (Armenia), Abastumani (Georgia), Borovoe (Kazakhstan) and Leovo II (Moldova).

The EU limit value for PM_{10} of $40 \mu\text{g m}^{-3}$ for the annual mean was not exceeded at any of the four sites, whereas the World Health Organization Air Quality Guidelines (WHO AQG) of $20 \mu\text{g m}^{-3}$ for PM_{10} for the annual mean was exceeded at the Leovo II site in Moldova. Samples were collected at a weekly time resolution at all four sites, hence no comparison to the EU limit value nor the WHO AQG for 24 hours could be made. Weekly maximum concentrations were a factor of 2 – 2.5 higher than the annual means, except for the Amberd site for which a factor of 4 was observed. The highest weekly mean concentration was observed at the Leovo II site, exceeding $45 \mu\text{g m}^{-3}$ during the first week of January 2011.

There was no apparent seasonal variability observed at the four sites, except for Leovo II, for which the mean winter time concentration was 25% higher than during summer. It should be noted though that poor data capture during certain periods of the year to some extent could confound the general impression of no seasonal variability. E.g. sampling was not conducted for periods of 2-3 months for the Borovoe site for unknown reasons.

7.3 Concentrations of EC and OC in PM_{10}

Thermal-optical analysis (TOA) is the method of choice to quantify the content of EC and OC in ambient aerosol filter samples. Carbonate (CO_3^{2-}) carbon is known to be detected by TOA as well, and thus has the potential to interfere with the EC/OC results. Depending on the thermal protocol used, the presence of carbonate will interfere with either OC or EC, or both. The evolution of CO_3^{2-} during EC/OC analysis is currently debated, and we will not go into detail on that here. Carbonate appears to be present in low concentrations in the European rural background environment, although with some exceptions, thus it is not considered a major confounding factor for EC/OC analysis. However, for regions

substantially influenced by mineral and soil dust, such as for selected EECCA countries, the potential presence of carbonate in the ambient aerosol should be addressed when performing thermal-optical analysis. For the Abastumani and Borovoe sites, additional and complementary thermal-optical analysis has been performed to account for the presence of CO_3^{2-} . Hence, for the two actual sites CO_3^{2-} - corrected levels of EC and OC are available for the entire one-year time series. CO_3^{2-} was found to evolve as both EC and OC for both sites.

EC is generated and emitted to the atmosphere during incomplete combustion of fossil fuel and biomass, and are typically associated with fine aerosol particles. Albeit crude, EC could be regarded as a tracer of anthropogenic emissions. Exceptions are wild fires when ignited by lightning, as seen during major Boreal fires in Canada and Siberia, however quite a few incidences when natural vegetation catches fire is likely due to human activity; E.g. agricultural burning which spreads to the natural vegetation.

The annual mean EC concentrations did not differ much between the two sites being $0.31 \pm 0.22 \mu\text{g C m}^{-3}$ at Abastumani and $0.32 \pm 0.17 \mu\text{g C m}^{-3}$ at Borovoe. This concentration range should be considered to be in the medium range of the annual mean EC concentrations reported for EMEP sites in 2010, ranging from $0.09 \mu\text{g C m}^{-3}$ to $1.4 \mu\text{g C m}^{-3}$. There was a pronounced seasonal variation in the EC concentration at the Abastumani site with winter time (May - September) concentrations ($0.36 \pm 0.24 \mu\text{g C m}^{-3}$) being 1.8 times higher than during summer (October - April) ($0.21 \pm 0.12 \mu\text{g C m}^{-3}$). For Borovoe it was the other way around with EC concentration being higher in summer ($0.36 \pm 0.14 \mu\text{g C m}^{-3}$) compared to winter ($0.31 \pm 0.18 \mu\text{g C m}^{-3}$), however the difference between the two seasons was not particularly pronounced; i.e. a factor 1.2. It should be noted that the samples were not uniformly collected throughout the year; at the Abastumani site 70% of the samples were collected during winter whereas for Borovoe 70% were collected during summer. It cannot be excluded that this might have had an effect on the observed seasonal variation for the parameters discussed.

When correcting for the influence of CO_3^{2-} a 10% reduction in the annual mean concentration of EC was observed for both sites. A 20-50% reduction in the EC concentration was observed for several samples. The observed annual mean EC/TC ratio, $14 \pm 4.2 \%$ at Abastumani and $11 \pm 5.1 \%$ at Borovoe, was comparable to that observed for EMEP sites in the Scandinavian countries and for high altitude sites in western/south-western Europe. At both sites the fraction of TC which could be attributed to EC was higher in winter (Abastumani: 15%; Borovoe 17%) compared to summer (Abastumani: 10%; Borovoe 8.4%; i.e. by as much as a factor of 2 for the Borovoe site. For Abastumani this can be explained by the increase in concentration of EC in winter, whereas for Borovoe the substantial reduction in OC going from summer to winter plays a more substantial role than the marginal increase observed for EC.

OC is emitted from a wide number of anthropogenic and natural sources and is typically thought to be associated with fine aerosol particles. As for EC, the major source of anthropogenic OC is incomplete combustion of fossil fuel and biomass. The major natural source of the carbonaceous aerosol is biogenic secondary organic aerosol (BSOA); i.e. biogenic VOCs emitted from vegetation which

oxidize in the atmosphere and which subsequently partition from the gas to the particulate phase, giving rise to BSOA. As for EC, OC emitted from wild fires can be regarded as both a natural source and of anthropogenic origin, depending on how it was ignited. There are also primary biogenic aerosol particles, i.e. primary biological aerosol particles (PBAP), contributing to the natural carbonaceous aerosol loading, however these would typically reside in the coarse fraction of PM₁₀.

The variability of the annual mean OC concentration was wider than observed for EC, ranging from $2.0 \pm 1.1 \mu\text{g C m}^{-3}$ at Abastumani to $2.8 \pm 1.3 \mu\text{g C m}^{-3}$ at the Borovoe site. These levels are in the upper range of the annual mean concentrations of OC in PM₁₀ reported for 2010 at EMEP sites, ranging from $0.83 - 2.3 \mu\text{g C m}^{-3}$. There was a pronounced seasonal variation in the OC concentration at the Borovoe site with summer time (May - September) concentrations ($3.2 \pm 1.2 \mu\text{g C m}^{-3}$) being 1.9 times higher than during winter (October - April) ($1.7 \pm 0.47 \mu\text{g C m}^{-3}$), which could indicate a noticeable biogenic contribution in summer. For Abastumani the winter time concentration was slightly higher than during summer, but only by minor margin; i.e. a factor 1.2.

There was an insignificant change in the annual mean concentration of OC when correcting for the influence of CO₃²⁻. For Abastumani >10% reduction in the OC concentration was observed for five of the samples.

7.4 Concentrations of CO₃²⁻ in PM₁₀

Quantifying carbonate is important not only in order to get more correct figures for EC and OC. For mass closure exercises it is important, as the conversion factor of carbonate-carbon to carbonate equals five, which is a pretty high number, thus even low concentrations of carbonate could make a substantial contribution to the particulate mass. For source apportionment studies it is of course important that one avoid attributing carbonate-carbon to either OC or EC, but rather to the mineral dust fraction where it rightfully belongs. Although the approach used to account for CO₃²⁻ in the present study is developed to provide corrected levels of EC and OC, it can be used to derive valuable information on the CO₃²⁻ content as well; as seen for the Abastumani and Borovoe sites.

For most samples collected at the Abastumani sites, levels of CO₃²⁻ were found to be rather low. I.e., for samples (n = 37) with a CO₃²⁻ concentration less than the annual mean ($< 0.5 \mu\text{g m}^{-3}$) the mean concentration was $0.15 \mu\text{g m}^{-3}$, whereas for those exceeding the annual mean (n = 7), the mean concentration was $2.3 \mu\text{g m}^{-3}$. Six of the seven samples with the highest CO₃²⁻ concentration also had a correspondingly high PM₁₀ concentration (i.e. within the 85 percentile), and for these samples CO₃²⁻ alone constituted 9% of the observed PM₁₀ concentration. This strongly suggests that mineral dust is a major contributing source to episodes of elevated concentrations of PM₁₀ at the Abastumani site.

The average CO₃²⁻ concentration at Borovoe was $0.2 \mu\text{g m}^{-3}$. As for Abastumani, peak values of CO₃²⁻ at Borovoe were associated with elevated concentrations of PM₁₀, although not as pronounced as observed for the Georgian site. Also, the peak CO₃²⁻ values at Borovoe was not nearly as high as those observed for the

Abastumani site; i.e. CO_3^{2-} MAX at Borovoe ($0.65 \mu\text{g m}^{-3}$) was nearly a factor of six less than CO_3^{2-} MAX at Abastumani ($3.7 \mu\text{g m}^{-3}$). Further, the contribution of CO_3^{2-} MAX to PM_{10} at Borovoe accounted for no more than 3.5% compared to 13.5% at Abastumani. Nevertheless, these findings suggest that mineral dust contributes substantially to episodes of elevated concentrations of PM_{10} also at the Borove site. More detailed information on the mineral dust composition, including the relative contribution of CO_3^{2-} , is needed to provide a quantitative estimate of the mineral dust contribution to PM_{10} at the two sites.

7.5 Concentrations of levoglucosan in PM_{10}

Levoglucosan is a thermal degradation product of cellulose and a unique tracer of particulate matter emissions from biomass burning, and thus used to study the influence of emissions from residential wood burning, wild and agricultural fires to the ambient aerosol particle loading. Estimates of carbonaceous aerosol (here: EC and OC) from biomass burning can be obtained by combining observed concentrations of levoglucosan and emission ratios for levoglucosan for wild/agricultural fires and for residential wood burning. For such calculations *a priori* knowledge of the actual biomass burning source is desirable, however typically not available. Here we have used the same OC/levoglucosan (10) and EC/Levoglucosan (2.5) emission ratios for the entire year when performing the calculations, despite that they are likely to change over the season. Thus, the results obtained should be regarded as estimates only. Here we briefly discuss the results from the Abastumani site in Georgia.

The annual mean concentration of levoglucosan in the PM_{10} size fraction at the Abastumani site was $52 \pm 39 \text{ ng m}^{-3}$. This is within the range reported for levoglucosan in the European rural background environment, but it should be considered to be in the medium to lower end. There was a pronounced seasonal variation with increased levels in winter ($70 \pm 36 \text{ ng m}^{-3}$) compared to summer ($14 \pm 4.0 \text{ ng m}^{-3}$), possibly reflecting increased wood burning for residential heating during the heating season. No pronounced correlation ($R^2 = 0.43$) was observed between levoglucosan and OC, suggesting that other sources dominated the ambient aerosol particle OC loading. A medium high correlation ($R^2 = 0.6$) was found when correlating levoglucosan and EC, suggesting that biomass burning was an important contributor to the observed levels of EC. The observed correlation was associated with samples collected during winter, indicating that residential wood burning was the biomass burning source. Figure 7.3 shows the rather similar temporal evolution of levoglucosan and EC on a monthly basis for the Abastumani site. Calculations suggested that 43% of the total EC loading could be attributed to biomass burning on an annual basis. The corresponding percentage for OC was 28%. The seasonal variation in the observed concentrations of levoglucosan, EC and OC caused EC from biomass burning to be relatively more abundant in winter (54% of EC) than in summer (21% of EC). For OC, 36% could be attributed to biomass burning in winter, whereas for summer the percentage was only 9.

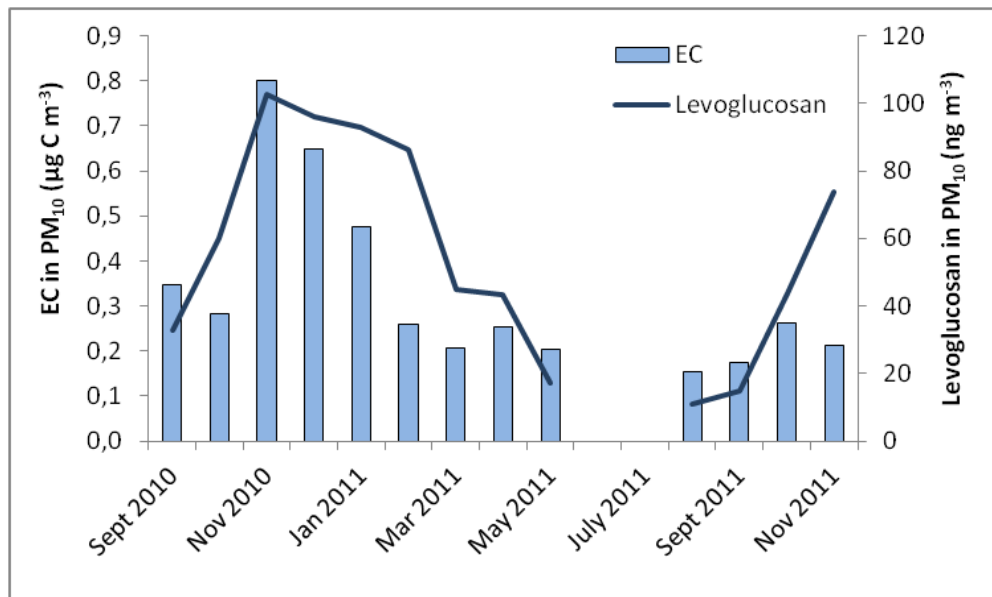


Figure 7.3: Monthly mean concentrations of EC and levoglucosan in PM₁₀ at the Abastumani site (Georgia).

7.6 Contribution of carbonaceous aerosol to PM₁₀

Chemical analysis of the ambient aerosol particle can provide important information about the various sources contributing to the ambient aerosol loading, including in a quantitative manner, e.g. when used as input to receptor models, as well as about chemical and physical processes taking place in the atmosphere. This is important as the ambient aerosol *pr.-se* is known to have adverse health effects, cause visibility degradation, contribute to acidification and eutrophication of ecosystems, causing material and crop damage, amongst others. Here we will use the results from the thermal-optical analysis to estimate the relative contribution of the carbonaceous aerosol to the mass concentration of PM₁₀. Further, we include CO₃²⁻ as part of the carbonaceous aerosol. In addition, levoglucosan has been used to apportion the part of EC and OC which can be attributed to biomass burning emissions.

To estimate the relative contribution of carbonaceous sub fractions to the mass concentration of PM₁₀ requires that OC (µg C m⁻³) is converted to organic matter (OM) (µg m⁻³) in order to account for other elements than carbon. Here we have applied a factor of 1.7 for OC, which is in line with the range applied for European EMEP sites. A conversion factor of 1.1 was used for EC. Unlike EC and OC, which are operational defined, CO₃²⁻ has a known empiric formula, however only the carbon content can be derived from the thermal-optical analysis, hence the conversion factor of 5 has been applied. For the fraction of OC that was apportioned to biomass burning a conversion factor of 2.4 was applied, which is similar to the levoglucosan-carbon to levoglucosan ratio of the tracer compound. This ratio should be considered in the upper range of conversion factors applied for this source. For EC originating from biomass burning a factor similar to that of EC from all sources was applied (i.e. 1.1).

The results show that on average 44% of the observed PM₁₀ mass concentration could be attributed to the carbonaceous aerosol on an annual basis at the Georgian Abastumani site (see Figure 7.4). Thus, the unknown fraction, likely to be dominated by secondary inorganic aerosol (SIA) constituents and mineral dust, were only slightly larger. A larger fraction of the observed PM₁₀ mass concentration was apportioned to the carbonaceous fraction in winter (47%) compared to summer (37%).

OM was the major carbonaceous fraction regardless of season, accounting for 40% of PM₁₀ in winter and 32% in summer. EC and CO₃²⁻ both contributed less than 4% to PM₁₀ regardless of season, but were more abundant in winter than for summer. OM from other sources than biomass burning dominated over OM from biomass burning regardless of season, but only by a marginal difference in winter; i.e. non-biomass burning OM accounted for 22% of PM₁₀ and biomass burning OM 18%. During summer the contribution of biomass burning OM to PM₁₀ was no more than approximately 4%, compared to 28% for OM from other sources.

The relative contribution of EC from other sources than biomass burning to PM₁₀ did not change between seasons (1.7 – 1.8%), whereas biomass burning EC was four times higher in winter (2.1% of PM₁₀) than during summer (0.5% of PM₁₀). Further, biomass burning EC was the major source of EC in winter.

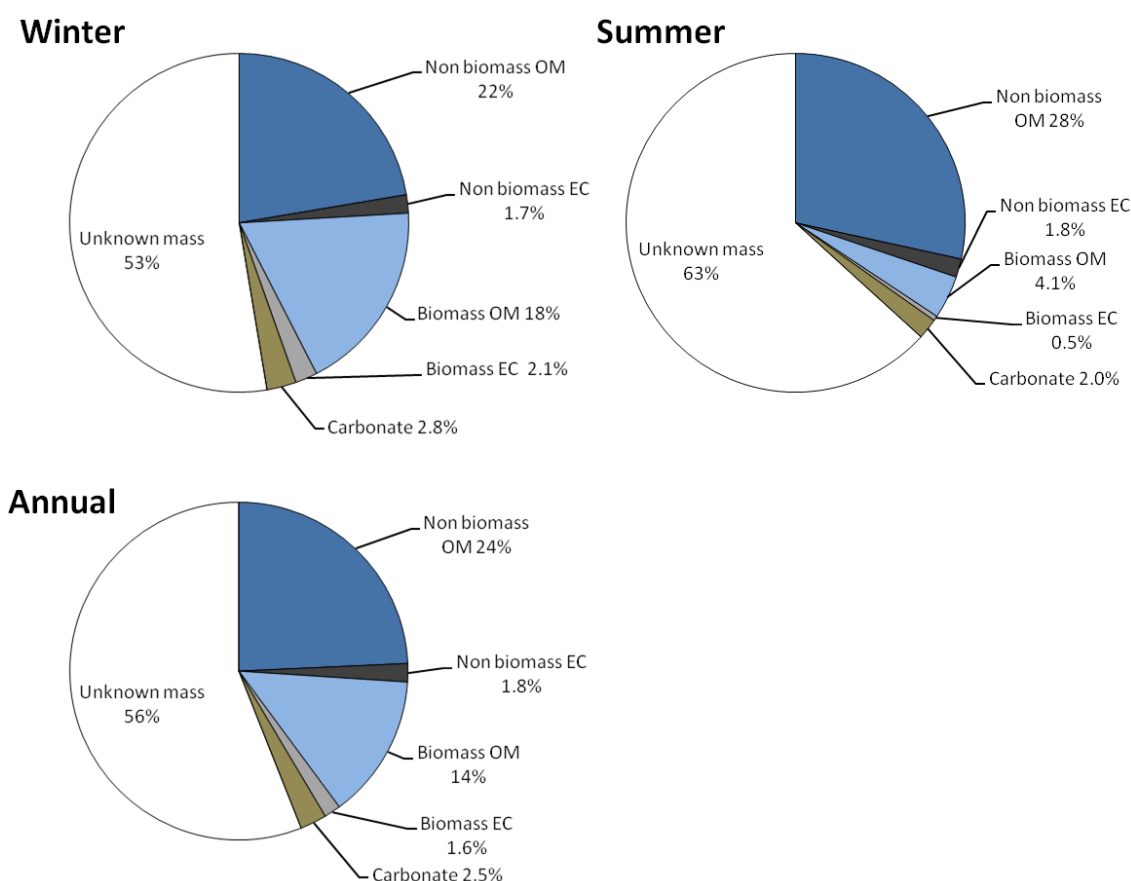


Figure 7.4: Relative contribution of carbonaceous sub fractions to the mass concentration of PM₁₀ at the Georgian rural background site Abastumani for winter, summer and the entire year.

7.7 General remarks

Although there is a positive trend with more measurements in the EECCA region there are still issues related to data quality and long term commitments, which needs to be addressed and improved. There are general problems with the regular EMEP measurements (level 1), as well as some specific issues for the campaign discussed in the current chapter. The various issues which need attention can be summarized as follows:

- Lack of long term funding from national governments to ensure proper maintenance of instruments and daily running costs. This may cause stop in measurements for longer periods and lack of compliance to the EMEP monitoring strategy, i.e. some parameters not measured at all.
- The ongoing activity appears to be too dependent on key personnel whom sometimes leave their positions. This makes the long term commitment vulnerable. It is a challenge to transfer knowledge from those persons which has been on training in field and which have had laboratory practices into permanent institutional knowledge.
- Data are not reported in standardised reporting routines. The data reporting, of routine data in particular, are somewhat ad hoc and often in a format which does not include all necessary metadata. This may cause additional uncertainties and errors in the reported data.

The standard operational routines (SOP) for sampling as well as recording necessary auxiliary data (flow, special events, start time etc) are often not followed. This might in some cases be due to not substantial and thorough enough field training from EMEP/CCC, as well as there might be problems with communication, often due to language barriers. There is a need to improve the understanding of and continuously emphasize that good quality data all depends on what is being done in the field, hence local involvements and the feeling of ownership and commitments is essential.

8 EMEP development endeavours towards better characterisation of atmospheric aerosol

8.1 Improved and extended measurement platform in EMEP

By Wenche Aas, Cathrine Lund Myhre

In the last decade, there has been a strong interaction between EMEP and several EU infrastructure projects. This has improved the measurement platform for especially aerosol properties on regional sites in Europe, typically joint EMEP/WMO GAW supersites. This collaboration with other networks and frameworks has been very important to develop EMEP, and this has explicitly been addressed in the monitoring strategy (ECE/EB.AIR/GE.1/2009/15).

In addition to being a catalyst for starting new measurements, the infrastructure projects contribute to quality assurance of measurements and are important for the development of new reference methods, and standardized format for data reporting. Figure 8.1 illustrates the development of new instrumentations providing measurements being available at the common database EBAS (<http://ebas.nilu.no/>) since the start of the FP5/GMES project CREATE (Construction, use and delivery of an European aerosol database) in 2002. CREATE was followed by the EU FP6 framework project EUSAAR (European Supersites for Atmospheric Aerosol Research) and now presently the EU FP7 framework project ACTRIS (Aerosols, Clouds and Trace gases Research InfraStructure Network). These two latter projects has been thoroughly presented in the two last EMEP PM reports, EMEP status report 4/2011 for EUSAAR and the EMEP status report 4/2012 for ACTRIS.

Not only have the atmospheric variables and number of instrument types reporting measurements to EMEP and EBAS (the y-axis in Figure 8.1) increased over this period, but also improvements of the methods and the data reporting formats as illustrated along the x-axis. The improved meta data description is an important documentation of the data quality. Within the ongoing project ACTRIS also development of new and improved new reference methods, and standardized format for reactive trace gases (NO_{xy} and VOCs) are included. Measurements employing the new reporting formats for these components are included for the first time in this year's EMEP-reporting.

The availability of new observational data for aerosol properties is a prerequisite for further development and improvement of the EMEP/MS-CW model as discussed in the next section.



Figure 8.1: Development of new data format and reporting of data to EMEP and WMO/GAW

8.2 EMEP-MAFOR: size-resolved aerosol model under development

By Svetlana Tsyro, Matthias Karl

Knowledge of the size distribution of atmospheric aerosols in the submicron size range is essential for estimation of aerosol radiative forcing and also health implications. Aerosol extinction of short and long wave radiation and interaction with clouds depends on their size. On the other hand, growing evidences suggest increased health effect from transport-related particles, in particular ultrafine ones (e.g. Oberdörster, 2001; WHO, 2005). As ultrafine particles contribute negligibly in PM_{10} and $PM_{2.5}$ mass, they should be described in terms of number concentrations.

Earlier developed UNI-AERO version of the EMEP model (Tsyro, 2008), based on the MONO-32 aerosol dynamics (Pirjola et al., 2003), has not been appropriately upgraded last years and consequently became outdated. The standard EMEP/MS-CW model deals with bulk aerosol mass, distinguishing solely between fine and coarse particles. Recently implemented calculations of Aerosol Optical Depth (AOD) and aerosol extinction coefficients are thus parameterized based on the aerosol total mass in the operational version. Obviously, the standard model version is not designed to calculate particle number density and size distribution.

Lately, a work has been initiated to develop the EMEP/MSC-W model towards simulating size-resolved particle number and mass concentrations. For this purpose, aerosol dynamics of the sectional aerosol model MAFOR (Karl et al., 2011; <http://mafor.nilu.no>) have been implemented in the EMEP/MSC-W model. The MAFOR (Marine Aerosol Formation) model has been developed for the specific purpose to simulate the formation and evolution of marine aerosols. Within the EU-project TRANSPHORM (“Transport related Air Pollution and Health impacts – Integrated Methodologies for Assessing Particulate Matter”), the MAFOR model has been further extended for use in simulations of particle number concentration (PNC) influenced by vehicular exhaust in urban environments (Karl et al., 2012). The interim name of the model under development is EMEP-MAFOR. The work is well in progress and the first tests are looking promising. Here, we make a brief summary of the approach applied and present some first model results and their comparison with measurements.

8.2.1 Short description of model approaches and process description

In the present version of EMEP-MAFOR, aerosol size distribution between 1 nm and 10 μm is represented with 16 size sections. Sectional models approximate the aerosol distribution by a finite number of size sections whose locations on the particle diameter axis can be variable with time or can be fixed. The fixed sectional method is the most convenient way to treat atmospheric transport and emission of particles, and nucleation of new particles, because the particle volume in one size section is always constant. Previous sectional models (Warren and Seinfeld, 1985; Jacobson and Turco, 1995; Pirjola and Kulmala, 2001) have focused on accurate treatment of the various aerosol dynamical processes in terms of number concentration but have not inherently secured that the initial mass concentrations of particulate compounds are consistent with initial particle numbers and that number and mass changes accordingly over time. The new approach consistently solves the time evolution of the particle number and mass concentration distribution of a multicomponent aerosol using the fixed sectional method in a robust manner on a 3-D atmospheric grid. The particles in each of the sections are assumed to be internally mixed. From the 16 size sections, four size “modes” are derived in the output, describing nucleation, Aitken, accumulation and coarse particles. Dependent on the modelling purpose and priorities, the number of size sections can be changed so that any multiple of 4 can be used (12, 16, 20, 24, etc.), where the minimum number of sections presently allowed is 12 (i.e. one aerosol mode is constructed based on 3 sections) and the maximum number is constrained by the available computational resources. MAFOR performs well in conserving mass during the condensation of vapours. That is, the overall mass balance for sulphate (as sum of gas phase and particle phase) was found to be quite accurately maintained and the total mass losses were within 1% in a one-day simulation, even for 12 size sections.

Certainly, for the purpose of regional and global size-resolve aerosol modelling, the computational efficiency of aerosol dynamics is essential requirement. The dependence of the computational demand (measured as CPU in seconds) on the number of size sections and the model-internal time step was tested with a box-version of the MAFOR model. CPU demand increases linearly when increasing the number of size sections (Figure 8.2a) and decreases following a power-law function when increasing the time step (Figure 8.2b). In the present version of

EMEP-MAFOR, the time step of the chemistry solver of the standard EMEP/MSC-W model is also used for the aerosol dynamics solver. For a full year run the EMEP-MAFOR with 16 size sections has a CPU demand which is a factor of 7-8 higher than the standard EMEP/MSC-W model with bulk aerosol.

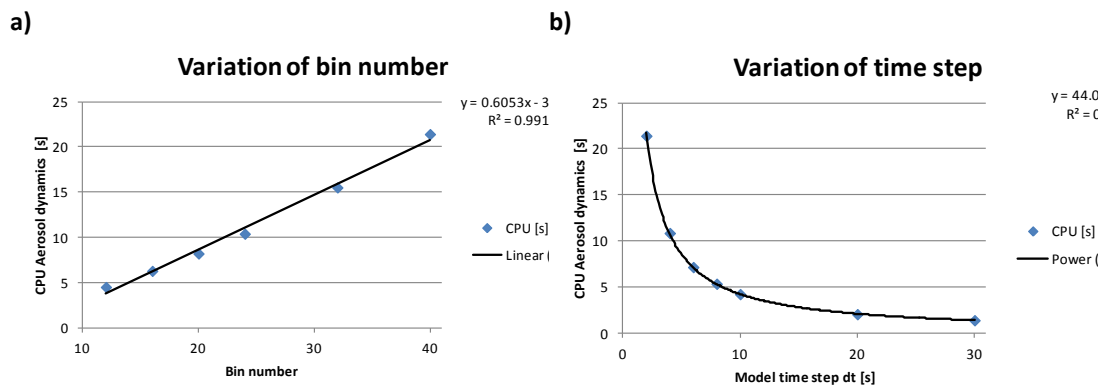


Figure 8.2: Dependence of the CPU demand for aerosol dynamics in the box-version of the MAFOR model: a) CPU vs. number of size sections, and b) CPU vs. length of model-internal time step.

The aerosol dynamic processes included in EMEP-MAFOR are: new particle formation by nucleation, particle growth due to coagulation (collision of two particles) and particle growth due to condensation of semi-volatile vapours (Figure 8.3 gives a schematic overview). The composition of particles in any size bin can change with time due to multicomponent condensation and/or due to coagulation of particles. The calculation of the water content in each size bin is parameterized with empirical polynomials for the mass fraction of solute.

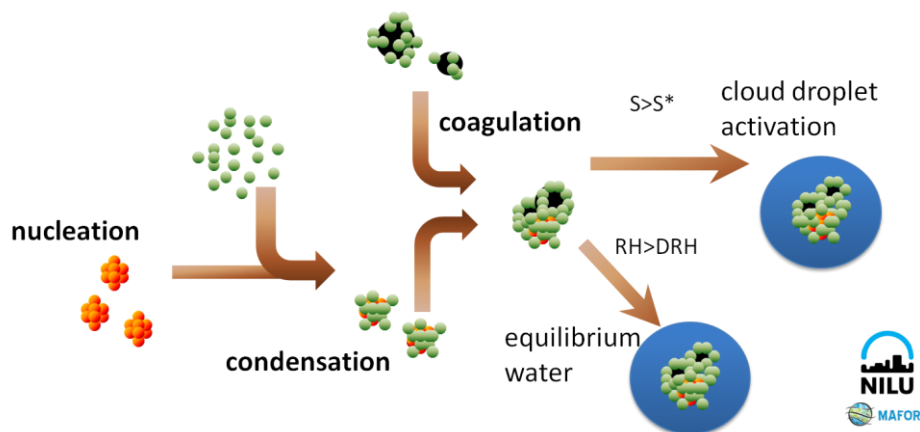


Figure 8.3: Illustration of particle nucleation and growth: condensation of organic molecules (green spheres) onto nucleated sulphuric acid clusters (orange), and coagulation of particles (black spheres denote pre-existing particles). Note: activation of particles into cloud condensation nuclei (CCN) is currently not implemented.

For nucleation, kinetic and activation approaches have so far been implemented. Sihto et al. (2006) reported that the nucleation mode particle concentration observed in a boreal forest (Hyytiälä, Southern Finland) typically depend on sulphuric acid concentration via a power-law relation with the exponent of 1 or 2. The proposed theory of atmospheric nucleation by cluster activation (Eq. 1) or kinetic nucleation (Eq. 2) could be used to explain the observed behaviour. The nucleation rate (production rate of 1 nm clusters, in $\text{cm}^{-3}\text{s}^{-1}$) for cluster activation can be written as (Kulmala et al., 2006):

$$J_{nucl} = A \cdot C_{g,H_2SO_4}, \quad (1)$$

and the nucleation rate for kinetic nucleation as:

$$J_{nucl} = B \cdot C_{g,H_2SO_4}^2, \quad (2)$$

with $A = 2.4 \times 10^{-7} \text{ s}^{-1}$ and $k = 3.2 \times 10^{-14} \text{ cm}^3 \text{ s}^{-1}$ from field measurements during the BACCI/QUEST IV campaign in Hyytiälä (Riipinen et al., 2007). The dependence of the nucleation rate on sulphuric acid concentration for the given nucleation parameters is illustrated in Figure 8.4.

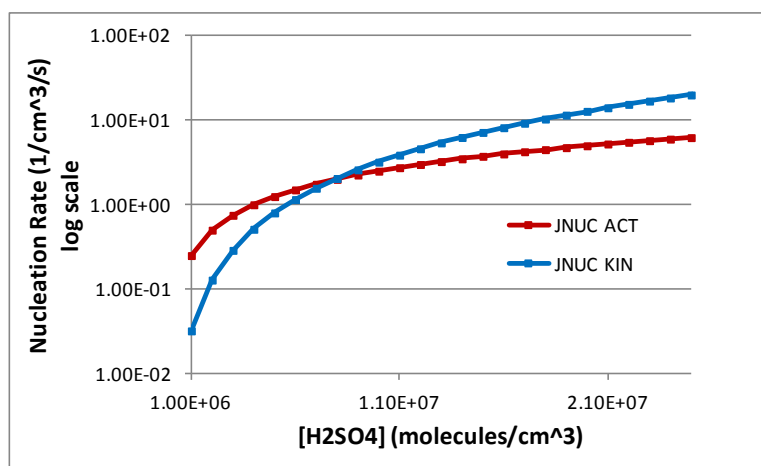


Figure 8.4: Dependence of nucleation rate on sulphuric acid (H_2SO_4) concentration for kinetic and activation approach.

Analysis of field and laboratory measurement data shows that the empirical nucleation coefficient A could range from 10^{-7} to 10^{-5} s^{-1} . Fountoukis et al. (2012) made assessments of aerosol number concentrations over Europe using the three-dimensional regional chemistry transport model PMCAMx-UF that included detailed aerosol microphysics. In the simulations, the values of $A = 2 \times 10^{-6} \text{ s}^{-1}$ and $k = 2.8 \times 10^{-13} \text{ cm}^3 \text{ s}^{-1}$ were used for activation and kinetic nucleation. With this configuration, Fountoukis et al. (2012) predicted that aerosol nucleation increased total particle number concentration (PNC) by a factor of 20 or more in areas with an extent of thousands of kilometres over the Balkans and Southeast Europe and during more localized events in Western and Central Europe.

The condensable vapours in the model are sulphuric acid and volatile organic compounds (VOCs). Growth of particles through multicomponent condensation is implemented according to the continuum/transition regime theory corrected by a

transitional correction factor (Fuchs and Sutugin, 1970). At the present stage, only biogenic VOCs, namely isoprene and α -pinene, are condensing on all particles. VOC condensation forms secondary organic aerosol (SOA), currently represented by one compound (“one-compound approach”). Saturation concentration of the condensable VOCs can be set by the model user. For the reference simulation we have used a saturation concentration of $C_{sat} = 0.1 \mu\text{g}/\text{m}^3$ for the condensable biogenic VOC. The following reactions have been added to the standard EMEP chemistry scheme, EMEP-EmChem09 (Simpson et al., 2012): reactions of SO_2 leading to sulphate and reactions of isoprene and α -pinene leading to biogenic SOA (as provided in Table 8.1).

Table 8.1: New reactions of SO_2 , isoprene and pinene included in EMEP/MSCW to produce vapours for nucleation and condensation (H_2SO_4 and BSOA). Squared brackets around species denote that the reaction is not included in the calculation of the gas phase concentration.

Rct. no.	Educts	Products	Rate constant
1	[OH] + [SO ₂]	H ₂ SO ₄	$K_{aq}(\text{OH}+\text{SO}_2) \cdot 2.0\text{e-}12$
2	[ISRO ₂] + [NO]	0.048 BSOA	KRO ₂ NO
3	[ISRO ₂] + [HO ₂]	0.078 BSOA	0.706·KHO ₂ RO ₂
4	APINENE + O ₃	TERPPeroxy	$6.3\text{e-}16 \cdot \exp(-580.0/T)$
5	APINENE + OH	TERPPeroxy	$1.2\text{e-}11 \cdot \exp(444.0/T)$
6	TERPPeroxy + NO	0.44 BSOA + NO ₂ + 1.2 HCHO + MGLYOX + 0.28 MAL + 1.70 HO ₂	KRO ₂ NO
7	TERPPeroxy + HO ₂	0.74 BSOA + HCHO + 0.3 MGLYOX + 0.7 CO + 0.46 OH + 0.60 HO ₂	KHO ₂ RO ₂

At this development stage, only sulphate and SOA mass from condensation of sulphuric acid and volatile organic compounds (VOCs) are explicitly size-resolved in calculations. The mass and number size distributions of the remaining primary and secondary particles (namely primary PM, SIA, sea salt and mineral dust) are currently derived from the bulk mass in a simplified manner. Henceforth, we refer to these particles as “bulk aerosols”. For this, assumptions are made regarding the modal distribution parameters of bulk aerosols (Geometric Mass Diameter, GMD; and Standard Deviation, σ) for the four size modes, namely GMD are 8, 60, 150 nm and 3 μm and σ are 1.45, 1.5, 1.55 and 1.80 for the nucleation, Aitken, accumulation and coarse modes respectively. These parameters are kept invariable within a model run. As the imposed size distribution greatly affects the resulting aerosol size distribution, we have performed a series of tests trying to constrain the distribution parameters through comparing model calculations with data from Asmi et al. (2011) and <http://www.atm.helsinki.fi/eusaar/>.

Dry deposition of the size-resolved aerosol distinguishes between nucleation mode, Aitken mode, accumulation mode and coarse mode which have deposition velocities calculated according to the new particle deposition scheme described in Simpson et al. (2012). Wet deposition of the size-resolved aerosol includes in-cloud and sub-cloud wet scavenging and also distinguishes the four aerosol modes.

8.2.2 Sensitivity studies

Modelling of VOC vapour condensation involves great uncertainties. A series of tests have been performed for biogenic SOA varying the saturation concentration. In a series of tests, saturation pressure C_{sat} was increased stepwise from 0.01 up to $1.0 \mu\text{g}/\text{m}^3$. Literature suggests to use very low values for C_{sat} within one-product approaches (e.g. Pierce et al., 2012) because only sufficiently low volatile vapours can enhance the growth of $<10 \text{ nm}$ particles to Aitken mode sizes to the degrees observed during new particle formation (NPF) events in forests. Figure 8.5 shows the simulated particle growth for various C_{sat} values for a selected period in June 2008 at the boreal station Hyytiälä in Southern Finland. Most drastic changes of the evolution of aerosol size spectrum are found for C_{sat} varying from 0.1 to $1.0 \mu\text{g m}^{-3}$. Decreasing C_{sat} below $0.1 \mu\text{g}/\text{m}^3$ does not appear to affect much aerosol growth probably due to the limited availability of the condensable vapours. In the case of $C_{sat} = 1.0 \mu\text{g}/\text{m}^3$, no apparent particle formation is predicted. In this case, particle condensation growth occurs mainly due to sulphuric acid. This process is not efficient enough to grow the nucleated clusters to any appreciable size before they are removed through coagulation on larger particles.

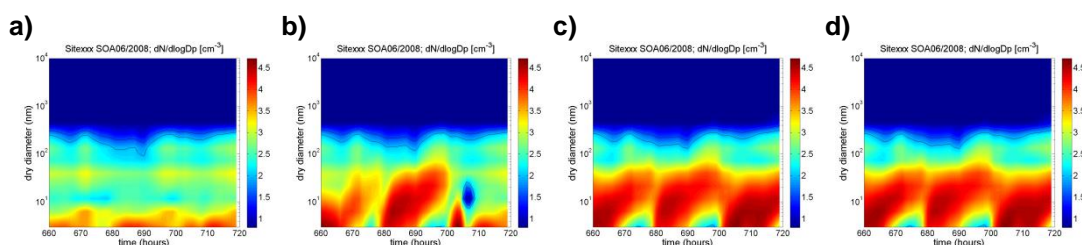


Figure 8.5: Simulated particle growth at Hyytiälä during a selected period in June 2008 with increasing C_{sat} of the condensable VOC: a) $1.0 \mu\text{g m}^{-3}$, b) $0.5 \mu\text{g m}^{-3}$, c) $0.1 \mu\text{g m}^{-3}$, and d) $0.01 \mu\text{g m}^{-3}$. Horizontal axis denotes dry diameter (nm) in logarithmic spacing and vertical axis denotes time in hours after 1st June 2008.

8.2.3 Preliminary results and comparison with measurements

In the following, we show results from EMEP-MAFOR calculations of size-resolved aerosol and first comparison of modelled number size distributions with a limited set of observations. A series of model runs has been performed in order to study the effect of some uncertain parameterisation parameters on calculation results (Table 8.2). Here, we look at the effects of (1) nucleation process; (2) VOC condensation (the lower saturation pressure the less volatile the VOC and thus the larger particle growth due to SOA formation); and (3) size distribution of bulk aerosols in Aitken mode.

The annual mean maps of calculated particle number concentrations (PNC) in 2008 are presented in Figure 8.6: shown are total PNC and respective PNCs in nucleation, Aitken and accumulation size modes from T0 run (Table 8.2). The nucleation mode particles contribute the most in the total PNC over Europe, followed by the contributions from Aitken and accumulation modes. The largest total PNC (and nucleation PNC) are associated with large SO_2 emission sources, where efficient nucleation of H_2SO_4 occur.

Table 8.2: Specification of parameters for model sensitivity runs.

	T0 (REF)	T1	T2	T3
Nucleation	Activation $A = 2.4 \times 10^{-7} \text{ s}^{-1}$	No	Activation $A = 2.4 \times 10^{-7} \text{ s}^{-1}$	Activation $A = 2.4 \times 10^{-7} \text{ s}^{-1}$
Csat	$0.1 \mu\text{g}/\text{m}^3$	$0.1 \mu\text{g}/\text{m}^3$	$1.0 \mu\text{g}/\text{m}^3$	$1.0 \mu\text{g}/\text{m}^3$
Bulk Aitken σ	1.5	1.5	1.5	2.0
Bulk Aitken GMD	60 nm	80 nm	80 nm	80 nm

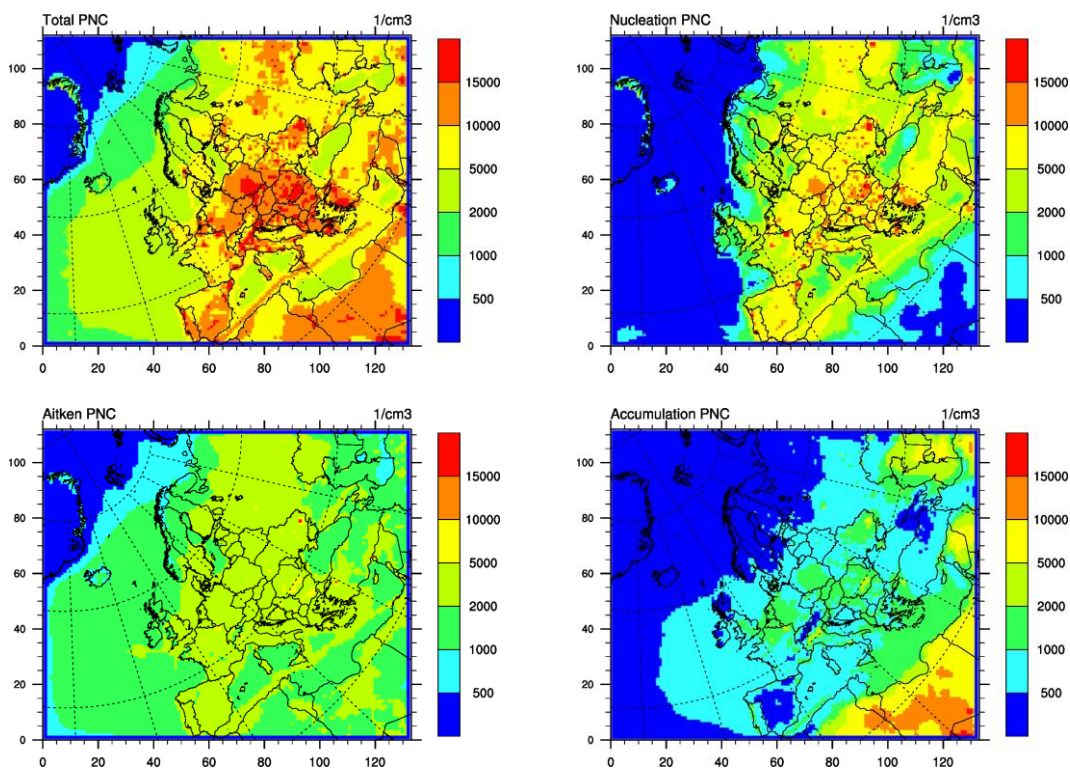


Figure 8.6: Model calculated annual mean particle number concentrations in 2008: total and in nucleation, Aitken and accumulation size modes (from T0 run in Table 8.2).

First evaluation of the model ability to reproduce observed particle size distributions has been performed using data presented in Asmi et al. (2011). Here, we have used statistics from the article and processed data available on <http://www.atm.helsinki.fi/eusaar/>, whereas the original observational data are stored at NILU EMEP database (EBAS) at <http://ebas.nilu.no/>. Note that the model calculations are performed for the year of 2008, whereas measurement data reported by Asmi et al. (2011) were collected in the period 2008-2009.

Asmi et al. (2011) found the general shape of aerosol size distributions, PNC histograms and their seasonal changes being relatively homogeneous over large geographical regions, also in areas with considerable contribution from anthropogenic sources. The smallest considered particles (with diameters between 30 and 50 nm) showed somewhat greater PNC variability because of their shorter lifetime (due to very efficient removal through coagulation scavenging and

deposition). Overall, this underlines the representativeness of the EUSAAR stations in terms of aerosol distribution properties and the suitability of the size distribution data for comparison with modelled size distributions from large-scale models that have relatively coarse spatial resolution.

Figure 8.7 shows model calculated and observed total PNC for particles in the diameter range of 10-1000 nm in different seasons for the Dutch site Cabauw. The model does reproduce the general pattern of the observed seasonal variation of PNC. Observed PNC has a clear minimum in springtime which is also seen in the model results although somewhat less pronounced. The model tends to underestimate the measured total PNC, greater in summer than in winter. In this way, EMEP-MAFOR predicts more particles in winter compared to summer PNC, whereas slightly more particles was observed in summer. The Reference model run (T0) and the run with a broader Aitken mode of bulk aerosols (T3) seem to produce PNC the closest to the observations, although summer and autumn PNC are much lower than observed. To understand the differences between modelled and observed total PNC, we look closer at PNCs in different size ranges and at number size distribution.

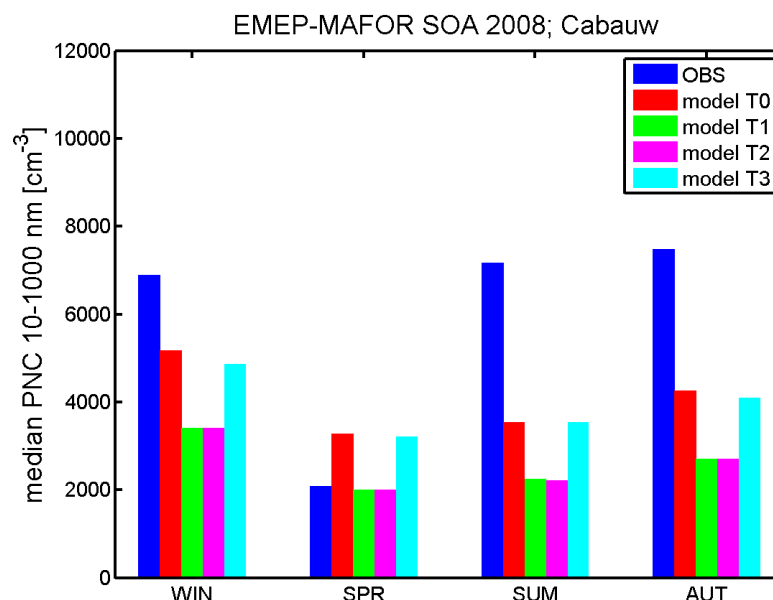


Figure 8.7: Seasonal mean number concentrations of particles in the diameter range of 10-1000 nm at Cabauw: observed (blue) and calculated in four model runs T0 – T3 (Table 8.2).

The comparison results of modelled number concentration in the sizes of 30-50 nm (N_{30-50}), 50 – 100 nm (N_{50-100}) and 100 - 500 nm ($N_{100-500}$) to observational data (2008-2009) published by Asmi et al. (2011), summarized in Table 8.3, suggests reasonable agreement (within a factor of 2-3) for most remote sites for the fraction of small particles (N_{30-50}) and accumulation mode ($N_{100-500}$), whereas the ultrafine fraction N_{50-100} is considerably underestimated by the model. The discrepancies are partly associated with uncertainties in the particle emission data, but are also due to currently deficient treatment of processes: better descriptions of particle deposition and of particle growth due to condensation of

inorganic and organic vapours, are expected to further improve the model's predictive capabilities.

Table 8.3: Median particle number concentrations in the size range 30 - 50 nm, 50 - 100 nm, and 100 - 500 nm. Model calculations are for 2008 from T0 run. Observed values in the period 2008-2009 adopted from Asmi et al. (2011).

Site	N₃₀₋₅₀ obs. (#/cm ³)	N ₃₀₋₅₀ model (#/cm ³)	N₅₀₋₁₀₀ obs. (#/cm ³)	N ₅₀₋₁₀₀ model (#/cm ³)	N₁₀₀₋₅₀₀ obs. (#/cm ³)	N ₁₀₀₋₅₀₀ model (#/cm ³)
Birkenes	156	683	293	162	218	237
Aspvreten	284	680	660	167	421	297
Hyytiälä	223	636	537	155	341	263
Pallas	89	337	94	93	111	100
K-Puszt	697	1068	1460	275	1660	866
Melpitz	860	1078	1023	269	1304	721
Kosetice	700	1063	1331	265	1863	743
Waldhof	878	1128	1245	275	1189	701
Cabauw	1914	1758	2435	421	952	1180
Finokalia	220	912	566	232	779	1212
Ispra	1341	1620	2319	386	2129	1156
Mace Head	105	912	99	214	142	386

Furthermore, we have compared modelled number size distribution with the observations separately for summer and winter seasons and results for Cabauw are presented in Figure 8.8. The results from four model sensitivity runs (Table 8.2) are shown.

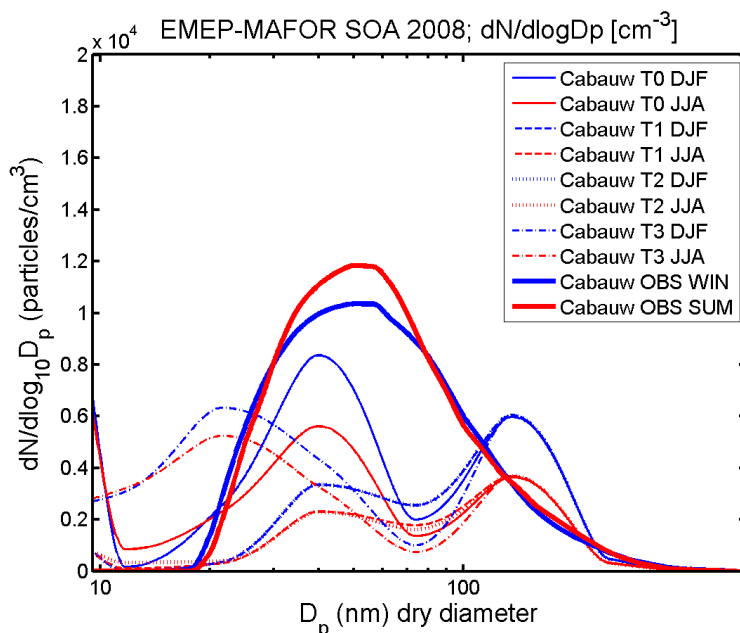


Figure 8.8: Average particle number size distribution observed (OBS) in 2008-09 and calculated (T0-T3) for 2008 in winter (DJF) and summer (JJA) at Cabauw, the Netherlands. Model test runs T0-T3 are described in Table 2.

The model predicts a pronounced bi-modal size distribution, with quite deep minimum between the Aitken and accumulation mode, which is not found in the observational data. Contrary to the measurements, calculated PNC densities of Aitken and accumulation mode are larger in winter (blue curves) than in summer (red curves) for all sizes and in all model runs. Most of accumulation particles are either primary emitted anthropogenic (PPM) and natural (sea salt and mineral dust) or secondary (SIA) from gaseous emissions. Overall, anthropogenic emissions are larger in winter in the EMEP model. The shape of PNC size distribution in the accumulation mode mostly relies on our initial assumptions for GMD and σ (Section 8.2.1).

It is more complicated for Aitken particles. The PNC and size distribution in the Aitken mode is affected by both PPM and SIA, but also on formation and evolution of nucleation particles. Dependent on the availability of condensable vapours, the freshly nucleated particles will either grow to Aitken sizes or will be scavenged by coagulation with Aitken particles. These competing processes modify the shape of Aitken size spectrum. The main findings from the sensitivity tests so far are:

- accounting for nucleation is a prerequisite for correct calculations of total PNC and number size distribution;
- appropriate description of nucleation particle growth, in particular through VOC condensation, is essential in order to reproduce observations, particularly during summer. Unfortunately, very limited PNC measurement data for particles below 10 nm concurrent with gas-phase sulphuric acid and VOC concentrations are available for constraining the new size-resolved model results;
- small changes in the distribution parameters of the Aitken mode of bulk aerosols have considerable effects on PNC and resulting size distribution in both nucleation and Aitken mode at the observation stations. In particular, the broader initial Aitken size spectrum in run T3 has resulted in a shift of Aitken mode to smaller sizes as compared to T2 (probably due to caused changes in the coagulation of nucleation particles onto Aitken ones).

Summarizing, the new EMEP-MAFOR model for calculating size-resolved aerosol is been under development. The first results and comparison with observations appear optimistic. The next working steps and model improvements, heavily relied on the extensive use of observational data, include:

- improvement of nucleation parameterisation;
- improvement of VOC condensation and SOA formation;
- implementation of size-resolved particle number emissions;
- implementation of size-resolved ammonium nitrate formation.

9 References

- Aas, W., Tsyro, S., Bieber, E., Bergström, R., Ceburnis, D., Ellermann, T., Fagerli, H., Frölich, M., Gehrig, R., Makkonen, U., Nemitz, E., Otjes, R., Perez, N., Perrino, C., Prévôt, A.S.H., Putaud, J.-P., Simpson, D., Spindler, G., Vana, M., Yttri, K. E. (2012) Lessons learnt from the first EMEP intensive measurement periods. *Atmos. Chem. Phys.*, *12*, 8073-8094. doi:10.5194/acp-12-8073-2012.
- Alemón, E., Herrera, L., Ortiz, E., Longoria, L.C. (2004). Instrumental nuclear activation analysis (INAA) characterization of environmental air filter samples. *Appl. Radiat. Isot.*, *60*, 6, 815-823.
- Alexandratos, N., Bruinsma, J. (2012) World agriculture towards 2030/2050, the 2012 revision. Rome, World Food and Agricultural Organization (ESA Working Paper, 12-3).
- Amann, M., Bertok, I., Borken, J., Chambers, A., Cofala, J., Dentener, F., Heyes, C., Hoglund, L., Klimont, Z., Purohit, P., Rafaj, P., Schöpp, W., Texeira, E., Toth, G., Wagner, F., Winiwarter, W. (2008) GAINS-Asia: A tool to combat air pollution and climate change simultaneously; Methodology. Laxenburg, International Institute for Applied Systems Analysis (IIASA). URL: <http://gains.iiasa.ac.at/gains/reports/GAINS-Asia-Methodology-20081205.pdf>
- Amann, M., Bertok, I., Borken-Kleefeld, J., Cofala, J., Heyes, C., Höglund-Isaksson, L., Klimont, Z., Nguyen, B., Posch, M., Rafaj, P., Sandler, R., Schöpp, W., Wagner, F., Winiwarter, W. (2011) Cost-effective control of air quality and greenhouse gases in Europe: modeling and policy applications. *Environ. Model. Software*, *26*, 1489–1501, doi:10.1016/j.envsoft.2011.07.012.
- Amann, M., Borken-Kleefeld, J., Cofala, J., Heyes, C., Klimont, Z., Rafaj, P., Purohit, P., Schöpp, W., Winiwarter, W. (2012) Future emissions of air pollutants in Europe – Current legislation baseline and the scope for further reductions. Laxenburg, International Institute for Applied Systems Analysis (TSAP Report #1).
- Amann, M., Klimont, Z., Wagner, F. (2013) Regional and global emissions of air pollutants: Recent trends and future scenarios. *Ann. Rev. Environ. Res.*, doi: 10.1146/annurev-environ-052912-173303. *In press*.
- Amato, F., Pandolfi, M., Escrig, A., Querol, X., Alastuey, A., Pey, J., Perez, N., Hopke, P.K. (2009) Quantifying road dust resuspension in urban environment by Multilinear Engine: a comparison with PMF2. *Atmos. Environ.*, *43*, 2770-2780.
- Asmi, A., Wiedensohler, A., Laj, P., Fjaeraa, A.-M., Sellegri, K., Birmili, W., and co-authors (2011) Number size distribution and seasonality of submicron particles in Europe 2008-2009. *Atmos. Chem. Phys.*, *11*, 5505-5538.
- Barnpadimos, I., Keller, J., Oderbolz, D., Hueglin, C., Prevot, A.S.H. (2012) One decade of parallel fine (PM_{2.5}) and coarse (PM₁₀-PM_{2.5}) particulate matter measurements in Europe: trends and variability. *Atmos. Chem. Phys.*, *12*, 3189–3203, doi:10.5194/acp-12-3189-2012.

- Bergametti, G., Dutot, A., Buat-Menard, P., Losno, R., Remoudaki, E. (1989) Seasonal variability of the elemental composition of atmospheric aerosol particles over the northwestern Mediterranean. *Tellus*, *41B*, 353-361.
- Bond, T.C., Doherty, S.J., Fahey, D.W., Forster, P.M., Berntsen, T., DeAngelo, B.J., Flanner, M.G., Ghan, S., Kärcher, B., Koch, D., Kinne, S., Kondo, Y., Quinn, P.K., Sarofim, M.C., Schultz, M.G., Schulz, M., Venkataraman, C., Zhang, H., Zhang, S., Bellouin, N., Guttikunda, S.K., Hopke, P.K., Jacobson, M.Z., Kaiser, J.W., Klimont, Z., Lohmann, U., Schwarz, J.P., Schindell, D., Storelvmo, T., Warren, S.G., Zender, C.S. (2013) Bounding the role of black carbon in the climate system: A scientific assessment. *J. Geophys. Res. Atmos.*, *118*, 5380-5552, doi:10.1002/jgrd.50171.
- Buhaus, Ø., Corbett, J.J., Endresen, Ø., Eyring, V., Faber, J., Hanayama, S., Lee, D.S., Lee, D., Lindstad, H., Markowska, A.Z., Mjelde, A., Nelissen, D., Nilsen, J., Pålsson, C., Winebrake, J.J., Wu, W., Yoshida, K. (2009) Second IMO GHG study 2009. London, International Maritime Organization (IMO).
- Calzolari, G., Chiari, M., Lucarelli, F., Mazzei, F., Nava, F., Prati, P., Valli, G., Vecchi, R. (2008) PIXE and XRF analysis of particulate matter samples: an inter-laboratory comparison. *Nucl. Instrum. Methods Phys. Res., Sect. B: Beam Interact. Mater. At.*, *266*, 2401-2404.
- Cofala, J., Amann, M., Klimont, Z., Kupiainen, K., Höglund-Isaksson, L. (2007) Scenarios of global anthropogenic emissions of air pollutants and methane until 2030. *Atmos. Environ.*, *41*, 8486-8499, doi:10.1016/j.atmosenv.2007.07.010.
- Drever, J.I. (1997) The geochemistry of natural waters: Surface and groundwater environments. Upper Saddle River, New Jersey, Prentice Hall.
- EEA (2009) Proposed gap-filling procedure for the European Community LRTAP Convention emission inventory. Technical paper for the meeting of the Air and Fuels Committee under Directive 96/62/EC, concerning 'Information on the Member States' reporting under the National Emission Ceilings Directive 2001/81/EC'. 28 September 2009, Brussels. European Environment Agency. Available upon request.
- EEA/CEIP (2013) Inventory review 2013. Review of emission data reported under the LRTAP Convention and NEC Directive. Stage 1 and 2 review. Review of emission inventories from shipping. Status of gridded and LPS data. By Mareckova K., Wankmueller, R., Murrels, T., Walker, H., Tista, M. Vienna, Umweltbundesamt (Technical report CEIP 1/2013).
- Elvidge, C.D., Baugh, K.E., Tuttle, B.T., Howard, A.T., Pack, D.W., Milesi, C., Erwin, E.H. (2007) A twelve year record of national and global gas flaring volumes estimated using satellite data: Final report to the World Bank. Boulder, NOAA National Geophysical Data Center. **URL:** http://ngdc.noaa.gov/eog/interest/flare_docs/DMSP_flares_20070530_b.pdf
- Elvidge, C.D., Baugh, K.E., Ziskin, D., Anderson, S., Ghosh, T. (2011) Estimation of gas flaring volumes using NASA MODIS fire detection products. Boulder, NOAA National Geophysical Data Center. **URL:** http://ngdc.noaa.gov/eog/interest/flare_docs/NGDC_annual_report_20110209.pdf

- EMEP (2013) Transboundary acidification, eutrophication and ground level ozone in Europe in 2010. Oslo, Norwegian Meteorological Institute (EMEP MSC-W & CCC & CEIP Status Report 1/2013).
- Escudero, M., Querol, X., Pey, J., Alastuey, A., Perez, N., Ferreira, F., Cuevas, E., Rodríguez, S., Alonso, S. (2007) A methodology for the quantification of the net African dust load in air quality monitoring networks. *Atmos. Environ.*, *41*, 5516–5524.
- EU (2008) Directive 2008/50/EC of the European Parliament and of the Council of 21 May 2008 on ambient air quality and cleaner air for Europe. *Off. J. Eur. Union: Legis*, L152, 1-44.
- Eyring, V., Isaksen, I.S.A., Berntsen, T., Collins, W.J., Corbett, J.J., Endresen, O., Grainger, R.G., Modanova, J., Schlager, H., Stevenson, D.S. (2010) Transport impacts on atmosphere and climate: Shipping. *Atmos. Environ.*, *44*, 4735-4771, doi:10.1016/j.atmosenv.2009.04.059.
- Fountoukis, C., Riipinen, I., Denier van der Gon, H.A.C., Charalampidis, P.E., Pilinis, C., Wiedensohler, A., O'Dowd, C., Putaud, J.P., Moerman, M., Pandis, S.N. (2012) Simulating ultrafine particle formation in Europe using a regional CTM: contribution of primary emissions versus secondary formation to aerosol number concentrations. *Atmos. Chem. Phys.*, *12*, 8663-8677.
- Fuchs, N.A., Sutugin, A.G. (1970) Highly dispersed aerosols. Ann Arbor, Mich., Ann. Arbor Sci., 1970.
- GEA (2012) Global energy Assessment: Toward a sustainable future. Cambridge, Cambridge University Press.
- Guenther, A.B., Jiang, X., Heald, C.L., Sakulyanontvittaya, T., Duhl, T., Emmons, L.K., Wang, X. (2012) The model of emissions of gases and aerosols from nature version 2.1 (MEGAN2.1): an extended and updated framework for modeling biogenic emissions. *Geosci. Model Dev. Discuss.*, *5*, 1503-1560, doi:10.5194/gmdd-5-1503-2012.
- Guinot, B., Cachier, H., Oikonomou, K. (2007) Geochemical perspectives from a new aerosol chemical mass closure, *Atmos. Chem. Phys.*, *7*, 1657-1670, doi:10.5194/acp-7-1657-2007.
- Hjellbrekke, A.-G., Fjæraa, A.M. (2012) Data report 2010. Acidifying and eutrophying compounds and particulate matter. Kjeller, NILU (EMEP/CCC-Report 1/2012).
- Höglund-Isaksson, L. (2012) Global anthropogenic methane emissions 2005–2030: technical mitigation potentials and costs. *Atmos. Chem. Phys.*, *12*, 9079-9096, doi:10.5194/acp-12-9079-2012.
- Huo, H., Yao, Z., Zhang, Y., Shen, X., Zhang, Q., He, K. (2012) On-board measurements of emissions from diesel trucks in five cities in China. *Atmos. Environ.*, *54*, 159-167, doi:10.1016/j.atmosenv.2012.01.068.
- IEA (2011) World Energy Outlook 2011. Paris, International Energy Agency.

- IPCC (2007) Climate Change 2007: The Physical Science Basis. Contribution of Working Group I to the Fourth Assessment Report of the Intergovernmental Panel on Climate Change. Ed. by S. Solomon, D. Qin, M. Manning, Z. Chen, M. Marquis, K.B. Averyt, M. Tignor and H.L. Miller. Cambridge, Cambridge University Press.
- Isaksen, I.S.A., Granier, C., Myhre, G., Berntsen, T.K., Dalsøren, S.B., Gauss, M., Klimont, Z., Benestad, R., Bousquet, P., Collins, W., Cox, T., Eyring, V., Fowler, D., Fuzzi, S., Jöckel, P., Laj, P., Lohmann, U., Maione, M., Monks, P., Prevot, A.S.H., Raes, F., Richter, A., Rognerud, B., Schulz, M., Shindell, D., Stevenson, D.S., Storelvmo, T., Wang, W.-C., van Weele, M., Wild, M., Wuebbles, D. (2009) Atmospheric composition change: Climate-chemistry interactions. *Atmos. Environ.*, *43*, 5138-5192, doi:10.1016/j.atmosenv.2009.08.003.
- Jacobson, M.Z., Turco, R.P. (1995) Simulating condensational growth, evaporation, and coagulation of aerosols using a combined moving and stationary grid. *Aerosol Sci. Technol.*, *22*, 73-92.
- Kallos, G., Papadopoulos, A., Katsafados, P., Nickovic, S. (2006) Transatlantic Saharan dust transport: Model simulation and results. *J. Geophys. Res.*, *111*, D09204, doi:10.1029/2005JD006207.
- Karanasiou, A., Diapouli, E., Cavalli, F., Eleftheriadis, K., Viana, M., Alastuey, A., Querol, X., Reche, C. (2011) On the quantification of atmospheric carbonate carbon by thermal/optical analysis protocols. *Atmos. Meas. Tech.*, *4*, 2409–2419.
- Karl, M., Denby, B.R., Lützenkirchen, S., Henzing, J.S., Keuken, M. (2012) Modelling PNC from kerbside to urban scale. In: *Proceedings of abstracts 8th International Conference on Air Quality - Science and Applications, Athens, 19-23 May 2012*. Red.: Singh, V., Price, H., Bartzis, J., Sohki, R.S. Athens, University of Hertfordshire, p. 77.
- Karl, M., Gross, A., Leck, C., Pirjola, L. (2011) A new flexible multicomponent model for the study of aerosol dynamics in the marine boundary layer. *Tellus*, *63B*, 1001-1025.
- Klein, H., Nickovic, S., Haunold, W., Bundke, U., Nillius, B., Ebert, M., Weinbruch, S., Schuetz, L., Levin, Z., Barrie, L. A., Bingemer, H. (2010) Saharan dust and ice nuclei over Central Europe. *Atmos. Chem. Phys.*, *10*, 10211–10221.
- Klimont, Z., Kupiainen, K., Heyes, Ch., Purohit, P., Cofala, J., Rafaj, P., Schoepp, W. (2013) Global anthropogenic emissions of particulate matter. *In preparation*.
- Klimont, Z., Smith, S.J., Cofala, J. (2013) The last decade of global anthropogenic sulfur dioxide: 2000-2011 emissions. *Environ. Res. Lett.*, *8*, 014003, doi:10.1088/1748-9326/8/1/014003.
- Klimont, Z., Streets, D. (2007) Emission inventories and projections for assessing hemispheric or intercontinental transport. In: *Hemispheric Transport of Air Pollution 2007*. Ed. by T. Keating and A. Zuber. New York and Geneva, United Nations, Economic Commission for Europe.

- Klimont, Z., Streets, D.G., Gupta, S., Cofala, J., Lixin, F., Ichikawa, Y. (2002) Anthropogenic emissions of non-methane volatile organic compounds (NMCOC) in China. *Atmos. Environ.*, *36*, 1309-1322, doi:10.1016/S1352-2310(01)00529-5.
- Kulmala, M., Lehtinen, K.E.J., Laaksonen, A. (2006) Cluster activation theory as an explanation of the linear dependence between formation rate of 3nm particles and sulphuric acid concentration. *Atmos. Chem. Phys.*, *6*, 787-793.
- Kulmala, M., Lehtinen, K.E.J., Laaksonen, A. (2006) Cluster activation theory as an explanation of the linear dependence between formation rate of 3nm particles and sulphuric acid concentration. *Atmos. Chem. Phys.*, *6*, 787-793.
- Lamarque, J.F., Bond, T.C., Eyring, V., Granier, C., Heil, A., Klimont, Z., Lee, D., Liousse, C., Mieville, A., Owen, B., Schultz, M.G., Shindell, D., Smith, S.J., Stehfest, E., Van Aardenne, J., Cooper, O.R., Kainuma, M., Mahowald, N., McConnell, J.R., Naik, V., Riahi, K., van Vuuren, D.P. (2010) Historical (1850-2000) gridded anthropogenic and biomass burning emissions of reactive gases and aerosols: Methodology and application. *Atmos. Chem. Phys.*, *10*, 7017-7039, doi:10.5194/acp-10-7017-2010.
- Landesamt für Natur, Umwelt und Verbraucherschutz NRW (2007) Luftqualitätsüberwachungssystem LUQS [webpage]. Recklinghausen. **URL:** <http://www.lanuv.nrw.de/luft/immissionen/luqs/e0.html> [Accessed 2013-08-05]
- Lee, D.S., Fahey, D.W., Forster, P.M., Newton, P.J., Wit, R.C.N., Lim, L.L., Owen, B., Sausen, R. (2009) Aviation and global climate change in the 21st century. *Atmos. Environ.*, *43*, 3520-3537, doi:10.1016/j.atmosenv.2009.04.024.
- Lucarelli, F., Nava, S., Calzolari, G., Chiari, M., Udisti, R., Marino, F. (2011) Is PIXE still a useful technique for the analysis of atmospheric aerosols? The LABEC experience. *X-Ray Spectrometry*, *40*, 162-167, doi: 10.1002/xrs.1312.
- Maenhaut, W., Vermeylen, R., Claeys, M., Vercauteren, J., Matheussen, C., Roekens, E. (2012) Assessment of the contribution from wood burning to the PM10 aerosol in Flanders, Belgium. *Sci. Total Environ.*, *437*, 226-236.
- Mitsakou, C., Kallos, G., Papantoniou, N., Spyrou, C., Solomos, S., Astitha, M., Housiadas, C. (2008) Saharan dust levels in Greece and received inhalation doses. *Atmos. Chem. Phys.*, *8*, 7181-7192.
- Mont, Z., Cofala, J., Xing, J., Wei, W., Zhang, C., Wang, S., Kejun, J., Bhandari, P., Mathus, R., Purohit, P., Rafaj, P., Chambers, A., Amann, M., Hao, J. (2009) Projections of SO₂, NO_x, and carbonaceous aerosols emissions in Asia. *Tellus*, *61B*, 602-617, doi:10.1111/j.1600-0889.2009.00428.x.
- Moreno, N., Querol, X., Andrés, J.M., López-Soler, A., Stanton, K., Towler, M., Nugteren, H., Janssen, M. (2004) Determining the Suitability of A Fly Ash for Silica Extraction and Zeolitisation. *J. Chem. Technol. Biotechnol.*, *79*, 1009-1018.
- Moreno, T., Querol, X., Castillo, S., Alastuey, A., Cuevas, E., Herrmann, L., Mounkaila, M., Elvira, J., Gibbons, W. (2006) Geochemical variations in aeolian mineral particles from the Sahara-Sahel Dust Corridor. *Chemosphere*, *65*, 261-270.

- Oberdörster, G. (2001) Pulmonary effects of inhaled ultrafine particles. *Int. Arch. Occup. Environ. Health*, 74, 1-8.
- Pandolfi, M., Gonzalez-Castanedo, Y., Alastuey, A., de la Rosa, J.D., Mantilla, E., Sanchez de la Campa, A., Querol, X., Pey, J., Amato, F., Moreno T. (2011) Source apportionment of PM₁₀ and PM_{2.5} at multiple sites in the strait of Gibraltar by PMF: impact of shipping emissions. *Environ. Sci. Pollut. Res.*, 18, 260-269.
- Pey, J., Querol, X., Alastuey, A., Forastiere, F., Stafoggia, M. (2013) African dust outbreaks over the Mediterranean Basin during 2001–2011: PM₁₀ concentrations, phenomenology and trends, and its relation with synoptic and mesoscale meteorology. *Atmos. Chem. Phys.*, 13, 1395-1410.
- Pfeffer, U., Breuer, L., Gladtke, D., Schuck, T. J. (2013) Contribution of wood burning to the exceedance of PM₁₀ limit values in North Rhine-Westphalia. *Gefahrstoffe Reinhaltung der Luft*, 6/2013, 239-245.
- Piazzalunga, A., Belis, C., Bernardoni, V., Cazzuli, O., Fermo, P., Valli, G., Vecchi, R. (2011) Estimates of wood burning contribution to PM by the macro-tracer method using tailored emission factors. *Atmos. Environ.*, 45, 6642 – 6649.
- Pierce, J.R., Leaitch, W.R., Liggio, J., Westervelt, D.M., Wainwright, C.D., Abbatt, J.P.D., and co-authors (2012) Nucleation and condensational growth to CCN sizes during a sustained pristine biogenic SOA event in a forested mountain valley. *Atmos. Chem. Phys.*, 12, 3147-3163.
- Pirjola, L., Kulmala, M. (2001) Development of particle size and composition distributions with a novel aerosol dynamics model. *Tellus*, 53B, 491-509.
- Pirjola, L., Tsyro, S., Tarrasòn, L., Kulmala, M. (2002) A monodisperse aerosol dynamics module – a promising candidate for use in long-range transport models: Box-model tests. *J. Geophys. Res.*, 108, D9, 4258, doi:10.1029/2002JD002867, 2003.
- Purohit, P., Amann, M., Mathus, R., Gupta, I., Marwah, S., Verma, V., Bertok, I., Borcken, J., Chambers, A., Cofala, J., Heyes, C., Hoglund, L., Klimont, Z., Rafai, P., Sandler, R., Schöpp, W., Toth, G., Wagner, F., Winiwarter, W. (2010) GAINS-Asia: Scenarios for Cost-Effective Control of Air Pollution and Greenhouse Gases in India. **URL:** <http://gains.iiasa.ac.at/images/stories/reports/Asia/IR-GAINS-India.pdf> (Accessed 9 August 2012)
- Putaud, J.-P., Van Dingenen, R., Alastuey, A., Bauer, H., Birmili, W., Cyrys, J., Flentje, H., Fuzzi, S., Gehrig, R., Hansson, H.C., Harrison, R.M., Herrmann, H., Hitenberger, R., Hüglin, C., Jones, A.M., Kasper-Giebl, A., Kiss, G., Koussa, A., Kuhlbusch, T.A.J., Löschau, G., Maenhaut, W., Molnar, A., Moreno, T., Pekkanen, J., Perrino, C., Pitz, M., Puxbaum, H., Querol, X., Rodriguez, S., Salma, I., Schwarz, J., Smolik, J., Schneider, J., Spindler, G., ten Brink, H., Tursic, J., Viana, M., Wiedensohler, A., Raes, F. (2010) A European aerosol phenomenology - 3: Physical and chemical characteristics of particulate matter from 60 rural, urban, and kerbside sites across Europe. *Atmos. Environ.*, 44, 1308-1320.

- Putaud, J.-P., Van Dingenen, R., Dell'Acqua, A., Raes, F., Matta, E., Decesari, S., Facchini, M. C., Fuzzi, S. (2004) Size-segregated aerosol mass closure and chemical composition in Monte Cimone (I) during MINATROC. *Atmos. Chem. Phys.*, 4, 889-902, doi:10.5194/acp-4-889-2004.
- Puxbaum, H., Caseiro, A., Sánchez-Ochoa, A., Kasper-Giebl, A., Claeys, M., Gelencsér, A., Legrand, M., Preunkert, S., Pio, C. (2007) Levoglucosan levels at background sites in Europe for assessing the impact of biomass combustion on the European aerosol background. *J. Geophys. Res.*, 112, D23S05, doi:10.1029/2006JD008114.
- Querol, X., Alastuey, A., Rodríguez, S., Plana, F., Ruiz, C.R., Cot, N., Massagué, G., Puig, O. (2001) PM₁₀ and PM_{2.5} source apportionment in the Barcelona Metropolitan Area, Catalonia, Spain. *Atmos. Environ.*, 35/36, 6407-6419.
- Querol, X., Pey, J., Pandolfi, M., Alastuey, A., Cusack, M., Pérez, N., Moreno, T., Viana, M., Mihalopoulos, N., Kallos, G., Kleanthous, S. (2009) African dust contributions to mean ambient PM₁₀ levels across the Mediterranean Basin. *Atmos. Environ.*, 43, 4266-4277.
- Riahi, K., Dentener, F., Gielen, D., Grubler, A., Jewell, J., Klimont, Z., Krey, V., McCollum, D., Pachauri, S., Rao, S., van Ruijven, B., van Vuuren, D.P., Wilson, C. (2012) Chapter 17 – Energy Pathways for Sustainable Development. In: *Global Energy Assessment – Toward a Sustainable Future*. Cambridge/Laxenburg, Cambridge University Press/International Institute for Applied Systems Analysis. pp. 1203-1306. **URL:** www.globalenergyassessment.org
- Riipinen, I., Sihto, S.-L., Kulmala, M., Arnold, F., Dal Maso, M., Birmili, W., Saarnio, K., Teinilä, K., Kerminen, V.-M., Laaksonen, A., Lehtinen, K.E.J. (2007) Connections between atmospheric sulphuric acid and new particle formation during QUEST III–IV campaigns in Heidelberg and Hyytiälä. *Atmos. Chem. Phys.*, 7, 1899-1914.
- Rodríguez, S., Alastuey, A., Querol, X. (2012) A review of methods for long term in situ characterization of aerosol dust. *Aeolian Res.*, 6, 55-74.
- Rodríguez, S., Querol, X., Alastuey, A., Kallos G., Kakaliagou, O. (2001) Saharan dust contributions to PM₁₀ and TSP levels in Southern and Eastern Spain, *Atmos. Environ.*, 35, 20 2433–2447.
- Schauer, J.J., Lough, G.C., Shafer, M.M., Christensen, W.F., Arndt, M.F., DeMinter, J.T., Park, J.-S. (2006) Characterization of metals emitted from motor vehicles. Boston, Health Effect Institute (Research report, 133). **URL:** <http://pubs.healtheffects.org/view.php?id=150>
- Schmidl, C., Luisser, M., Padouvas, E., Lasselsberger, L., Rzaca, M., Ramirez-Santa Cruz, C., Handler, M., Peng, G., Bauer, H., Puxbaum, H. (2011) Particulate and gaseous emissions from manually and automatically fired small scale combustion systems. *Atmos. Environ.*, 45, 7443 – 7454.
- Schmidl, C., Marr, I.L., Caseiro, A., Kotianova, P., Berner, A., Bauer, H., Kasper-Giebl, A., Puxbaum, H. (2008) Chemical characterisation of fine particle emissions from wood stove combustion of common woods growing in mid-European Alpine regions. *Atmos. Environ.*, 42, 126 - 141

- Sciare, J., Oikonomou, K., Favez, O., Markaki, Z., Liakakou, E., Cachier, H., Mihalopoulos, N. (2008) Long-term measurements of carbonaceous aerosols in the Eastern Mediterranean: Evidence of long-range transport of biomass burning. *Atmos. Chem. Phys.*, 8, 5551-5563.
- Sihto, S.-L., Kulmala, M., Kerminen, V.-M., Dal Maso, M., Petäjä, T., Riipinen, I., Korhonen, H., Arnold, F., Janson, R., Boy, M., Laaksonen, A., Lehtinen, K.E.J. (2006) Atmospheric sulphuric acid and aerosol formation: Implications from atmospheric measurements for nucleation and early growth mechanisms. *Atmos. Chem. Phys.*, 6, 4079-4091.
- Simpson, D., Benedictow, A., Berge, H., Bergström, R., Emberson, L.D., Fagerli, H., Hayman, G.D., Gauss, M., Jonson, J.E., Jenkin, M.E., Nyiri, A., Richter, C., Semeena, V.S., Tsyro, S., Tuovinen, J.-P., Valdebenito, A., Wind, P. (2012) The EMEP MSC-W chemical transport model – technical description, *Atmos. Chem. Phys.*, 12, 7825-7865, doi:10.5194/acp-12-7825-2012.
- Stohl, A., Klimont, Z., Eckhardt, S., Kupiainen, K. (2013) Why models struggle to capture Arctic Haze: the underestimated role of gas flaring and domestic combustion emissions. *Atmos. Chem. Phys. Discuss.*, 13, 9567-9613, doi:10.5194/acpd-13-9567-2013.
- Stohl, A., Berg, T., Burkhardt, J.F., Fjæraa, A.M., Forster, C., Herber, A., Hov, Ø., Lunder, C., McMillan, W.W., Oltmans, S., Shiobara, M., Simpson, D., Solberg, S., Stebel, K., Ström, J., Tørseth, K., Treffeisen, R., Virkkunen, K., Yttri, K.E. (2007) Arctic smoke – record high air pollution levels in the European Arctic due to agricultural fires in Eastern Europe in spring 2006. *Atmos. Chem. Phys.*, 7, 511-534.
- Tørseth, K., Aas, W., Breivik, K., Fjæraa, A.M., Fiebig, M., Hjellbrekke, A.G., Lund Myhre, C., Solberg, S., Yttri, K.E. (2012) Introduction to the European Monitoring and Evaluation Programme (EMEP) and observed atmospheric composition change during 1972–2009. *Atmos. Chem. Phys.*, 12, 5447-5481, doi:10.5194/acp-12-5447-2012.
- Tsyro, S. (2008) Regional model for formation, dynamics, and long-range transport of atmospheric aerosol: Study of atmospheric aerosol properties in Europe. *Russ. Meteorol. Hydrol.*, 33, 300-309.
- Umweltbundesamt (2012) Luftqualität 2011 - Feinstaubepisoden prägten das Bild. Dessau-Roßlau, UBA. URL: <http://www.umweltdaten.de/publikationen/fpdf-1/4211.pdf>
- UNECE (2009) Guidelines for reporting emission data under the Convention on Long-Range Transboundary Air Pollution. Geneva (ECE/EB.AIR/97). URL: http://www.ceip.at/fileadmin/inhalte/emep/reporting_2009/Rep_Guidelines_ECE_EB_AIR_97_e.pdf [07-08-2012]
- UNEP (2011) Near-term climate protection and clean air benefits: Actions for controlling short-lived climate forcers. Nairobi, United Nations Environment Programme (UNEP). URL: http://www.unep.org/dewa/Portals/67/pdf/Near_Term_Climate_Protection_&Air_Benefits.pdf (Accessed 12 March 2012)

- UNEP/WMO (2011) Integrated assessment of black carbon and tropospheric ozone. Nairobi, Kenya. **URL:** www.unep.org/dewa/Portals/67/pdf/BlackCarbon_report.pdf
- Van Loy, M., Bahadori, T., Wyzga, R., Hartsell, B., Edgerton, E. (2000) The aerosol research and inhalation epidemiology study (ARIES): PM_{2.5} mass and aerosol component concentrations and sampler intercomparisons. *J. Air Waste Manag. Assoc.*, 50, 1446-1458.
- van Vuuren, D.P., Edmonds, J., Kainuma, M., Riahi, K., Thomson, A., Hibbard, K., Hurtt, G.C., Kram, T., Krey, V., Lamarque, J.-F., Masui, T., Meinshausen, M., Nakicenovic, N., Smith, S.J., Rose, S.K. (2011) The representative concentration pathways: an overview. *Climatic Change*, 109, 5-31, doi:10.1007/s10584-011-0148-z.
- Vestreng, V., Myhre, G., Fagerli, H., Reis, S., Tarrasón, L. (2007) Twenty-five years of continuous sulphur dioxide emission reduction in Europe. *Atmos. Chem. Phys.*, 7, 3663-3681.
- Viana, M., Kuhlbusch, T.A.J., Querol, X., Alastuey, A., Harrison, R.M., Hopke, P.K., Winiwarter, W., Vallius, M., Szidat, S., Prévôt, A.S.H., Hueglin, C., Bloemen, H., Wählín, P., Vecchi, R., Miranda, A.I., Kasper-Giebl, A., Maenhaut, W., Hitznerberger, R. (2008) Source apportionment of particulate matter in Europe: a review of methods and results. *J. Aerosol Sci.*, 39, 827-849.
- Warren, D.R., Seinfeld, J.H. (1985) Simulation of aerosol size distribution evolution in systems with simultaneous nucleation, condensation, and coagulation. *Aerosol Sci. Technol.*, 4, 31-43.
- Wei, W., Wang, S., Chatani, S., Klimont, Z., Cofala, J. (2008) Emission and speciation of non-methane volatile organic compounds from anthropogenic sources in China. *Atmos. Environ.*, 42, 4976-4988, doi:10.1007/s10584-011-0148-z.
- WHO (2005) Air quality guidelines for particulate matter, ozone, nitrogen dioxide and sulfur dioxide - Global update 2005. Copenhagen, World Health Organization. **URL:** http://www.who.int/phe/health_topics/outdoorair_aqg/en/ [2011-08-16].
- WHO (2005) Health effects of transport-related air pollution. Ed. by Krzyzanowski, M., Kuna-Dibbert, B., Schneider, J. Copenhagen, World Health Organization.
- Xu, Y. (2011) Improvements in the operation of SO₂ scrubbers in China's coal power plants. *Environ. Sci. Technol.*, 45, 380-385, doi:10.1021/es1025678.
- Xu, Y., Williams, R.H., Socolow, R.H. (2009) China's rapid deployment of SO₂ scrubbers. *Energy Environ. Sci.*, 2, 459-465, doi:10.1039/B901357C.
- Zhang, Q., Streets, D.G., Carmichael, G.R., He, K.B., Huo, H., Kannari, A., Klimont, Z., Park, I.S., Reddy, S., Fu, J.S., Chen, D., Duan, L., Lei, Y., Wang, L.T., Yao, Z.L. (2009) Asian emissions in 2006 for the NASA INTEX-B mission. *Atmos. Chem. Phys.*, 9, 5131-5153, doi:10.5194/acp-9-5131-2009.

APPENDIX A

Table A.1: Statistic analysis of model calculated PM₁₀ against observations in 2011.

Here, Obs – the measured mean, Mod – the calculated mean, Bias is calculated as $\Sigma(\text{Mod-Obs})/\text{Obs} \times 100\%$, R– the temporal correlation coefficient and RMSE – the Root mean Square Error= $1/\text{Ns} \times \Sigma(\text{Mod-Obs})^2$ ^{1/2}.

Site	Name	Obs	Mod	Bias	R	RMSE	IOA
AT0002	Illmitz	24.37	14.82	-39	0.63	16.51	0.67
AT0005	Vorhegg	9.24	10.01	8	0.39	9.03	0.57
AT0048	Zoebelboden	11.24	12.72	13	0.34	9.15	0.59
CH0001	Jungfrauoch	2.98	7.41	149	0.11	9.95	0.23
CH0002	Payerne	17.28	12.09	-30	0.64	10.50	0.73
CH0003	Tänikon	15.56	12.81	-18	0.53	10.31	0.71
CH0004	Chaumont	9.18	12.14	32	0.54	8.14	0.7
CH0005	Rigi	8.33	10.89	31	0.45	8.77	0.63
CY0002	Ayia Marina	23.32	24.29	4	0.34	22.20	0.54
CZ0001	Svratouch	16.06	13.71	-15	0.53	9.54	0.71
CZ0003	Košetice	17.56	14.23	-19	0.61	10.10	0.73
DE0001	Westerland	22.07	18.33	-17	0.70	10.31	0.8
DE0002	Waldhof	18.72	14.42	-23	0.58	12.21	0.68
DE0003	Schauinsland	9.27	10.49	13	0.45	7.39	0.66
DE0007	Neuglobsow	16.55	13.16	-20	0.68	9.81	0.76
DE0008	Schmücke	11.13	12.73	14	0.35	9.33	0.59
DE0009	Zingst	18.65	14.71	-21	0.71	10.67	0.78
DE0044	Melpitz	24.12	14.55	-40	0.62	14.42	0.64
DK0012	Risoe	27.28	14.82	-46	0.67	17.12	0.63
ES0005	Noia	8.37	13.17	57	0.66	7.70	0.71
ES0006	Mahon	12.91	16.82	30	0.55	8.62	0.64
ES0007	Viznar	17.29	13.95	-19	0.59	11.23	0.75
ES0008	Niembro	18.41	10.52	-43	0.59	11.03	0.63
ES0010	Cabo de Creus	17.03	14.97	-12	0.55	7.12	0.72
ES1778	Montseny	18.52	18.33	-1	0.48	7.74	0.69
FI0050	Hyytiälä	6.35	5.25	-17	0.39	4.81	0.61
GB0036	Harwell	13.97	13.92	0	0.72	7.27	0.84
GB0048	Auchencorth Moss	7.80	9.12	17	0.73	4.84	0.83
IT0001	Montelibretti	29.23	13.26	-55	0.43	21.16	0.54
LV0010	Rucava	14.38	9.17	-36	0.42	10.10	0.58
MD0013	Leova II	15.92	15.96	0	0.32	22.31	0.48
PL0005	Diabla Gora	17.04	11.53	-32	0.37	11.97	0.57
RO0008	EM-3	17.85	8.80	-51	0.42	12.40	0.54
SE0005	Bredkälen	3.94	3.24	-18	0.61	2.45	0.75
SE0012	Aspvreten	8.06	6.92	-14	0.58	4.89	0.74
SE0014	Råö	16.97	14.00	-18	0.65	8.22	0.78
SI0008	Iskrba	16.33	14.02	-14	0.48	10.34	0.67
Hourly							
CZ0003	Košetice	20.00	13.29	-34	0.60	12.21	0.66
FI0017	Virolahti II	11.10	7.44	-33	0.33	10.54	0.48
FR0009	Revin	27.65	13.52	-51	0.52	17.51	0.51
FR0013	Peyrusse Vieille	21.43	11.48	-46	0.36	13.40	0.47
FR0014	Montandon	18.91	10.24	-46	0.56	11.46	0.6
FR0015	La Tardière	20.73	14.27	-31	0.56	11.27	0.66
FR0018	La Coulonche	11.16	11.51	3	0.72	4.31	0.84
GB0006	Lough Navar	9.58	9.22	-4	0.57	6.44	0.74
GB0036	Harwell	18.20	13.70	-25	0.73	8.75	0.8
GB0043	Narberth	11.73	15.27	30	0.59	9.81	0.74
GB0048	Auchencorth Moss	7.18	9.41	31	0.73	5.23	0.82
GR0001	Aliartos	29.28	13.94	-52	0.55	17.42	0.52
MK0007	Lazaropole	15.78	13.72	-13	0.22	10.37	0.51
NL0007	Eibergen	26.67	18.19	-32	0.63	14.68	0.69
NL0009	Kollumerwaard	23.15	18.13	-22	0.58	12.20	0.71
NL0010	Vreedepeel	28.57	18.25	-36	0.66	15.18	0.68
NL0091	De Zilk	23.70	20.93	-12	0.58	11.98	0.74
SE0011	Vavihill	16.13	12.90	-20	0.64	8.83	0.77
Weekly							
NO0002	Birkenes II	7.01	5.86	-16	0.64	3.40	0.76
NO0039	Kårvatn	3.58	2.62	-27	0.44	1.94	0.64
NO0056	Hurdal	5.87	6.07	3	0.42	3.01	0.67

Table A.2: *Statistic analysis of model calculated daily PM_{2.5} against observations in 2011.*

Site	Name	Obs	Mod	Bias	R	RMSE	IOA
AT0002	Illmitz	19.27	12.62	-35	0.59	13.66	0.68
CH0002	Payerne	12.18	9.36	-23	0.61	8.60	0.74
CH0005	Rigi	6.91	8.84	28	0.32	8.36	0.53
CY0002	Ayia Marina	16.55	16.78	1	0.45	11.22	0.61
CZ0003	Košetice	16.08	11.29	-30	0.63	9.16	0.71
DE0002	Langenbrügge/Waldhof	14.24	10.71	-25	0.60	10.95	0.69
DE0003	Schauinsland	7.16	8.11	13	0.48	5.89	0.67
DE0007	Neuglobsow	13.14	9.91	-25	0.68	9.94	0.73
DE0008	Schmücke	8.48	9.99	18	0.38	8.20	0.60
DE0044	Melpitz	20.08	11.51	-43	0.65	13.08	0.65
ES0007	Víznar	8.98	7.22	-20	0.59	4.51	0.74
ES0008	Niembro	7.75	7.15	-8	0.68	3.93	0.81
ES0009	Campisábalos	4.88	5.33	9	0.50	2.76	0.70
ES0010	Cabo de Creus	8.06	8.93	11	0.56	5.22	0.72
ES0011	Barcarrota	8.36	5.99	-28	0.30	7.31	0.49
ES0012	Zarra	5.63	8.54	52	0.66	4.58	0.67
ES0013	Penausende	5.23	5.36	2	0.66	2.76	0.80
ES0014	Els Torms	7.61	10.56	39	0.53	6.93	0.67
ES0016	O Saviñao	8.49	7.30	-14	0.81	4.18	0.87
ES1778	Montseny	11.79	14.73	25	0.41	6.80	0.59
FI0050	Hyytiälä	4.90	4.09	-17	0.53	3.23	0.72
GB0036	Harwell	10.14	9.27	-9	0.78	5.92	0.87
GB0048	Auchencorth Moss	4.62	5.26	14	0.78	3.35	0.87
IT0004	Ispra	22.15	16.09	-27	0.34	19.88	0.58
LV0010	Rucava	11.40	6.33	-44	0.59	8.07	0.62
NL0009	Kollumerwaard	12.83	11.92	-7	0.68	9.15	0.80
NL0010	Vreedepeel	15.97	13.39	-16	0.69	9.85	0.80
NL0011	Cabauw	15.25	13.42	-12	0.66	10.60	0.78
NL0091	De Zilk	12.67	12.66	0	0.67	9.86	0.80
PL0005	Diabla Gora	12.79	8.75	-32	0.42	9.54	0.59
SE0005	Bredkälen	1.94	2.25	16	0.61	1.45	0.76
SE0014	Råö	7.90	7.56	-4	0.53	6.02	0.71
SI0008	Iskrba	14.31	11.65	-19	0.52	9.62	0.68
Hourly							
CZ0003	Košetice	15.08	11.4	-24	0.56	9.53	0.66
FI0009	Utö	6.33	5.08	-20	0.56	4.95	0.71
FI0017	Virolahti II	7.24	5.33	-26	0.39	5.98	0.59
FR0009	Revin	15.65	10.26	-34	0.63	9.59	0.7
FR0013	Peyrusse Vieille	14.85	7.63	-49	0.53	10.07	0.58
FR0015	La Tardière	13.24	10.14	-23	0.61	9.31	0.74
GB0036	Harwell	11.83	8.83	-25	0.83	6.21	0.87
GB0048	Auchencorth Moss	4.34	5.26	21	0.79	3.36	0.88
Weekly							
NO0002	Birkenes II	4.13	3.65	-12	0.5	2.73	0.68
NO0039	Kårvatn	2.59	1.93	-25	0.41	1.51	0.59
NO0056	Hurdal	4.34	4.64	7	0.47	2.43	0.69

Table A.3: *Statistic analysis of model calculated EC and OC in PM₁₀ and PM_{2.5} against observations in 2011 based on daily and weekly (cursive) data.*

Site	Name	Obs	Mod	Bias	R	RMSE	IOA
EC in PM ₁₀							
ES1778	Montseny	0.34	0.73	115	0.04	0.51	0.30
GB0036	Harwell	0.36	0.38	6	0.82	0.35	0.82
NO0002	<i>Birkenes II</i>	<i>0.11</i>	<i>0.08</i>	<i>-27</i>	<i>0.67</i>	<i>0.08</i>	<i>0.72</i>
NO0039	<i>Kaarvatn</i>	<i>0.07</i>	<i>0.03</i>	<i>-57</i>	<i>0.34</i>	<i>0.06</i>	<i>0.48</i>
NO0056	<i>Hurdal</i>	<i>0.17</i>	<i>0.22</i>	<i>29</i>	<i>0.70</i>	<i>0.11</i>	<i>0.78</i>
EC in PM _{2.5}							
CY0002	Ayia Marina	0.22	0.12	-45	0.37	0.14	0.49
CZ0003	Košetice	0.46	0.32	-30	0.73	0.28	0.78
DE0002	Langenbrügge/Waldhof	0.39	0.32	-18	0.55	0.34	0.66
DE0003	Schauinsland	0.15	0.26	73	0.29	0.18	0.51
DE0007	Neuglobsow	0.37	0.27	-27	0.75	0.36	0.72
DE0008	Schmücke	0.23	0.34	48	0.21	0.27	0.40
DE0044	Melpitz	1.08	0.38	-65	0.57	1.45	0.41
ES0009	Campisábalos	0.13	0.10	-23	0.68	0.07	0.77
IT0004	Ispra	1.71	0.74	-57	0.47	1.75	0.50
NL0011	Cabauw	0.54	0.65	20	0.45	0.49	0.65
PL0005	Diabla Gora	0.58	0.26	-55	0.44	0.55	0.52
SI0008	Iskrba	0.35	0.52	49	0.64	0.39	0.65
NO0002	<i>Birkenes II</i>	<i>0.11</i>	<i>0.07</i>	<i>-36</i>	<i>0.68</i>	<i>0.08</i>	<i>0.68</i>
NO0039	<i>Kaarvatn</i>	<i>0.07</i>	<i>0.03</i>	<i>-57</i>	<i>0.45</i>	<i>0.06</i>	<i>0.50</i>
NO0056	<i>Hurdal</i>	<i>0.16</i>	<i>0.21</i>	<i>31</i>	<i>0.71</i>	<i>0.1</i>	<i>0.78</i>
OC in PM ₁₀							
GB0036	Harwell	2.27	0.98	-57	0.68	1.7	0.58
NO0002	<i>Birkenes II</i>	<i>0.91</i>	<i>0.87</i>	<i>-4</i>	<i>0.62</i>	<i>0.52</i>	<i>0.67</i>
NO0039	<i>Kaarvatn</i>	<i>0.88</i>	<i>0.66</i>	<i>-25</i>	<i>0.52</i>	<i>0.57</i>	<i>0.48</i>
NO0056	<i>Hurdal</i>	<i>1.28</i>	<i>1.42</i>	<i>11</i>	<i>-0.01</i>	<i>0.88</i>	<i>0.34</i>
OC in PM _{2.5}							
CY0002	Ayia Marina	1.68	1.54	-8	0.41	1.01	0.63
CZ0003	Košetice	2.98	1.44	-52	0.20	2.86	0.43
DE0002	Langenbrügge/Waldhof	3.14	1.11	-65	0.31	3.75	0.41
DE0003	Schauinsland	1.48	1.15	-22	0.57	0.85	0.73
DE0007	Neuglobsow	3.01	1.12	-63	0.42	3.85	0.40
DE0008	Schmücke	1.59	1.17	-26	0.25	1.14	0.51
DE0044	Melpitz	2.15	1.27	-41	0.36	2.24	0.46
ES0009	Campisábalos	1.81	0.99	-45	0.79	0.92	0.59
IT0004	Ispra	7.51	2.35	-69	0.08	8.84	0.44
NL0011	Cabauw	2.24	1.15	-49	0.47	2.27	0.47
PL0005	Diabla Gora	3.45	1.25	-64	0.15	3.5	0.43
SI0008	Iskrba	3.80	1.85	-51	0.27	2.99	0.44
NO0002	<i>Birkenes II</i>	<i>0.67</i>	<i>0.86</i>	<i>28</i>	<i>0.60</i>	<i>0.44</i>	<i>0.70</i>
NO0039	<i>Kaarvatn</i>	<i>0.67</i>	<i>0.66</i>	<i>-1</i>	<i>0.53</i>	<i>0.37</i>	<i>0.50</i>
NO0056	<i>Hurdal</i>	<i>0.88</i>	<i>1.40</i>	<i>59</i>	<i>0.36</i>	<i>0.78</i>	<i>0.50</i>

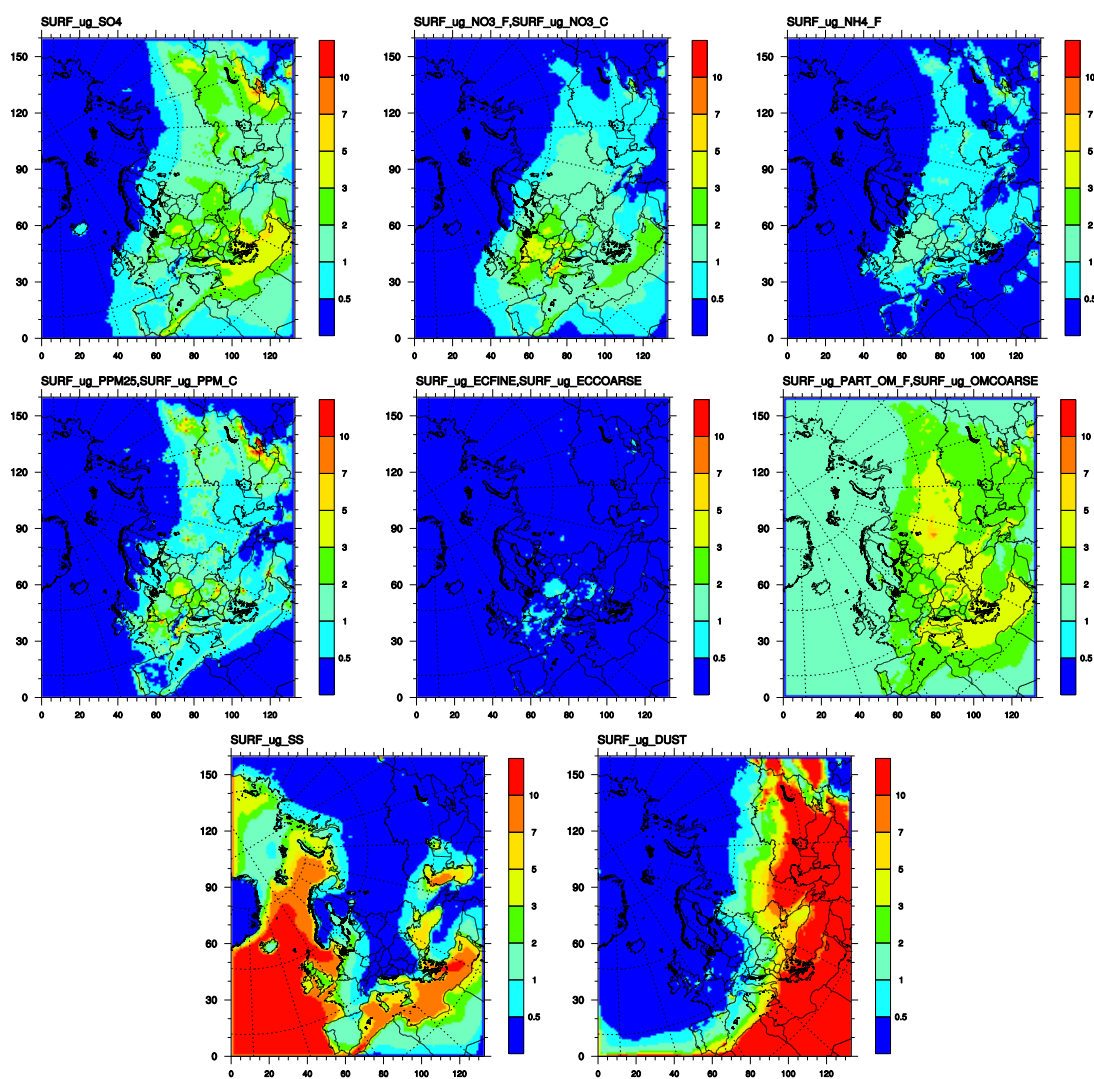


Figure A.1: Annual mean concentrations of the individual aerosol components of PM_{10} in 2010 calculated with the EMEP/MSC-W model. Here, upper panel: SO_4^{2-} , NO_3^- , NH_4^+ ; middle panel: primary PM_{10} , elemental carbon, organic aerosols; lower panel: sea salt and mineral dust. Units: $\mu g/m^3$.

